MEDICAL UNIVERSITY OF VIENNA

The underdogs: How small immune cell populations shape lung macrophage development

Doctoral thesis at the Medical University of Vienna
for obtaining the academic degree

Doctor of Philosophy

Submitted by

Anna-Dorothea Gorki, M.Sc.

Supervisor:
Univ.Prof. Sylvia Knapp, MD, PhD

Department of Internal Medicine I, Laboratory of Infection Biology, Medical University of Vienna

Research Center for Molecular Medicine (CeMM) of the Austrian Academy of Siences

Vienna, 12/2018

Declaration

The doctoral candidate, Anna-Dorothea Gorki, conducted her PhD studies under the supervision of Prof. Dr. Sylvia Knapp, PhD at the (i) Department of Medicine I, Laboratory of Infection Biology, Medical University of Vienna and (ii) the Research Center for Molecular Medicine (CeMM) of the Austrian Academy of Sciences. Additionally, parts of her PhD studies were conducted abroad, at the Department of Immunology, Weizmann Institute of Science, Rehovot, Israel where the doctoral candidate spent 8 months as a research fellow under the supervision of Dr. Ido Amit. The work abroad was granted by the FWF-funded PhD program 'Cell Communication in Health and Disease' (CCHD) at the Medical University of Vienna.

For the publication "First-breath-induced type 2 pathways shape the lung immune environment" included in chapter 2.1 of this thesis, Anna-Dorothea Gorki, helped to perform experiments and analyzed data. Simona Saluzzo performed the majority of experiments, analyzed the data and wrote the manuscript. While Simona Saluzzo worked in Cambridge in the lab of Andrew McKenzie during her stay abroad, Anna-Dorothea Gorki performed FACS experiments in transgenic mouse models, which resulted in an overview of cell composition changes in the lung of transgenic mice such as ST2 deficient mice compared to WT mice. Together with Simona Saluzzo she optimized the cell surface staining and gating strategies for lung cell populations used for the final publication. Anna-Dorothea Gorki also conducted in-vitro experiments to establish the macrophage polarization pattern of tissue-resident macrophages of WT and knock-out mice after stimulation with heat inactivated bacteria. Sylvia Knapp funded the project, supervised the work and wrote the manuscript. Andrew McKenzie provided intellectual input and supervised the experiments conducted in Cambridge. Batika Rana and Philipp Starkl performed some of the in-vivo experiments. Rui Martins and Seth Scanlon provided assistance with the confocal microscopy and image processing. Omar Sharif and Joanna Warszawska provided intellectual inputs and assistance for the *in vivo* and *in vitro* experiments with *S. pneumoniae*. Karin Lakovits, Anastasiya Hladik and Ana Korosec provided technical assistance with *in vivo* and *in vitro* experiments.

For the publication "Lung single-cell signaling interaction map reveals basophil role in macrophage imprinting" included in chapter 2.2 of this thesis, Merav Cohen, Amir Giladi and Anna-Dorothea Gorki share first authorship. Anna-Dorothea Gorki conceived, designed, performed and analyzed experiments. Merav Cohen conceived, designed, performed and analyzed experiments and wrote the manuscript. Amir Giladi conceived, designed and analyzed experiments, developed computational methods, performed bioinformatics analysis and wrote the manuscript. Anna-Dorothea Gorki joined the project after the optimization of the technical pipeline, around 2 month after the first experiment. During her 8 month stay at

the Weizmann Institute, Anna-Dorothea Gorki and Merav Cohen performed all sorting experiments and library preparations together and discussed the next steps together with Amir Giladi, who was performing the bioinformatic analysis of the single cell experiments, and Ido Amit as the supervisor of the study. After Anna-Dorothea Gorki returned to Vienna she set up important, timed breedings of transgenic mice and continued cell sorting from ST2- and basophil-deficient animals, the latter being the main mouse model in the paper. In addition, she established and optimized the staining for tissue-resident lung macrophages together with Anastasiya Hladik and acquired the pictures used for TissueFAXS analysis. Using tissue clearing as a newly established technique in the Knapp laboratory, Anna-Dorothea Gorki could provide light sheet microscopy pictures and videos in collaboration with Anastasiya Hladik, Andras Miklosi and Tibor Harkany. To establish the impact of basophils in lung development, Anna-Dorothea Gorki performed phagocytosis assays with primary cells, thereby providing important data on macrophages developing in basophil deficient mice. Dikla Gelbard Solodkin developed computational methods and performed bioinformatic analysis. Mor Zada, Anastasiya Hladik, Andras Miklosi, Tomer-Meir Salamem, Keren Bahar Halpern, Eyal David, Shalev Itzkovitz and Tibor Harkany contributed to the experiments. Sylvia Knapp conceived, designed and supervised experiments. Ido Amit directed the project, conceived, designed and analyzed experiments and wrote the manuscript.

Table of Contents

List of Figures

Thesis figures

Published figures

First-Breath-Induced Type 2 Pathways Shape the Lung Immune Environment

Lung Single-Cell Signaling Interaction Map Reveals Basophil Role in Macrophage Imprinting

List of Tables

Published tables

First-Breath-Induced Type 2 Pathways Shape the Lung Immune Environment

Lung Single-Cell Signaling Interaction Map Reveals Basophil Role in Macrophage Imprinting

Abstract

With the first breath, the lung is suddenly exposed to the outer environment leading to substantial structural and cellular changes. It is not completely understood how immune and non-immune cells in the lung develop and how essential interactions between the two niches are for these processes. Here we show in two publications that microenvironmental factors derived from non-immune cells lead to the activation of two small immune cell populations of the lung, innate lymphoid cells type 2 (ILC2s) and basophils. Factors released by these cells shape the identity of the tissue-resident macrophages of the lung, alveolar macrophages (AM).

In the first study we showed that the alarmin interleukin-33 (IL-33), an epithelial-derived cytokine, is up-regulated shortly after birth due to mechanical stress. This subsequently leads to the activation of tissue resident ILC2s. The resulting expansion of ILC2s around postnatal day 3 is accompanied by the arrival of AMs that obtain a rather anti-inflammatory phenotype, which is driven by ILC2-derived IL-13. This M2-like polarization state of AMs is required to secure tissue homeostasis by preventing excessive inflammation that otherwise would be induced by the constant exposure to airborne particles and pathogens. This comes at the expense of a delayed response in WT mice when challenged with a bacterial infection like pneumococcal pneumonia while IL-13 deficient or ILC2 deficient mice show an increased bacterial clearance due to a more pro-inflammatory phenotype of AMs.

In the second part we studied lung development on a single-cell level from early fetal development until adulthood. In addition to the lung cell atlas we generated, we went on to investigate possible interaction ligand and receptor pairs. Next to the ILC2-AM axis described in the previous paper, we found a population of basophils that had a lung-specific expression pattern that was IL-33 dependent. Deletion of these lung-specific basophils *in vivo* resulted in a premature monocyte-like gene expression profile of AMs. In a genetic model of adult basophil-deficient mice we found a decreased number of alveolar macrophages in the bronchoalveolar lavage, which in addition had a reduced phagocytic capacity.

Both studies provide new insights into lung development shortly before and after birth, a time that was shown to be critical in premature babies and infants. By broadening our understanding of the pathways involved in the early events of immune cell maturation, we hope to get a few steps closer to understand how lung immune and non-immune cells behave in health and disease.

Kurzfassung

Der erste Atemzug eines Neugeborenen stellt eine Herausforderung für das Lungengewebe dar: Die Lungenbläschen entfalten sich und sind dabei zum ersten Mal der äußeren Umgebung ausgesetzt. Die dadurch verursachten strukturellen, aber auch zellulären Änderungen, sind bisher wenig erforscht. In den zwei in der Thesis enthaltenen Publikationen geht es um das Zusammenspiel von Struktur- und Immunzellen während den verschiedenen Phasen der Lungenentwicklung. Wir konnten dabei zeigen, dass die Interaktion zwischen Epithelzellen und den angeborenen Typ-2-Lymphozyten (ILC2s), sowie zwischen Epithelzellen und Basophilen zur Produktion von Interleukinen und Zytokinen führt, die für die Entwicklung von Alveolarmakrophagen (AM) wichtig sind.

In der ersten Studie konnten wir in dem Lungengewebe von neugeborenen Mäusen einen deutlichen Anstieg des Zyotkins Interleukin-33 (IL-33) beobachten. IL-33 ist bekannt dafür, dass es als Antwort auf mechanischen Stress von Strukturzellen gebildet wird. Kurz darauf folgt eine Aktivierung der sich im Gewebe teilenden ILC2 Population und dem parallel einhergehenden Auftreten von AMs. Das von ILC2 produzierte Interleukin-13 (IL-13) führt zur Polarisierung der AMs in eine entzündungshemmende Richtung. Dieser sogenannte M2-Phäntotyp ist später im voll entwickelten Gewebe wichtig um unnötige Entzündungsreaktionen zu vermeiden. Es führt jedoch auch dazu, dass AMs aus WT Mäusen eine verzögerte Immunreaktion im Vergleich zu AMs aus IL-13 oder ILC2-defizienten Mäusen aufweisen, sobald sie mit einem bakteriellen Erreger konfrontiert werden.

Im zweiten Teil der Thesis geht es um Basophile, einer bisher wenig beachteten Population in der Lunge. Durch Einzelzell-Untersuchungen auf RNA Ebene konnten wir einen „Entwicklungsatlas der Lunge“ erstellen, der von sehr frühen Stadien im Embryo bis zum Erwachsenenalter reicht. Dabei haben wir mögliche Interaktionen zwischen Zellpopulationen verglichen und nicht nur die vorher beschriebenen Signalwege zwischen Epithelzellen und ILC2s bestätigt, sondern auch eine Lungen-spezifische Basophilen Population entdeckt, die ebenfalls IL-33 abhängig ist. In einem Antikörper basierten Versuch konnten wir eine signifikante Verminderung der Basophilen im Mausmodell erreichen, was zu einem unreifen AM Phänotyp führte. Wenn man ein genetisches Modell verwendet, findet man weniger AMs in einer bronchoalveolären Lavage von Basophil-defizienten Mäusen im Vergleich zu WT Mäusen. Zudem weisen die AMs reduzierte phagozytotische Eigenschaften auf.

Die Studien, die in dieser Thesis präsentiert werden, ermöglichen erstmals einen genauen Blick auf die Lungenentwicklung kurz vor und kurz nach der Geburt zu werfen, einer Zeit, die vor allem in frühgeborenen Babys eine wichtige Rolle spielt. Die Hoffnung ist, dass durch ein besseres Verständnis der involvierten Signalwege und Immunzellpopulationen, ein Schritt in die Richtung verbesserter Therapieansätze gemacht wurde.

Publications arising from this thesis

1) **First-Breath-Induced Type 2 Pathways Shape the Lung Immune Environment.**

Simona Saluzzo, Anna-Dorothea Gorki, Batika M.J. Rana, Rui Martins, Seth Scanlon, Philipp Starkl, Karin Lakovits, Anastasiya Hladik, Ana Korosec, Omar Sharif, Joanna M. Warszawska, Helen Jolin, Ildiko Mesteri, Andrew N.J. McKenzie and Sylvia Knapp

Cell Reports, published: 21 February 2017, DOI: 10.1016/j.celrep.2017.01.071, (Volume 18, Issue 8, Pages 1893–1905).

2) **Lung single-cell signaling interaction map reveals basophil role in macrophage imprinting.**

Merav Cohen*, Amir Giladi*, Anna-Dorothea Gorki*, Dikla Gelbard Solodkin, Mor Zada, Anastasiya Hladik, Andras Miklosi, Tomer-Meir Salame, Keren Bahar Halpern, Eyal David, Shalev Itzkovitz, Tibor Harkany, Sylvia Knapp, Ido Amit
* These authors contributed equally

Cell, published: 11 October 2018, DOI: 10.1016/j.cell.2018.09.009, (Volume 175, Issue 4, Pages 1031–1044).

This publication was highlighted in the preview article “Tissue uni-ted: Lung cells team up to drive alveolar macrophage development” by Scott&Guilliams in Cell (Scott and Guilliams, 2018).

Abbreviations

AEC I	Alveolar epithelial cells type I
AEC II	Alveolar epithelial cells type II
AM	Alveolar macrophage
Arg1	Arginase 1
BAL	Bronchoalveolar lavage
BASC	Bronchoalveolar stem cell
Bmp4	Bone morphogenetic protein-4
BPD	Bronchopulmonary dysplasia
CCSP	Club cell secretory protein
CD	Cluster of differentiation
C/EBPα	CCAAT/enhancer-binding protein-α
CO_2	Carbon dioxide
Csf2rb	Colony stimulating factor 2 receptor beta common subunit
DAMPs	Damage-associated molecular patterns
DNA	Deoxyribonucleic acid
DT	Diphtheria toxin
Fgf	Fibroblastic growth factor
Fgfr	Fibroblastic growth factor receptor
FISH	Fluorescence *in situ* hybridization
GATA2	GATA binding protein 2
GM-CSF	Granulocyte-macrophage colony-stimulating factor
Id2	Inhibitor of DNA binding 2
IFN	Interferon
Ig	Immunoglobulin
IL	Interleukin
ILC	Innate lymphoid cell
iNOS	Nitric oxide synthase
Ly-6C	Lymphocyte antigen 6 complex, locus C1
Mcpt8	Mast cell protease 8
MHC	Major histocompatibility complex
NANCI	Nkx2.1-associated noncoding intergenic RNA
NET	Neutrophil extracellular trap
NK cell	Natural killer cell
Nkx2.1	NK2 homeobox 1
NO	Nitric oxide

PAMPs	Pathogen-associated molecular patterns
PAP	Pulmonary alveolar proteinosis
PPARγ	Peroxisome proliferator-activated receptor gamma
RA	Retinoic acid
RDS	Respiratory distress syndrome
RNA	Ribonucleic acid
ROS	Reactive oxygen species
Scgb1a1	Secretorglobin family 1a member 1
Sftpc	Surfactant protein C
Shh	Sonic hedgehog
Siglec-F	Sialic acid bining Ig-like lectin F
Slc7a2	Solute carrier family 7 member 2
SLE	Systemic lupus erythematosus
Sox2	Sex determining region Y-box 2
Sox9	Sex determining region Y-box 9
SP	Surfactant protein
STAT	Signale transducer and activator of transcription
ST-2	Suppression of tumorigenicity 2
TGFβ	Transforming growth factor β
TSLP	Thymic stromal lymphopoietin
TTF-1	Thyroid-specific transcription factor 1
Wnt2/2b	Wingless-type MMTV integration site family, member 2
ZEB2	Zinc finger E box binding homeobox 2

Acknowledgements

After 5 years of working hard to finally get to this point I couldn't possibly come up with a complete list of all the people that helped and supported me along the way. So I want to say: Thank you all for your help and encouragement!

First and foremost, I would like to thank Sylvia, who believed from the beginning that I would be a match for the lab. She always supported me in every possible way and encouraged me when I wanted to break fresh ground and pursue a Masters in Bioinformatics. I couldn't have asked for a better supervisor and mentor!

Special thanks also to my partners in crime, the first month we spent together as the CCHD group I will never forget (even if I forgot most of the Hungarian phrases that I learnt during that time). To the people from my year at CeMM and the additional Bad Toro group members, especially Paul&Niki, Juliane, Adrian, Ceci, Aniko&Michel and Mate: thank you for all the (late) G&T nights, settler of Catan rounds and the various trips we took together and all the scientific and non-scientific discussions we had.

I also want to say thanks to all the Ex-Knappsies, Minibabs, Rui, Omar and Simona, who helped me when I just had started in the lab by creating such a friendly environment, that I immediately felt welcomed. That brings me to best labmates one could imagine Fede, Sophie, Philipp, Martin and Stefanie: You girls (& guys ;-)) are amazing! Special thanks go to Nina, who not only helped with all the formatting requirements but also with organizational things throughout the years.

When I started my PhD, I could have never imagined that colleagues can become such good friends. I have clearly underestimated the Supergirls: Ana, Riem, Babsi, Karin und Anastasiya. Thank you for your friendship and all-round support! Karin, Ana and Anastasiya I want to mention once more for their help and outstanding technical support and of course Karin's world famous cakes.

A huge adventure during my PhD was my time at the Weizmann Institute. I can only say that it was a fantastic opportunity to work in the Amit lab. So many thanks to all the group members and Ido for being such a good mentor. I especially want to mention Merav and Amir, who I really enjoyed working with. Thanks for including me in the project from the beginning and all the interesting and fruitful discussion we had during my time there but also later on. I'm grateful that I could share some of the experiences in Israel with the best unit in MK: Laura, Amal and Deborah, I'm so happy that we met and got such good friends in a very short time. I know that after Tel Aviv, Paris, Budapest and Vienna there are many more places that want to be explored by us. Another person, listening to the spy name "Dante", made my stay in Israel even more fun, so I'm very happy to have you around.

Gratitude also goes to my soulmate at the end of the world, Marion, thanks for all the long skype calls about everything and nothing. I'm looking forward to next year!
I want to thank my parents and my siblings for their continuous support, critical input and encouragement when I needed it most. Last, but not least, the biggest thanks go to the person who accompanied me to the lab for late night experiments, who encouraged me over and over again, who listened to all the small and big complaints, who cooked me dinner when I had a long day in the lab, who makes me laugh, even when my experiments fail and who is always there for me, Paul, thanks again for your love, support and encouragement throughout the last years.

1. Introduction

The work presented in this thesis is using single cell sequencing to study the complex and precise mechanisms and signaling pathways during lung development. Single cell sequencing is a fast developing and powerful technology to distinguish gene expression profiles of separate cell types on a single cell level within a heterogeneous cell population. This allowed us to generate a mouse cell atlas that shows immune and non-immune cell types in perinatal lung development and thereby provides an important resource tool for researchers worldwide.
The following chapters provide an overview about the multi-step process of lung development as well as the origin and polarization of alveolar macrophages, the tissue-resident macrophages of the lung. Further, function of basophils and innate lymphoid cells, populations that have previously not been known for their role in lung development, will be described in more detail. Together, this provides the framework required to understand the rationale of the experiments conducted and the results found.

1.1. Lung development

Together the lung and the trachea form the mammalian respiratory system, whose main vital function is to facilitate gas exchange. Despite the importance of a proper development of the lung, the exact mechanisms involved in the maturation before and after birth are not understood in their entire complexity. However, clinical evidence clearly supports the importance of pre- and postnatal events in shaping lung homeostasis, as it is well known that complications in the perinatal period can lead to serious diseases after birth. Examples are the respiratory distress syndrome (RDS) or bronchopulmonary dysplasia (BPD), which are associated with lung immaturity and hence are major causes of morbidity and mortality in premature infants. Lung development consists of three phases, the embryonic, the fetal and the postnatal phase, that are described in the following sections.

1.1.1. Lung development before birth

From the first breath on, the lung is constantly in contact with the outside environment and is thereby exposed to changing temperatures, inhaled particles, allergens or pathogens, and therefore needs to be fully functional at the time of birth. It is not surprising that a complex multi-step process like lung development starts very early in embryogenesis and continues even after birth until young adulthood.
Before birth, an embryonic and a fetal period can be distinguished and at the end of the fetal period the conducting airways and the associated vasculature are established, ready to

adapt to the transitions occurring during the first breath. The embryonic period can be divided into the embryonic stage and the beginning of the pseudoglandular stage. The pseudoglandular stage together with the canalicular and the saccular stage as well as the beginning of the alveolar stage are characteristics of the fetal period (Fig.1).

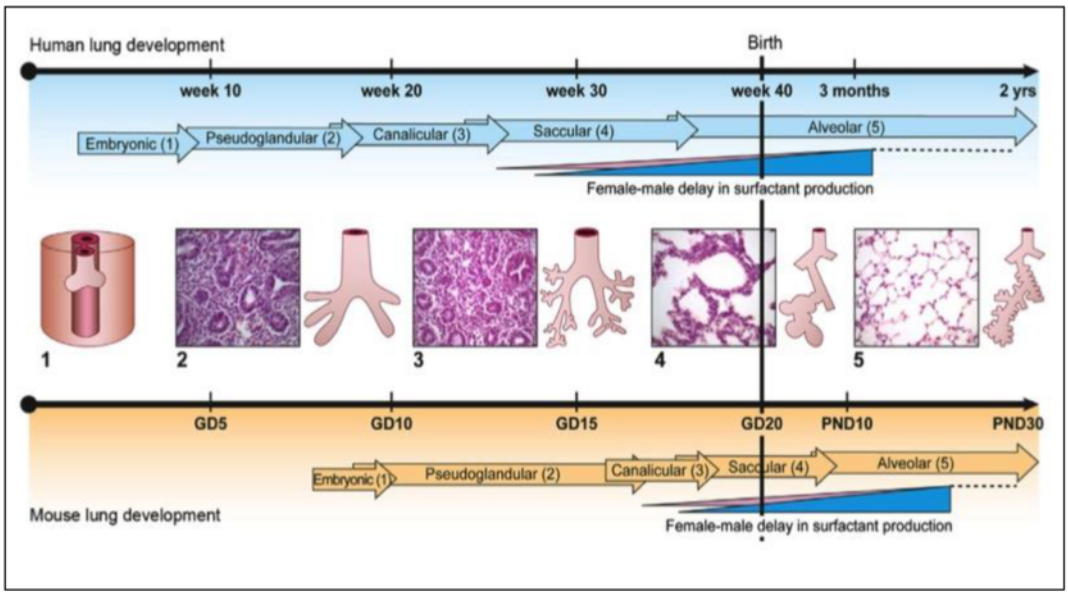

Fig. 1 – Stages of lung development in human (blue) and mouse (orange). Before birth lung development is divided into an embryonic (stage 1 and beginning of stage 2) and a fetal period (stage 2- 4). Adapted from (Boucher et al., 2015).

At embryonic day (E) 9.0 in mice and 28 days after gestation in humans the lung starts to form from two small primordial buds, which result from a specification of endoderm at the ventral wall of the anterior foregut due to NK2 homeobox 1 (Nkx2.1) expression (Herriges and Morrisey, 2014). Nkx2.1, also known as TTF-1 (thyroid-specific transcription factor 1), is a transcription factor that plays not only an important role in the differentiation of the lung but also in the organogenesis of the brain and the thyroid gland (Minoo, 2000). Only recently it was shown that Nkx2.1 expression is regulated by formation of a duplex with the long noncoding RNA NANCI (Nkx2.1-associated noncoding intergenic RNA), which leads to the establishment of a negative feedback loop (Herriges et al., 2014, 2017). In addition, Wnt2/2b and bone morphogenetic protein-4 (Bmp4) signaling from the surrounding mesoderm are required for the correct patterning of lung endoderm progenitors (Goss et al., 2009; Mucenski et al., 2003; Shu et al., 2005). While Wnt2 and Wnt2b promote expression of Nkx2.1 through accumulation and nuclear translocation of β-catenin, Bmp4 inhibits the transcription factor Sox2, a known repressor of Nkx2.1 during foregut development (Domyan et al., 2011). Concurrently, the antagonizing effect of Nkx2.1 and Sox2 plays a role during development of the trachea from the ventral foregut tube, a process that is characterized by Nkx2.1 expression, whereas dorsally the future esophagus is marked by Sox2 expression (Que et al., 2007).

In the next step the two independently formed primary lung buds start to extend into the surrounding mesenchyme and begin to develop into complex tree-like structures. This important process is called branching morphogenesis and is a main feature of the pseudoglandular stage. The first 10% of the final gas exchange surface are formed at this point by branching morphogenesis; the remaining 90% are established postnatally in a process called alveolarisation (Schittny, 2017). Critical signaling components that control the repeated splitting of the tip during branching morphogenesis include members of the fibroblastic growth factor family (FGFs). One of the main signaling molecules is Fgf 10, which is expressed at the distal lung mesenchyme that forms the developing branching points, whereas its receptor, Fgfr2, is expressed in the developing endoderm. Loss of either Fgf10 or Fgfr2 leads to complete abrogation of branching (Herriges and Morrisey, 2014). Expression of Fgf10 is restricted by expression of sonic hedgehog (Shh) in the lung epithelium (Pepicelli et al., 1998). In parallel, distinct cell types form along the proximal-distal axis including neuroendocrine cells as well as secretory, ciliated and mucosal cells in the proximal endoderm lineage. The distal lineage consists of alveolar epithelial cells type I and type II (AECI, AEC II) and is marked by the expression of the transcription factor Sox9 together with Id2, a transcription regulator. The transcription factor important for the accurate development of the proximal endoderm progenitor lineage is Sox2 (Morrisey and Hogan, 2010). The role and function of the distinct cell types is described in a later chapter (1.1.3). At the end of the pseudoglandular stage fetal breathing movements start, induced by the spontaneous contraction of smooth muscle cells that leads to a stretching of lung tissue and secretion of lung fluid. This mechanical stimulus leads to enhanced differentiation of lung epithelial cells due to increased serotonin levels (Pan et al., 2006). A reduction in fetal breathing movement and lung volume is associated with pulmonary hypoplasia often found in newborn disorders like BPD (Liu and Post, 2000).

Around E 15 (mice) or week 18 (human) the canalicular stage starts, where the terminal buds are getting narrower and are more closely associated with the surrounding vasculature. As the alveolar epithelium gets into contact with the mesenchymal capillary network, the first future blood-air barrier is formed. A special characteristic of the human fetus is that AEC II differentiation starts and intracellular lamellar bodies are formed to act as a storage form of surfactant protein (Schittny, 2017). For preterm infants, it is important to reach this stage to have a first air/blood barrier as well as minimal surfactant production. In most other species including mouse, surfactant production starts only shortly before birth.

In the saccular stage, the last prenatal stage, the airways widen by mesenchyme condensation, which results from reduced fibroblast proliferation and induced cell death (apoptosis) (Rogelj et al., 1989). This leads to the formation of thick, immature septae that are defined by a double-layered capillary network (Fig. 2).

1.1.2. First breath and lung maturation after birth: environmental and structural changes

The first breath is associated with substantial structural changes within the lungs, including the absorption of fetal lung fluid from the alveoli and the first exposure to air and the outside environment. At the same time, pulmonary immune cells gradually expand and differentiate to their mature phenotypes in order to fulfill their tasks of protecting from infection and establishing tissue homeostasis. As the lung increases in size due to progressive expansion of the airways and interstitial thinning, the large surface area needed for the transition to lung gas exchange is formed. This last stage of lung development is the alveolar stage, which is characterized by the process of alveolarisation (Joza and Post, 2015). Alveolarisation continues until young adulthood and leads to the subdivision of the alveoli into functional units to efficiently facilitate gas exchange. The process of branching morphogenesis during lung organogenesis leads to the formation of primary septae with an underlying dual capillary layer, also called pre-alveolarisation (Fig. 2).

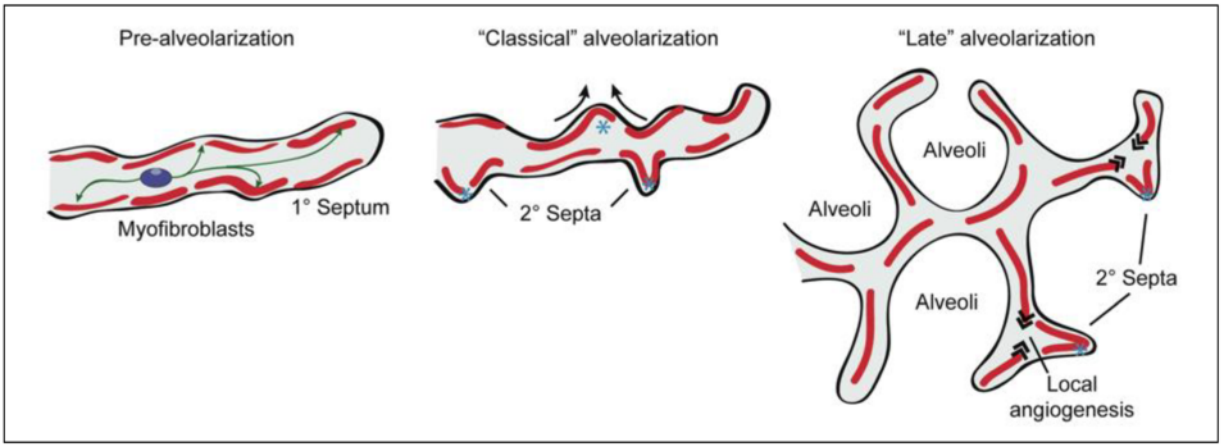

Fig. 2 – Septae formation process. After elastin deposition (blue star) by alveolar myofibroblasts, secondary septae are formed. In the final step the capillary bilayer is reduced to a monolayer and additional septation takes place. Adapted from (Joza and Post, 2015).

During "classical alveolarisation" smaller units are created by formation and extension of secondary septae that form through the accumulation of elastin at the inner walls of primary septae. Subsequently, during microvascular maturation, reduction of the separating connective tissue by apoptosis of fibroblasts leads to the fusion of the capillary bilayer into a monolayer. In a second "late alveolarisation" step, additional septation takes place, which requires local angiogenesis at the base of the newly established secondary septae (Schittny, 2017). Signaling molecules that are involved in the orchestration of developmental processes before birth are also key players in the postnatal lung development. One of these players is Nkx2.1. Its inactivation during fetal development leads to defective epithelial lineage differentiation as well as disruption of branching morphogenesis, which results in death of Nkx2.1 deficient mice at birth due to absent lungs (Kimura et al., 1996). Postnatally, Nkx2.1 also plays a role in epithelial homeostasis as its loss leads to epithelial hyperplasia and

decreased surfactant production, which can ultimately result in respiratory failure (Snyder et al., 2013). Immature alveolar structures have been shown to be risk factors for asthma and recurrent infections in preterm infants. As part of respiratory care, preterm infants were frequently exposed to high oxygen therapy, which is now known to be associated with the development of a chronic lung disease called bronchopulmonary dysplasia (BPD) (D'Angio and Maniscalco, 2004; Madurga et al., 2013). BPD is the leading cause of mortality and long-term morbidity in prematurely born infants and is characterized by an arrest in alveolar development. Consequently, these infants have a reduced gas exchange area and an impaired respiratory potential (Bourbon et al., 2005).

Considering the rapid switch from placental oxygenation to lung ventilation, high oxygen concentrations are one of the most important environmental changes at the first breath. Hence, unrestricted oxygen supplementation was thought to induce tissue oxygenation and stabilize irregular breathing patterns but it was shown that exposure to hyperoxia shortly after birth leads to formation of reactive oxygen species, which can cause cell cycle arrest and cell death. This in turn triggers the release of inflammatory cytokines and the recruitment of innate immune cells, resulting in lung inflammation, destruction of the alveolar-capillary barrier and pulmonary edema. In addition, the mechanical ventilation used to support immature lungs often leads to overinflation of the alveoli and results in lung injury (Jobe and Ikegami, 1998; Ryan et al., 2008). New therapies for BPD include gentle ventilation and only restricted oxygen treatment but also the use of prenatal corticosteroids and surfactant replacement (Coalson, 2003). The lack of pulmonary surfactant is characteristic for premature infants with respiratory distress syndrome (RDS). These infants produce less than 10mg/kg of surfactant compared to healthy infants with around 100mg/kg (Nkadi et al., 2009). Pulmonary surfactant consists of phospholipids and proteins, which are important to lower the alveolar surface tension and thereby prevent alveolar collapse during exhalation. Furthermore, surfactant proteins (SP)-A and SP-D are known to play a role in the innate host defense against pathogens by binding to structures on the surface of bacteria or viral particles and activating immune cells (LeVine et al., 2000). Synthesis and secretion of surfactant proteins can be induced by mechanical stimulation of the epithelium especially during the process of birth. Also, hormones, purines and beta-agonists binding beta-adrenergic receptors are important stimulators of surfactant secretion (Mason and Voelker, 1998; Nkadi et al., 2009). While AEC II account only for 5%-10% of the alveolar surface area, they are responsible for the synthesis of surfactant but also the clearance of inactive surfactant together with alveolar macrophages that reside inside the alveoli.

It is apparent that lung development before and after birth requires a coordinated and precise orchestration of signaling pathways and cell-cell interactions. It is crucial to further explore the precise mechanisms to develop therapeutics against disorders such as BPD or RDS.

1.1.3. Role of non-immune cell types in lung development

In the previous sections the focus has been on lung formation through defined interactions between the endodermal derived epithelium and the mesoderm. Here, the function and differentiation potential of the different cell types will be described.

The respiratory tree is lined by a variety of epithelial cells that are not only involved in mucociliary clearance but also respond to danger molecules and pathogens and thereby can initiate the recruitment of immune cells. Along the proximal-distal axis a change in cell composition can be observed, from basal cells that form 30% of the pseudostratified epithelium in the larger airways (Barkauskas et al., 2017) to the two types of pneumocytes, AEC I and AEC II, that line the alveoli (Fig. 3).

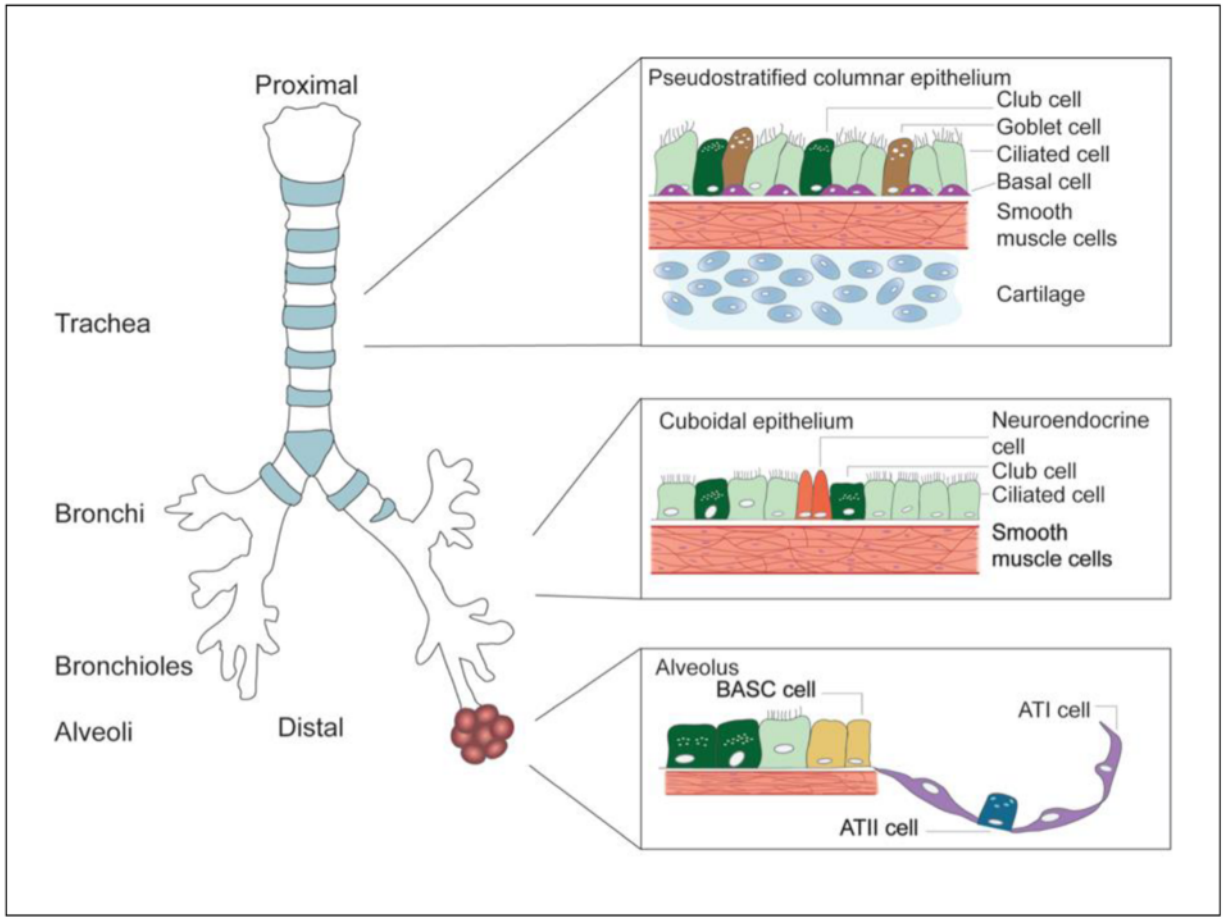

Fig. 3 – Cellular composition of the adult lung.

Basal cells closely adhere to the basal membrane and function as progenitors for ciliated and secretory cells. The environmental cues that induce fate decision are not completely understood but Notch signaling has been associated with lineage determination (Rock et al., 2011). During homeostasis the rate of cellular turnover is very low, whereas following lung damage or injury basal cells induce the prompt restoration of the epithelial barrier function by regeneration of the epithelium (Hong et al., 2004; Pardo-Saganta et al., 2015). Adult stem cells in the lung express long-term self-renewal capacities and give rise to specialized cell

types as it was depicted for basal cells. Not all lung stem cells need to be undifferentiated, as trans-differentiation or phenotypic reprogramming was also described. Depletion of basal cells, as one of the main stem cell populations of the lung, leads to reprogramming of so called 'variant' club cells that continue to function as basal cells afterwards (Barkauskas et al., 2017; Giangreco et al., 2002). This prevents the outgrowth of underlying stromal cells, which was seen in lung disease models where the basal lamina was not sufficiently covered by basal cells (O'Koren et al., 2013) and ensures the constant renewal of the epithelium. If they are not functioning as stem cells, club cells are non-ciliated secretory cells that produce secretoglobins, such as club cell secretory protein (CCSP), that play an important role in immune cell activation (Reynolds et al., 2007; Snyder et al., 2010). Goblet cells are also secretory cells but they are specialized in the synthesis of mucins, large glycoproteins that are a major component of the mucosal barrier. The coordinated movement of the ciliated cells interacting with the mucus is responsible for the mucociliary transport of inhaled particles and pathogens out of the lung (Hiemstra et al., 2015).

The role of pulmonary neuroendocrine cells, which are often clustered in neuroendocrine bodies at branching points, is not completely understood but they seem to act as sensors of airborne allergens and are important for stimulating immune cells such as innate lymphoid cells as part of the allergen-induced immune response (Kobayashi and Tata, 2018). The respiratory bronchioles act as the end of the air-conducting zone and the beginning of the respiratory zone. This transition is characterized by the appearance of fewer ciliated and club cells and the localization of BASC, bronchoalveolar stem cells, at the bronchoalveolar duct junctions (Fig. 3). BASC co-express Scgb1a1 (secretorglobin family 1a member 1), a marker for club cells, and the prominent AEC II marker surfactant protein C (Sftpc) (Kim et al., 2005). *In vitro* and after bleomycin-induced lung injury, these cells were shown to have the potential to differentiate into alveolar and bronchiolar lineages (Hogan et al., 2014; Zheng et al., 2014).

The alveolar epithelial cell differentiation starts around E16.5 in mice with a common bi-potential progenitor population that later gives rise to flat AEC I that are responsible for gas exchange and cuboidal, surfactant-secreting AEC II (Treutlein et al., 2014). In the mature lung, AEC II can self-renew and trans-differentiate into AEC I not only after injury (Desai et al., 2014; Evans et al., 1975) but also under homeostatic conditions (Volckaert and De Langhe, 2014).

For the mesoderm-derived mesenchyme, which among others includes smooth muscle cells, pericytes and fibroblasts, undifferentiated progenitor cells were shown to proliferate and disseminate to seed progenitor "niches" at different sites of the lung (Kumar et al., 2014).

All in all, the mature lung can undergo repair and regeneration after injury but prenatal deficiencies in progenitor populations can result in lifelong respiratory problems. Therefore, a better understanding of lung development before and shortly after birth is needed.

1.2. Lung immune cell populations

The pulmonary immune system's function is to preserve tissue integrity that is required for the lungs to perform their main function, i.e. the oxygenation of blood and removal of CO_2. This implies the delicate tasks of rapidly removing inhaled particles or microbes while at the same time maintaining a quiescent milieu and even a certain degree of tolerance towards the constant exposure to inhaled irritants. The precise mechanisms and immune-modulatory factors that enable the lungs to remain at - and return to - homeostasis are not yet appreciated in their entire complexity. In the following section the origin of tissue-resident macrophages and the development of alveolar macrophages will be described, followed by a brief overview of basophils and innate lymphoid cells (ILC) as these were the two cell types we found to play a role during alveolar macrophage maturation shortly after birth.

1.2.1. Alveolar macrophages – the tissue-resident macrophages of the lung

Origin and development of tissue-resident macrophages

Macrophages were first described for their ability to engulf pathogens, hence the name 'big eaters'. Over the last years, the role of tissue-resident macrophages has been redefined as they also shape and execute the response to danger and infection by mounting an inflammatory response, while at the same time playing a crucial role in the preservation of tissue homeostasis and organ function. By constantly sensing the surrounding area, tissue-resident macrophages can adapt to the local environment and can perform organ-specific functions (Amit et al., 2016; Gautier et al., 2012) such as the clearance of senescent erythrocytes by splenic red pulp macrophages or like peritoneal cavity macrophages that regulate the immunoglobulin A (IgA) production in the gut by interacting with peritoneal B-1 cells (Okabe and Medzhitov, 2014).

For a long time, it was thought that all macrophages are regularly replenished by circulating bone marrow-derived monocytes at steady state (van Furth and Cohn, 1968; van Furth et al., 1972). This dogma has been challenged in the past years, as it was shown that most tissue-resident macrophages populate the according tissue early during fetal development and are long living populations with self-renewing capacities (Hashimoto et al., 2013; Schulz et al., 2012). Therefore, three possibilities arise how tissue-macrophages can develop (Fig.4): if they are of embryonic origin they either derive from yolk sac macrophages as it was shown for microglia (Ginhoux et al., 2010), the brain's tissue macrophages, or they develop from fetal liver monocytes like the tissue-resident macrophages in liver, spleen and lung (Guilliams et al., 2013; Hoeffel et al., 2015). Upon arrival at different body sites, local tissue-derived signals are shaping macrophage identity by activating transcription factors that are inducing very distinct transcriptional programs that lead to the phenotypic diversity of tissue-resident

macrophages (Amit et al., 2016; Gautier et al., 2012; Gosselin et al., 2014; Lavin et al., 2014). For the before mentioned peritoneal macrophages (PMs), tissue-derived retinoic acid (RA) induces a PM-specific gene expression profile including the expression of the transcription factor GATA6. GATA6 was shown to be dispensable for the development of PMs but it is needed to control their correct localization that allows the interaction with B-1 cells, which is in turn important for functional IgA production (Okabe and Medzhitov, 2014).
The third possibility for the origin of tissue-macrophages is that they are not of embryonic origin but are constantly replenished by bone marrow-derived monocytes as it was described for intestinal, dermal and cardiac macrophages (Bain et al., 2014; Epelman et al., 2014; Tamoutounour et al., 2013). Except for the aforementioned populations, mature tissue-resident macrophages were shown to be independent of adult hematopoiesis at homeostatic conditions. Only after an infection or an insult such as irradiation, which results in an emptied macrophage niche, incoming bone marrow-derived monocytes can take over tissue-macrophage functions and restore tissue integrity (van de Laar et al., 2016).

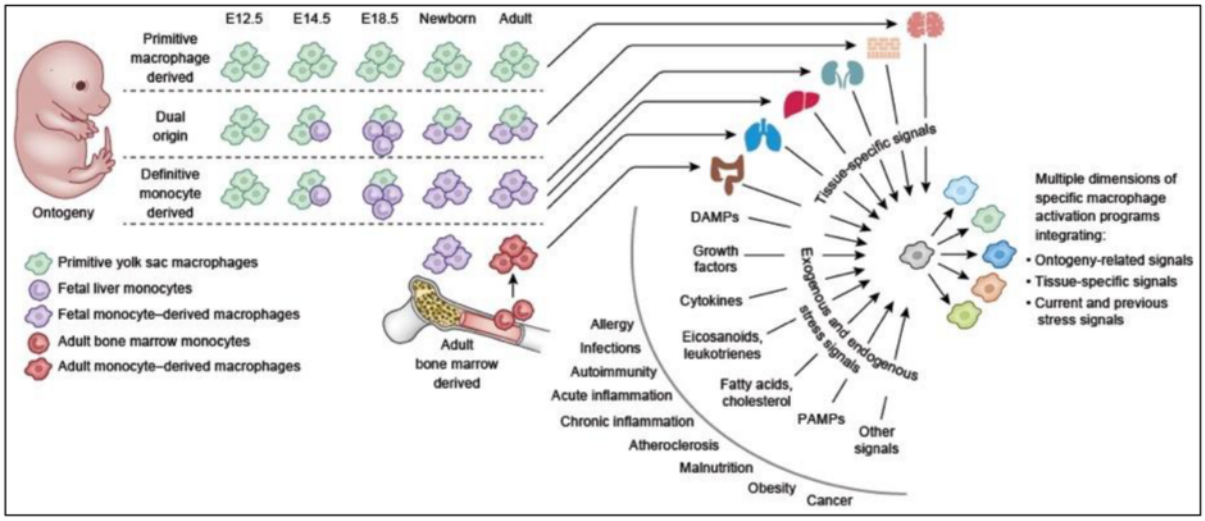

Fig. 4 – Origin of tissue-resident macrophages. Three different possibilities are depicted how tissue-resident macrophages develop: arise from primitive yolk sac derived macrophages, a mix of yolk sac macrophages and fetal liver monocytes or are constantly replenished by adult bone marrow-derived monocytes. Adapted from (Ginhoux et al., 2016).

These findings underline once more the importance of microenvironmental factors in inducing organ-specific macrophage profiles. Even if macrophages are considered a very heterogeneous lineage that develop independently of each other, there are some conserved features such as the role of the lineage-determining transcription factor PU.1 (Heinz et al., 2010) or the transcription factor ZEB2 (zinc finger E box binding homeobox 2) that in a recent study was shown to be required for macrophage maintenance (Scott et al., 2018). Tissue-resident macrophages also seem to retain sufficient plasticity to adapt to a new microenvironment as the transfer into another body site results in up-regulation of genes specific for this alternate tissue (Lavin et al., 2014).

Therefore, identifying the microenvironmental signals that shape and regulate the profile of individual tissue-resident macrophage populations is important for understanding their behavior in response to diseases as well as in homeostatic conditions.

Development of alveolar macrophages

Alveolar macrophages (AMs), the tissue-resident macrophages of the lung, and microglia, the brain's macrophages, are the most distant populations in a hierarchical tree comparing all tissue-resident macrophage populations (Lavin et al., 2014). This is a result of differences in their ontogeny but it also reflects the unique microenvironmental conditions AMs and microglia are exposed to.

AMs reside in the alveoli of the lung and are important for the clearing of inactivated surfactant and cellular debris. In addition, as they are the sentinels of the lung, they are key players in orchestrating innate immune responses during bacterial infections like pneumococcal pneumonia (Knapp et al., 2003). Next to their important role in the initiation of inflammation they are indispensable at later stages of disease, where they phagocytose apoptotic neutrophils and thereby contribute to resolution of infection and maintenance of tissue integrity (Hussell and Bell, 2014). AMs were shown to derive from fetal liver-derived monocytes that differentiate via granulocyte-macrophage colony-stimulating factor (GM-CSF) induced expression of the transcription factor PPARγ (peroxisome proliferator-activated receptor gamma) (Guilliams et al., 2013; Schneider et al., 2014). Upon arrival in the pre-mature lung, fetal monocytes expand and develop into a pre-AM state by embryonic day 17.5 (Fig.5). Respiratory epithelial cells provide GM-CSF, illustrating the importance of tissue-derived signals in instructing AM identity.

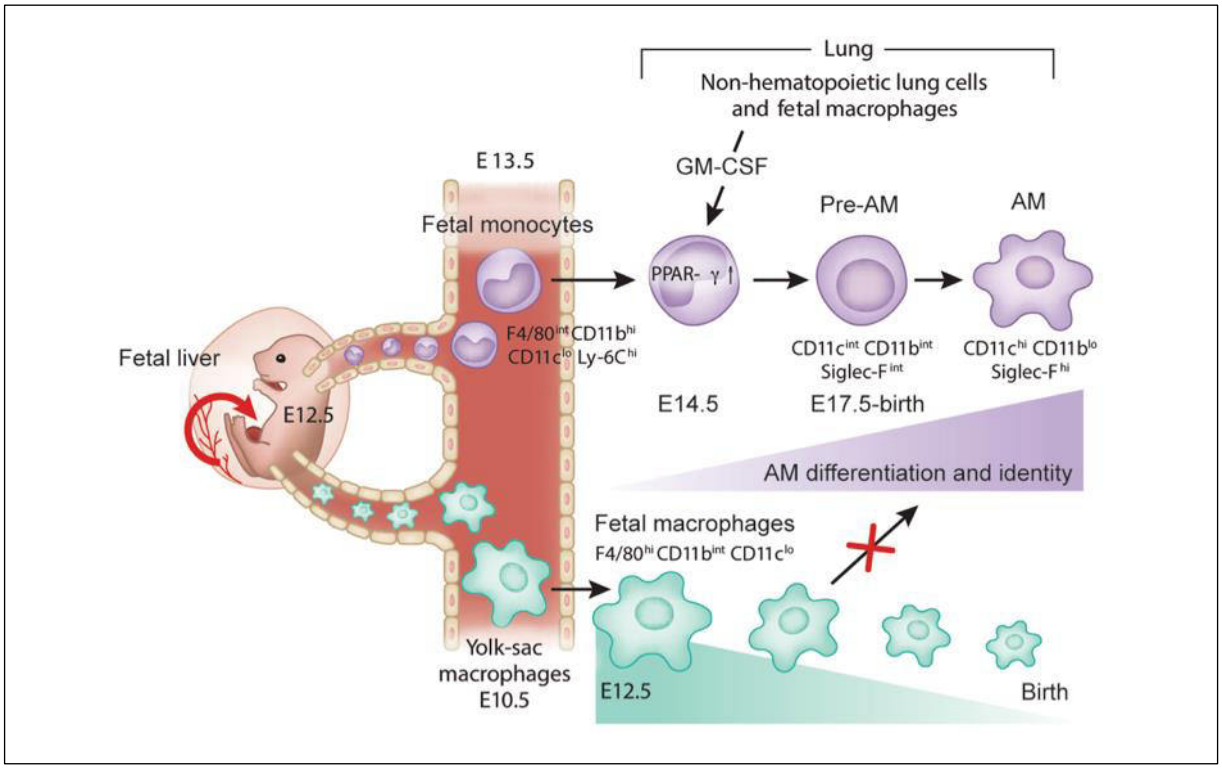

Fig. 5 – Development of alveolar macrophages. AMs derive from fetal liver monocytes and develop into pre-AM, which is GM-CSF and PPARγ dependent. Adapted from (Ginhoux, 2014).

Only perinatally, around D3, AMs as we find them in adult mice start to emerge, showing the characteristic up-regulation of the cell surface markers sialic acid-binding immunoglobulin-like lectin F (Siglec-F) and CD11c (Ginhoux, 2014; van de Laar et al., 2016).

Another cell population that expresses high levels of Siglec-F but not CD11c on their surface are mature circulating eosinophils, a granulocytic cell type. On eosinophils, Siglec-F is up-regulated in an asthma-like allergy mouse model and it was shown that SiglecF deficient mice have elevated eosinophil accumulation partially due to a block in apoptosis (Cho et al., 2010; Nutku et al., 2003; Zhang et al., 2007). In contrast, the role of SiglecF on AMs remains one of the open questions that still need to be answered. The cell surface marker CD11c, a β2 integrin, has a role in adhesion of monocytes to the endothelium and is involved in cellular activation. Several ligands including bacterial lipopolysaccharides, complement factor fragments or fibrinogen are described (Bilsland et al., 1994; López-Rodríguez et al., 1995).

In a more recent study, TGFβ (transforming growth factor β) was found to drive AM development via the activation of the key transcription factor PPARγ, but independent of the GM-CSF signaling pathway. In addition, it was shown that TGFβ is equally important for self-maintenance of mature AMs, as in adult mice inhibition of autocrine TGFβ signaling leads to increased surfactant and protein content in the bronchoalveolar lavage (BAL) (Yu et al., 2017). Mice that completely lack mature alveolar macrophages, e.g. GM-CSF receptor knockout mice (*Csf2rb-/-*), show an accumulation of surfactant and develop pulmonary alveolar proteinosis (PAP) over time (Robb et al., 1995). PAP is a rare lung syndrome that

leads to dyspnea and increased susceptibility to infections and therefore can even result in death. In patients, auto-antibodies against GM-CSF are the main cause for PAP development but also mutations in the GM-CSF receptor chain were reported (Suzuki et al., 2011). By better understanding the drivers of AM development and maintenance, we get a step closer to find promising targets for treatments of lung diseases.

1.2.2. Macrophage polarization

So far, I described how the developmental process together with microenvironmental factors shape macrophage identity. In addition to this locally defined program, the activation status of macrophages is a dynamic and reversible process that can tremendously influence their response pattern. Macrophages are activated through stimulation with cytokines, growth factors or microbial products, which can be crucial for the outcome of diseases but can also result in non-resolving inflammation (Murray et al., 2014). The potential activation states are as diverse as the range of stimuli macrophages can encounter, which leads to the renewed definition of an activation spectrum instead of fixed activation states. On the edges of this spectrum are the intensely investigated, and well described, so-called M1 and M2 macrophages. When the concept of M1 and M2 was introduced 25 years ago (Mills et al., 2000; Stein et al., 1992), the names should mimic the opposite programs observed in T cell responses, Th1 and Th2 respectively, and were based on differences in the arginine metabolism in two different mouse strains, BL/6 and BALB/c. M1 was termed the pro-inflammatory response characterized by nitric oxide (NO) and other inflammatory mediators such as interleukin-6 (IL-6) or interleukin 1β (IL-1β), which lead to high microbicidal activity. This can also be observed when macrophages are stimulated *in vitro* with interferon-gamma (IFN-γ) (Murray and Wynn, 2011). On the other hand, interleukin-4 (IL-4) stimulation *in vitro* gives rise to M2 macrophages. These are characterized by the up-regulation of the mannose receptor as well as the release of high amounts of anti-inflammatory cytokines such as IL-4 and IL-10, thereby driving the response against helminth infections but also wound healing and tissue repair (Gordon and Martinez, 2010). That BL/6 mice have a deletion in the promoter region of the cationic amino acid transporter 2 (Slc7a2), which results in decreased uptake of arginine, was not known at that time (Sans-Fons et al., 2013). Arginine conversion to ornithine, a precursor of polyamines and collagen, is increased in M2 macrophages as IL-4 stimulates arginase expression. This contributes to the production of extracellular matrix, an important feature for promoting wound healing (Mosser and Edwards, 2008).

The concept of the M1-M2 polarization was afterwards expanded including more and more subpopulations for example M2a, M2b and M2c (Mantovani et al., 2004). As not all phenotypes of macrophage activation can be described with the M1-M2 concept, the most recent idea for the activation spectrum is that one extreme are macrophages that resemble

the M1 phenotype M(IFN-γ) and on the other end are macrophages that behave like M2 macrophages, termed M(IL-4), but in between macrophage subsets are distinguished by the source they derive from and the activator combination used in the experimental set-up (Fig.6) (Murray et al., 2014).

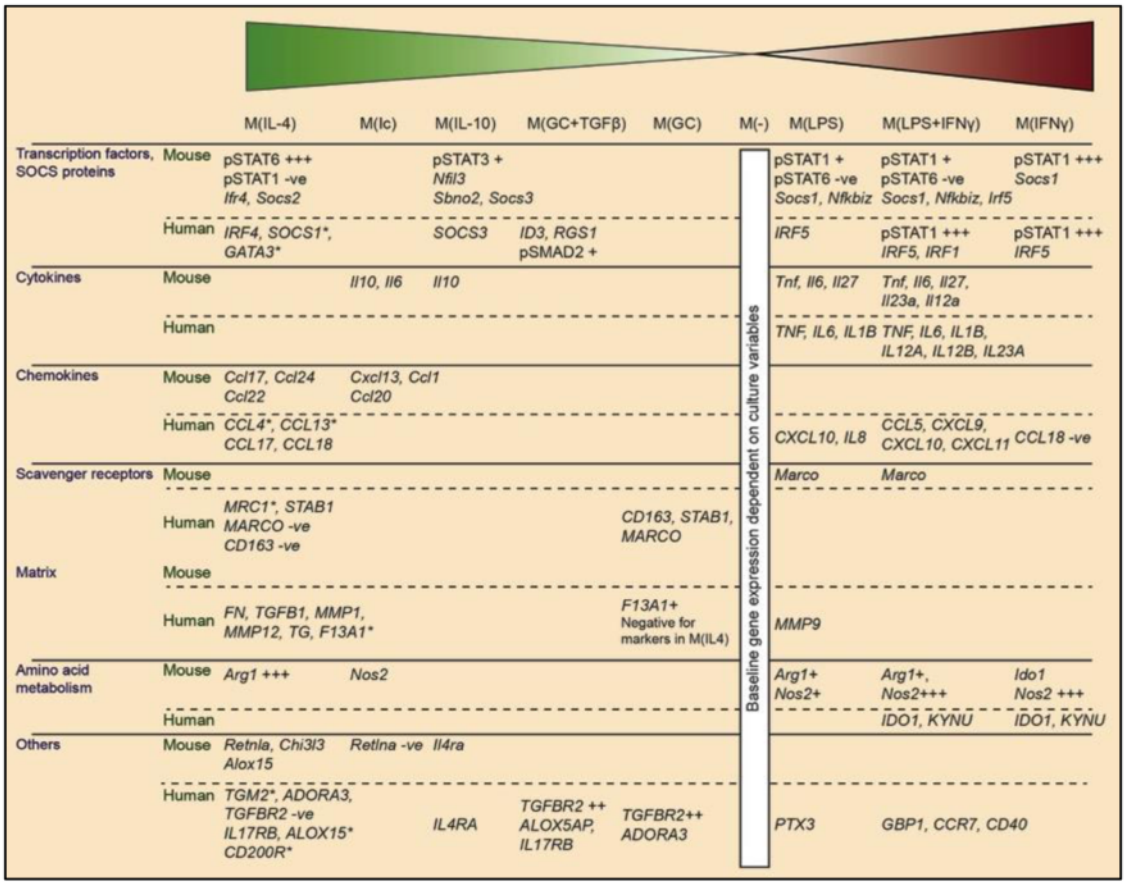

Fig. 6 – Polarization spectrum of *in vitro* generated macrophages. Adapted from (Murray et al., 2014).

The use of established markers like chitinase-like 3 (Chil3 or Ym1), resistin like alpha (Retnla, Relmα) or arginase 1 (Arg1) for M2 and inducible nitric oxide synthase 2 (iNOS) for M1 macrophages might give a hint about the polarization state of the macrophage population studied (Mills et al., 2000), but can also be misleading as for example arginine can be increased in macrophages that rather belong to the M1 side of the spectrum (El Kasmi et al., 2008). Therefore additional markers should be used as specified in Fig. 6. Good indicators are the phosphorylation states of the transcription modulators signal transducer and activator of transcription-1 (STAT1) that stimulates M1 polarization or STAT3 and STAT6, which are activated by IL-4 or IL-13 signaling and induce a M2-like expression profile (Lawrence and Natoli, 2011).

To clarify the activation status of macrophages, the name of *in vitro* generated macrophages should derive from the stimulus that was used in the experiment and for *in vivo* macrophages the closest relative in the activation spectrum should be identified (Murray et al., 2014). This would also allow the introduction of activation states that are the result of multiple, often

conflictive stimuli as it occurs in tumors or infections, where the pathogen is still present but inflammation should be dampened to quickly restore tissue homeostasis (Xue et al., 2014).

1.2.3. Role of basophils in type 2 immunity

Discovered by the German scientist Paul Ehrlich over 130 years ago, basophils are a long neglected and understudied cell population. This view slowly changes and fast developing technologies like single-cell sequencing allow us to further discover their potential functions and activation states. Basophils belong to the family of granulocytes, which also includes neutrophils and eosinophils. Granulocytes are short-lived innate immune cells that exert beneficial functions especially during the early phase of infections but are also known for their detrimental functions when they are not tightly controlled.

Neutrophils are the most abundant leukocytes in the blood and their antimicrobial activity was extensively studied (Nicolás-Ávila et al., 2017). In addition to reactive oxygen species (ROS) generation, release of granule content and phagocytosis, a mechanism specific for neutrophils was described in 2004: the formation of neutrophil extracellular traps (NETs) (Brinkmann et al., 2004). NETs are composed of decondensed chromatin fibers, DNA, histones and granular proteins, which are released by neutrophils to enhance killing of pathogens. Where it is beneficial in infections, it was shown that NETs contribute to the pathogenesis of autoimmune diseases such as systemic lupus erythematosus (SLE), tumors and thrombosis (Albrengues et al., 2018; Sørensen and Borregaard; Yu and Su, 2013).

Basophils, on the other hand, represent a very small fraction of blood leukocytes and are pro-inflammatory effector cells that are involved in allergic reactions but also have a role in protection against helminth infections (Chirumbolo, 2012). They are characterized by the expression of the high affinity receptor for immunoglobulin (Ig) E, which is one of the similarities they share with mast cells. Others are overlapping effector molecules e.g. histamine, mast cell-associated proteases or cytokines, that are partially pre-stored in cytoplasmic granules (Voehringer, 2017).

During pathogen elimination, the immune response is often classified into type 1 or type 2 immunity, based on the cell types, the production of specific cytokines and the immunoglobulin subtypes that are involved. As it was described in the previous chapter, there are two pronounced naïve helper T cell types, Th1 and Th2 respectively (Mosmann et al., 1986). But as already seen for the polarization states of macrophages, there were additional CD4 T cell subsets described in the following years. The most important ones are Th17 cells, which are important for the response against extracellular bacteria and fungi (Weaver et al., 2006) and subsets of regulatory T cells.

In response to bacterial, viral or fungal pathogens type 1 immunity is activated, which is mediated by Th1 as well as Th17 cells and results in cell-mediated cytotoxicity. Important for

the type 1 response are pro-inflammatory cytokines such as IFN-γ (Bradley et al., 1996), as well as IL-2 and tumor necrosis factor-beta (TNF-β). Moreover, type 1 immunity is characterized by the production of immunoglobulin G (IgG) class by B cells (Snapper and Paul, 1987). Excessive type 1 responses can lead to tissue damage and need to be tightly regulated. It was thought for a long time, that the only function of the type 2 immunity is to suppress type 1 responses (Berger, 2000). But it was shown later that in addition, type 2 immunity is important for the defense against helminth infections and other extracellular parasites as well as for the activation of tissue-regenerative mechanisms. Type 2 immunity is characterized by the production and secretion of IL-4, IL-5, and IL-13 by Th2 cells. IL-4 induces the production of IgE by B cells, whereas IL-5 promotes the development and recruitment of eosinophils leading to additional hallmarks of type 2 immunity: high IgE levels and eosinophilia. If type 2 immune responses are dysregulated or repair processes become chronic, they can result in the development of tissue fibrosis (Gieseck et al., 2018).

Several studies show that basophils are involved in type 2 responses where they can regulate Th2 cell function, can act as antigen-presenting cells and are producers of IL-4 and thymic stromal lymphopoietin (TSLP). Unlike Th2 cells, which develop from naïve T helper cells upon stimulation, basophils do not require the differentiation step and can produce IL-4 even without prior activation via the high affinity Ig E receptor cascade that follows after crosslinking of receptor-bound IgE by antigen binding (Marone et al., 2007). As basophils are the least abundant granulocytes in the blood, low cell counts and difficulties in the isolation process made it hard to study basophils in detail. There are two in vivo models that induce depletion of basophils: the first model is based on monoclonal antibodies such as MAR-1, which is directed against the high affinity IgE receptor (FcεRI) (Denzel et al., 2008). As the high affinity IgE receptor is not solely expressed on basophils, this can introduce bystander effects such as the activation of mast cells resulting in unwanted cytokine release. In addition, Ab treatment can influence phagocytes and dendritic cells that partially express the receptor on their surface (Hammad et al., 2010). Therefore a genetic model was generated, the Mcpt8^{DTR} mouse strain. Mast cell protease 8 (Mcpt8) is a serine protease that is solely expressed in basophils but not in mast cells as the name would suggest. In this model, treating mice with diphtheria toxin (DT) results in a transient depletion of basophils, while the majority of mast cells are unaffected (Wada et al., 2010).

Basophils derive from CD34 expressing progenitor cells in the bone marrow and are thought to expand during helminth infection (Ohnmacht and Voehringer, 2009). Transcription factors that are involved in basophil development are GATA2 and CCAAT/enhancer-binding protein-α (C/EBPα) (Arinobu et al., 2009). The IL-3/STAT5 signaling pathway induces differentiation into progenitor cells when STAT5 binds to regulatory elements of GATA2. It is also known that IL-3 and TSLP (thymic stromal lymphopoietin) promote basophil survival but are

dispensable for basophil development as IL-3 KO as well as TSLP-receptor KO or double mutant mice have normal basophil baseline numbers (Siracusa et al., 2011).
In patients with allergic asthma, which is controlled by type 2 cytokines, high basophil numbers were found in the lung and sputum (Gauvreau et al., 2000). In an allergic asthma mouse model, where allergic inflammation is induced by cysteine proteases, innate lymphoid cells type 2 (ILC2s) release IL-5 and IL-13, which results in eosinophilia. It was shown, that the release of IL-5 and IL-13 by ILC2s is enhanced by IL-4, which was produed by basophils. In mice that specifically lack IL-4 in basophils, the phenotype of eosinophilia in the lung was resolved (Motomura et al., 2014).
This shows that basophils are playing a role in type 2 immune responses but still need to be studied in more detail. In the next chapter I will depict the family of ILC and their role in health and disease.

1.2.4. Innate lymphoid cells

Innate lymphoid cells (ILCs) are located at the barrier sites of the body such as lung, intestine, mucosal tissues, adipose tissue or skin, where they can secrete high amounts of cytokines associated with the different T helper cell responses described before (Artis and Spits, 2015; Eberl et al., 2015). As ILCs are not dependent on the recognition of antigens via diversified adaptive antigen receptors found on T and B cells, they are part of the innate immune system. The discovery of ILCs has led to a new perception of how tissue homeostasis is maintained. In response to cytokines, damage signals or pathogens, ILCs contribute to multiple pathways and modulate immune responses by potentiating adaptive immune responses or regulating tissue inflammation. ILCs can be divided in three main subgroups, where ILC1, ILC2 and ILC3 mirror Th1, Th2 and Th17 cells respectively (Fig.7). Also natural killer (NK) cells are part of the ILC family and mimic CD8 positive cytotoxic T cells (Vivier et al., 2018).

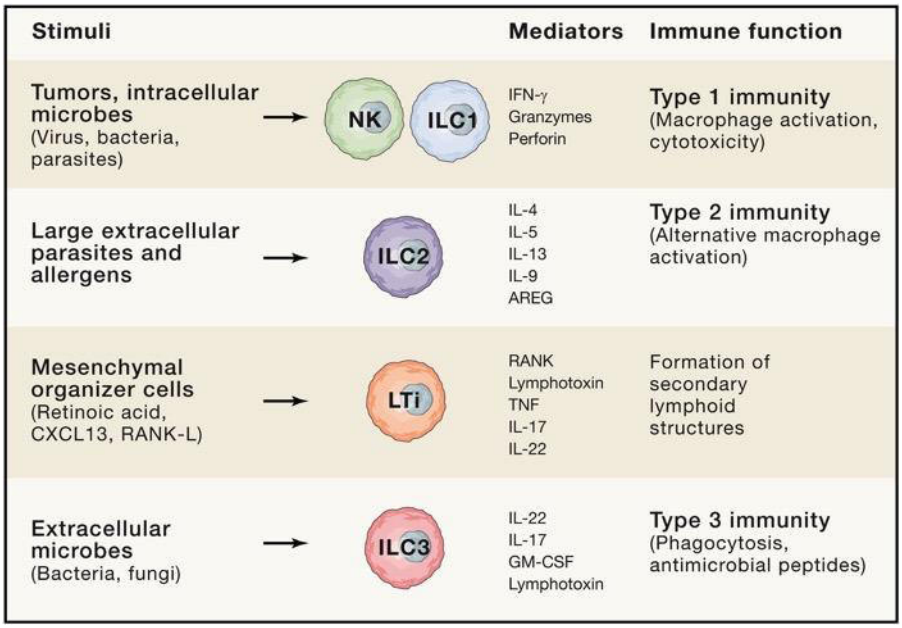

Fig. 7 - Immune function of distinct ILC subsets. In addition, effector molecules that are produced upon activation are shown. Taken from (Vivier et al., 2018).

As T cells have to undergo clonal expansion, the T cell response takes several days, whereas ILCs as well as subsets of γδ T cells or resident memory T cells can react immediately. Later on ILCs and T cells can cross-regulate each other by expression of major histocompatibility complex class II molecules (MHCII) and processing of antigen by ILCs that results in the activation of antigen-specific T cells (Oliphant et al., 2014). On the other hand, production of interleukin-2 (IL-2) by T cells modulates ILC activity. It was shown recently that ILCs also have an immunomodulatory role and are involved in the resolution of inflammation (Artis and Spits, 2015; Mattner and Wirtz, 2017). Following acute viral infections, ILC3s are involved in the repair of lymphoid tissue (Scandella et al., 2008) and were also shown to drive tissue repair and regeneration in an inflamed intestine (Sawa et al., 2011). In an influenza mouse model amphiregulin secreted by ILC2s was important for the restoration of bronchial epithelium (Monticelli et al., 2011), emphasizing the role of ILC in tissue healing and repair.

Like tissue-resident macrophages, ILCs arrive at the organ site during early embryogenesis. There they can act as lymphoid tissue-inducing cells by interacting with mesenchymal stromal cells to produce cytokines that attract additional hematopoietic cells (Mebius et al., 1997). In non-lymphoid tissues, ILC progenitors are recruited from the blood and survival is maintained by production of local survival factors such as interleukin-7 (IL-7) (Kang and Coles, 2012). Even if most ILCs are tissue-resident cells, some subsets like NK cells or inflammatory ILC2s can circulate in the bloodstream and can be recruited during inflammation.

By studying ILCs using single-cell sequencing up to 50 distinct ILC clusters were found (Gury-BenAri et al., 2016) that need to be further analyzed and studied to distinguish between different activation states and role of the microenvironment on ILC development.

1.3. Advancing technologies: Single-cell sequencing

Next-generation sequencing technologies are advancing rapidly and allow us to distinguish transcriptional changes of individual cells within complex tissues. Single-cell RNA sequencing (scRNA-seq) has not only been successfully used for the reconstruction of cell lineage trees but also to study the heterogeneity of immune responses in different cell populations. With the regulation of immune responses being of particular importance, these new tools allow for the systematic characterization of previously unknown subpopulations and their role in the course of disease and developmental processes. For the lung more and more studies are published using scRNA-seq in different models and already in 2014 Treutlein et al. started to resolve the stages of embryonic alveolar development (Treutlein et al., 2014). They showed that instead of implementing a lineage priming model, downregulation of factors in a common bipotent progenitor cell leads to the development of AEC I and AEC II cells.

Starting from transcriptome measurements based on microarrays, technology has been improved rapidly, resulting in the development of several distinct sequencing methods (Linnarsson and Teichmann, 2016). The sensitivity and cost efficiency of the six most established techniques are compared in Fig. 8. The sensitivity is thereby the probability of capturing and converting mRNA transcripts of single cells into cDNA that can be found in the sequencing library. As seen in Fig. 8 some techniques are based on a microfluidic set-up as for example Drop-seq (Macosko et al., 2015), whereas other methods such as MARS-Seq are based on sorting of single cells using fluorescence-activated cell sorting (FACS) (Jaitin et al., 2014). The incorporation of cell-specific barcodes allows the increase of scRNA-seq library generation due to multiplexing possibilities as well as the use of unique molecular identifiers (UMIs) that enables the separation of original mRNA molecules and background noise introduced during amplification steps.

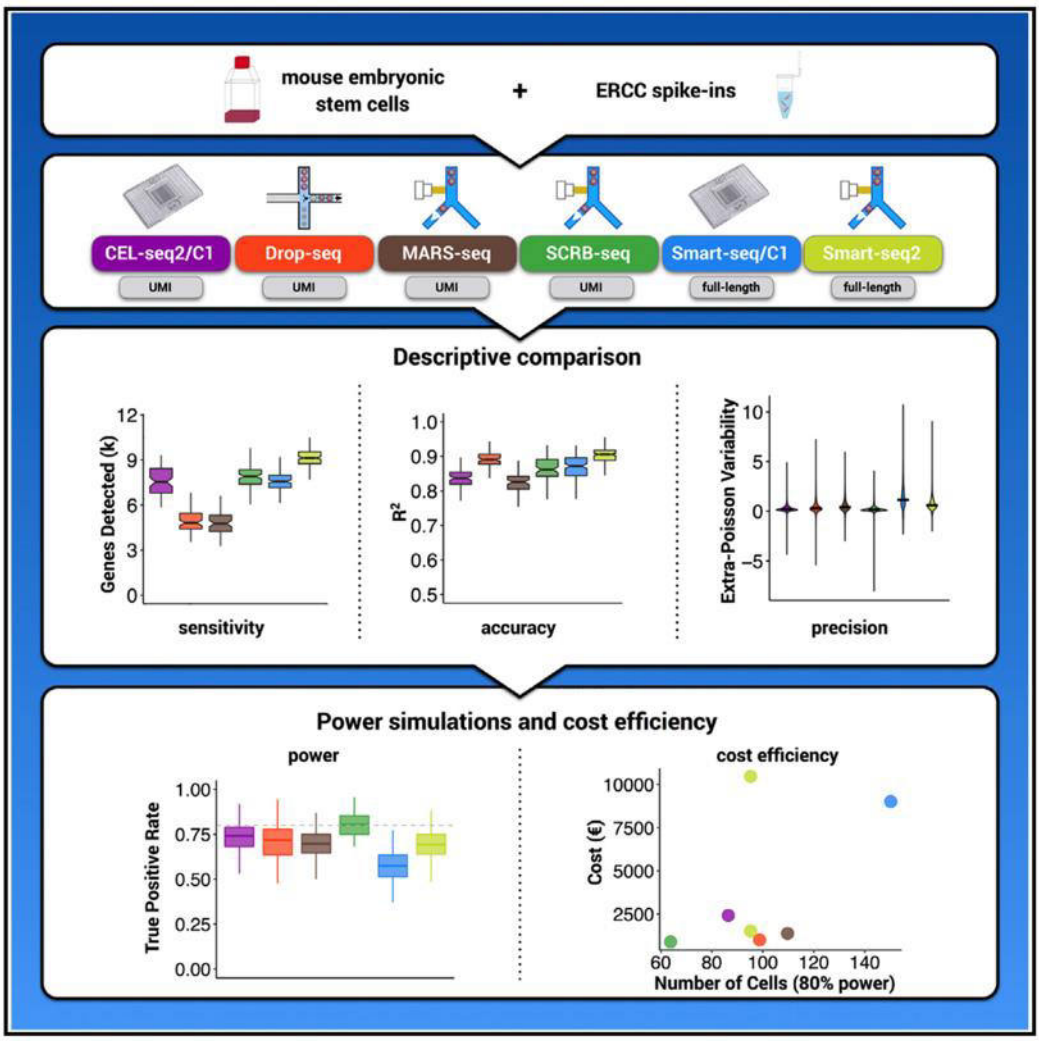

Fig. 8 – Comparison of scRNA-seq protocols. Adapted from (Ziegenhain et al., 2017).

The biggest challenge next to the technical optimization is the development of analytical pipelines that help to analyze and visualize the enormous amount of data that is generated already within a single experiment. New pipelines like the velocity algorithm even allow the prediction of the differentiation status of cells over time. Transcriptomic measurements are only a snapshot of the cell at a specific time but by taking the ratio of spliced and unspliced transcripts, we can now predict how the cell will develop in the future (La Manno et al., 2018). This will allow us to better interpret the difference between cell type and cell state. Another disadvantage in the beginning was the need to dissociate the tissue to generate single cell suspensions but new techniques have been developed that for example combine multiplex single-molecule fluorescence *in situ* hybridization (FISH) and a imaging based spatial genomic analysis (SGA) to preserve spatial information (Lignell et al., 2017). All in all scRNA-seq is an accessible and powerful tool that is used more and more by labs worldwide as also costs further decrease. It will nourish our knowledge about cell biology and in combination with other techniques like measurement of chromatin accessibility will allow a better understanding of the dynamics in complex systems.

1.4. Thesis aim

The first breath is associated with substantial structural changes within the lung, while in parallel pulmonary immune cells gradually expand and differentiate to their mature phenotypes. It is a very delicate time frame to establish tissue homeostasis but also ensure protection from infection. The activation of alveolar macrophages (AM), the tissue-resident macrophages of the lung, is tightly controlled via cell-cell interactions and soluble mediators that prevent unwanted inflammatory signaling. Despite the importance of a proper development of the lung, the exact mechanisms involved in the immune maturation after birth are not understood in their entire complexity.

With this thesis we therefore aimed to:

- Characterize tissue-derived signals that shape lung immune cell maturation and especially AM identity within the first weeks after birth
- Generate a resource tool by using single-cell RNA sequencing to generate a 'lung developmental cell atlas' that provides a detailed overview about the expression profiles of non-immune and immune cells at different stages of lung development
- Unravel the role of ILC2s and a newly described population of lung-specific basophils on AM maturation at birth and during adult life.

2. Results

2.1. First-breath-induced type 2 pathways shape the lung immune environment

In the first part of this chapter the publication “First-breath-induced type 2 pathways shape the lung immune environment” will be presented. In this work, we aim to understand the role of the epithelium-derived stress induced cytokine interleukin-33 (IL-33) on the newest players of innate immunity: innate lymphoid cells (ILCs). We found that up-regulation of IL-33 at birth activates ILC2s and leads to their expansion that coincided with the detection of alveolar macrophages (AM) in the lung. The release of IL-13 by ILC2s causes a shift of AMs to the M2-side of the macrophage activation spectrum and thereby enables the development of homeostatic conditions. This rather anti-inflammatory phenotype of AMs results in a delayed response in a pneumococcal pneumonia model when compared to mice deficient for IL-13 or ILC2s. This work not only gives a first hint of the complex interactions happening during immune cell maturation but can also help to provide a better understanding of disease development in newborns.

Cell Reports
Article

OPEN ACCESS
CellPress

First-Breath-Induced Type 2 Pathways Shape the Lung Immune Environment

Simona Saluzzo,[1,2,3] Anna-Dorothea Gorki,[1,2] Batika M.J. Rana,[3] Rui Martins,[1,2] Seth Scanlon,[3] Philipp Starkl,[1,2] Karin Lakovits,[1,2] Anastasiya Hladik,[1,2] Ana Korosec,[1,2] Omar Sharif,[1,2] Joanna M. Warszawska,[1,2] Helen Jolin,[3] Ildiko Mesteri,[4] Andrew N.J. McKenzie,[3,*] and Sylvia Knapp[1,2,5,*]

[1]CeMM Research Center for Molecular Medicine of the Austrian Academy of Sciences, Vienna 1090, Austria
[2]Department of Medicine I, Laboratory of Infection Biology, Medical University of Vienna, Vienna 1090, Austria
[3]MRC Laboratory of Molecular Biology, Francis Crick Avenue, Cambridge CB2 0QH, UK
[4]Institute of Pathology Überlingen, Überlingen 88662, Germany
[5]Lead Contact
*Correspondence: anm@mrc-lmb.cam.ac.uk (A.N.J.M.), sylvia.knapp@meduniwien.ac.at (S.K.)
http://dx.doi.org/10.1016/j.celrep.2017.01.071

SUMMARY

From birth onward, the lungs are exposed to the external environment and therefore harbor a complex immunological milieu to protect this organ from damage and infection. We investigated the homeostatic role of the epithelium-derived alarmin interleukin-33 (IL-33) in newborn mice and discovered the immediate upregulation of IL-33 from the first day of life, closely followed by a wave of IL-13-producing type 2 innate lymphoid cells (ILC2s), which coincided with the appearance of alveolar macrophages (AMs) and their early polarization to an IL-13-dependent anti-inflammatory M2 phenotype. ILC2s contributed to lung quiescence in homeostasis by polarizing tissue resident AMs and induced an M2 phenotype in transplanted macrophage progenitors. ILC2s continued to maintain the M2 AM phenotype during adult life at the cost of a delayed response to *Streptococcus pneumoniae* infection in mice. These data highlight the homeostatic role of ILC2s in setting the activation threshold in the lung and underline their implications in anti-bacterial defenses.

INTRODUCTION

The integrity of the alveolar-capillary barrier is essential to ensure sufficient blood oxygen levels, and the mechanisms driving its maintenance, renewal, and protection are flourishing fields of research (Beers and Morrisey, 2011; Chiu and Openshaw, 2015; Hogan et al., 2014; Hussell and Bell, 2014; Kopf et al., 2015; Peng et al., 2015). Lung development begins at embryonic day 9 (E9) in mice and proceeds through stages of branching morphogenesis, giving rise to pre-alveolar spaces at the saccular stage and the differentiation of type 1 and type 2 airway epithelial cells (AEC1s and AEC2s) by E18.5 (Mund et al., 2008; Woik and Kroll, 2015). At birth, alveolar sacs are suddenly exposed to the external environment and subjected to the mechanical forces of spontaneous ventilation (Orr et al., 2006; Wirtz and Dobbs, 2000). It is after the previously sterile lung tissue has been exposed to the outside environment, around postnatal day 4 (P4), when the process of alveologenesis continues with the formation of primary septa (Hogan et al., 2014). These postnatal adaptations are paralleled by the development of the early innate immune environment. Alveolar macrophages (AMs) differentiate on P3 from $CD11b^{hi}F4/80^{int}Ly6C^{hi}$ fetal monocyte progenitors into long-lived, self-renewing cells (Guilliams et al., 2013; Murphy et al., 2008). Since tissue-derived signals were found to govern the gene expression signature of macrophages (Lavin et al., 2014; Okabe and Medzhitov, 2014), the lung cytokine milieu in newborns likely determines the phenotype of AMs during this delicate developmental period. However, the postnatal immunological environment in lungs is largely unexplored, as are the innate immune signals that influence the function of AMs early in development and during homeostasis.

Under different pathological conditions, AMs have the ability to assume either an interferon-γ (IFN-γ) and Toll-like receptor (TLR) ligand-induced inflammatory phenotype (M1) or an interleukin-4 (IL-4)-, IL-13-, or IL-10-induced wound healing and tissue remodeling phenotype (M2) (Gordon and Martinez, 2010). M1 macrophages are potent producers of inflammatory cytokines such as tumor necrosis factor (TNF) and CXCL1 (Guery et al., 2011; Mantovani et al., 2004). CXCL1 is a chemokine that critically determines the early recruitment of neutrophils (De Filippo et al., 2013), thereby exerting a protective role in bacterial lung infections (Schliehe et al., 2015; Warszawska et al., 2013). M2 macrophages, phenotypically defined by the expression of *Retnla* (referred to here as *Fizz1*), *Mrc1*, *Chil3* (referred to here as *Ym1*), and *Arg1* are less efficient in triggering inflammatory responses to bacterial pathogens than M1 macrophages (Warszawska et al., 2013).

IL-33 is an alarmin belonging to the IL-1 family of cytokines best known for its capacity to drive type 2 immune responses (Liew et al., 2010; Schmitz et al., 2005) and is increasingly recognized as an important mediator of homeostasis and tissue tolerance (Molofsky et al., 2015). Upon mechanical strain or cell necrosis (Kakkar et al., 2012; Lamkanfi and Dixit, 2009; Sanada et al., 2007), IL-33 is released from cells, activating the ST2 receptor expressed on several lung cell types, including regulatory T cells (T_{reg}), dendritic cells (DCs), mast cells, group 2 innate

lymphoid cells (ILC2s), natural killer (NK) cells, and AMs (Lu et al., 2015). At steady state, lung resident ILC2s are the most abundant ST2-expressing cells and are found in close proximity to bronchovascular structures (Halim et al., 2014; Nussbaum et al., 2013), where they can be rapidly activated by IL-33 to secrete IL-13, IL-5, IL-6, IL-9, granulocyte-macrophage colony-stimulating factor (GM-CSF), and amphiregulin (Roediger and Weninger, 2015). ILC2s are involved in host protection against parasitic helminths and promotion of airway hyperreactivity in asthma or upon influenza infection and are important for adipose tissue homeostasis (Barlow et al., 2012; Brestoff et al., 2015; Chang et al., 2011; Molofsky et al., 2013; Monticelli et al., 2011; Neill et al., 2010).

Human lungs are highly susceptible to bacterial infections. Pneumonia caused by *Streptococcus pneumoniae* is the primary cause of death by an infectious disease in Western countries (van der Poll and Opal, 2009). Notably, risk factors for developing community-acquired pneumonia are asthma and influenza (Chien et al., 2009; Talbot et al., 2005), which are both characterized by IL-13-induced airway hyperreactivity (Kim et al., 2012; Lambrecht and Hammad, 2015) and the presence of M2 polarized AMs (Chen et al., 2012). Here, we investigated the physiological role of the IL-33/ILC2/IL-13 axis in shaping the pulmonary immune environment from birth to adult life and the consequences of these pathways on the innate defense against *S. pneumoniae*.

RESULTS

Postnatal Lung Inflation Is Associated with the Upregulation of IL-33 by AEC2

With the first breath, a number of profound changes occur in the newborn's lung. We hypothesized that the sudden inflation of the previously liquid-filled lungs may cause considerable mechanical stress and potential tissue injury, which could result in IL-33 induction (Kakkar et al., 2012). We discovered a substantial increment in pulmonary IL-33 on P1 compared to E19 at both the protein (Figure 1A) and mRNA levels (Figure 1B). To investigate if an abrupt exposure to negative pressure, occurring upon spontaneous breathing in the alveolar space, might cause the induction of *Il33*, we placed the lungs of E19 $Il33^{Cit/+}$ reporter (Hardman et al., 2013) and WT mice in a vacuum chamber (Figure S1A) and discovered a significant induction of Citrine$^+$ viable cells (Figures 1C, 1D, S1B, and S1C) and IL-33 protein (Figure 1E) in lungs 6 hr post-exposure to negative pressure as compared to ambient atmospheric pressure.

To study the cellular origin of pulmonary IL-33 over time, we analyzed lungs of $Il33^{Cit/+}$ reporter mice by flow cytometry. We observed a strong upregulation of *Il33* among the CD45$^-$ cell fraction starting on P1 (Figures 1F, 1G, S1D, and S1E). Approximately 60% of CD45$^-$ citrine$^+$ cells were further classified as EpCam$^+$CD31$^-$ cells (Figures 1H and 1I). Immunohistochemistry revealed that AEC2 (surfactant protein C$^+$) was the most abundant cell population upregulating *Il33* in the first few days after birth (Figure 1J). Postnatally infiltrating CD45$^+$ cells (Figure 1F, top, and Figure S1F) did not show substantial *Il33* expression (Figure S1G), except for few citrine$^+$ cells in the fetal macrophage fraction (CD45$^+$F4/80$^+$CD11b$^+$CD11c$^-$ SiglecF$^-$) (Figures S1H and S1I). In summary, we determined that postnatal lung inflation or exposure to abrupt changes in pressure was associated with the immediate induction of IL-33.

IL-33 Shapes the Neonatal Lung Environment

To understand IL-33-dependent effects on the immune environment in neonatal lungs, we first analyzed a panel of pulmonary cytokines and chemokines at P7 in wild-type (WT) and IL-33-deficient ($Il33^{Cit/Cit}$) mice. $Il33^{Cit/Cit}$ mice showed reduced expression of the type 2 cytokines IL-5 and IL-9 and of inflammatory mediators like IL-6, IFN-γ, IL-1α, IL-1β, CCL5, and CXCL10 (Figures 2A and S2A). Since ST2$^+$ ILC2s are major producers of IL-5 and Il-9 and considered the primary targets of IL-33 in the lung (Halim et al., 2014; Kearley et al., 2015), we analyzed newborn lungs for the presence of ILC2s (Lin$^-$ CD127$^+$ST2$^+$ICOS$^+$). We detected few ILC2s at E19 but markedly increased numbers by P7 that stabilized by week 6 (Figures 2B and S2B). We found IL-33 to be contributory in populating lungs with ILC2s, as illustrated by reduced ILC2 numbers in $Il33^{Cit/Cit}$ (Figure 2C) and ST2-deficient ($Il1rl1^{-/-}$) mice at P7 (Figure 2D). In accordance with the ability of ILC2s to regulate eosinophil homeostasis via IL-5 secretion (Nussbaum et al., 2013), eosinophils populated the lungs a few days after ILC2s (Figures 2E and S2C), with clear reductions in the absence of IL-33 (Figure 2F) or ST2 (Figure 2G). IL-5+ ILC2s expanded locally in the lungs (Figures S2E–S2G), whereas eosinophil numbers increased systemically (Figure 2H). The numbers of AMs, polymorphonuclear (PMNs) cells, B cells, and T cells were not changed in $Il33^{Cit/Cit}$ mice (Figures 2F, 2G, and S2D). Importantly, the postnatal alveolarization process (Hogan et al., 2014) was not affected by the absence of IL-33 (Figure S2H).

Collectively, these data indicate a critical role for IL-33 in shaping the immune cell infiltrate in the neonatal lung by promoting the appearance of ILC2s and eosinophils. This early period, in which the lung immunological environment is being established, may have subsequent effects on adult lung homeostasis and host defense.

AM Development in Neonatal Lungs Coincides with ILC2 Activation

We next examined the activation state of postnatally expanded ILC2s in lungs using *Il13* tdTomato ($Il13^{Tom/+}$) reporter mice (Barlow et al., 2012). IL-13-expressing ILC2s began to expand at P3, peaked at 70% on P10, and started to decline by P14 (Figures 3A, 3B, and S3A–S3C). Perinatal IL-13 expression was restricted to Lin$^-$ cells (Figure S3D) and depended on the presence of IL-33 (Figure S3E). The expansion of activated ILC2s coincided with the emergence of AMs (Figures 3C, 3D, and S3F).

Considering the critical role of IL-13 in driving the alternative activation of macrophages, we tested to what degree this postnatal wave of ILC2-derived IL-13 might contribute to the immediate polarization of newly differentiated AMs (Gordon and Martinez, 2010). We discovered reduced expression levels of the M2 markers *Ym1*, *Arg1*, and *Fizz1* in $Il13^{-/-}$ and $Il1rl1^{-/-}$ AMs (Figures 3E and S3G). Further, we found elevated spontaneous expression levels of *Cxcl1* and *Tnf* in $Il13^{-/-}$ as compared to WT AMs on P7 (Figures 3E and 3F). Remarkably, the amount of CXCL1 released by WT AMs declined with age, whereas

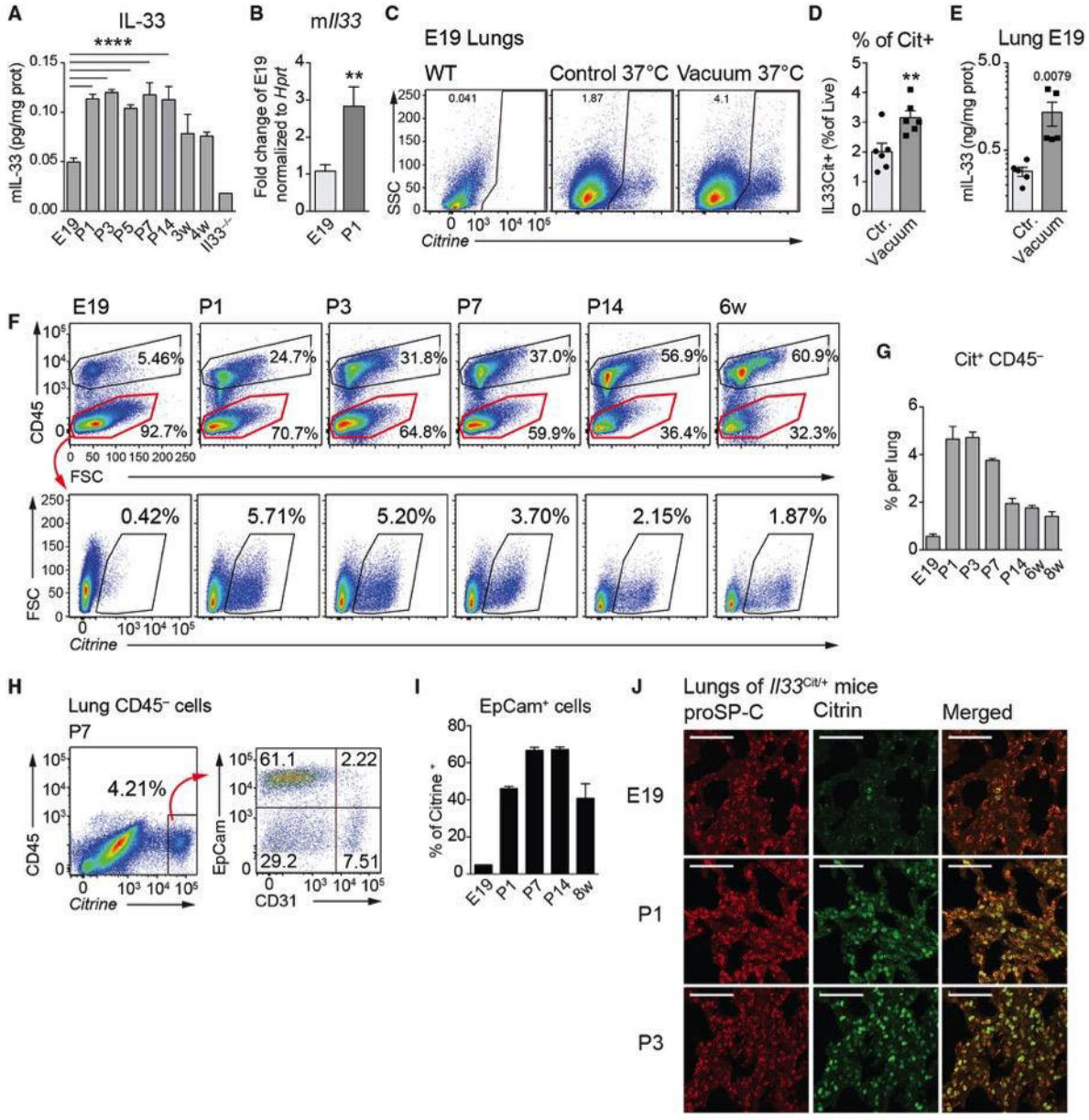

Figure 1. Type 2 Alveolar Epithelial Cells Induce IL-33 at Birth

(A) Whole-lung IL-33 quantification by ELISA at E19; postnatal days 1, 3, 5, 7, and 14 (P1–P14); and 3 and 4 weeks (3–4w) after birth.

(B) qRT-PCR of pulmonary *Il33* expression in WT mice at E19 and P1.

(C) FACS analysis of viable citrine$^+$ cells from *Il33*$^{Cit/+}$ mice at E19 exposed to vacuum or atmospheric pressure (control) for 6 hr.

(D) Quantification of (C).

(E) Whole-lung IL-33 quantification by ELISA of WT lungs at E19 exposed to vacuum or atmospheric pressure (control) for 6 hr.

(F) FACS analysis of lung CD45 and citrine expression in *Il33*$^{Cit/+}$ reporter mice at the indicated time points (gates are set using WT as controls).

(G) Percentage of Cit$^+$CD45$^-$ cells among lung cells, gated as in (F).

(H) Flow cytometry of viable CD45$^-$ lung cells from *Il33*$^{Cit/+}$ mice at P7, stained for EpCam and CD31.

(I) Quantification of the *Cit*$^+$ proportion of EpCAM$^+$ cells between E19 and 8 weeks of age.

(J) Micrographs of lung sections at E19, P1, and P3 from *Il33*$^{Cit/+}$ reporter mice. Red, surfactant protein C (SP-C); green, IL-33-driven citrine. Scale bars represent 75 μm.

Data are representative of two independent experiments with three to five mice per time point, and graph bars represent mean ± SEM. $^{**}p < 0.01$ and $^{****}p < 0.0001$.

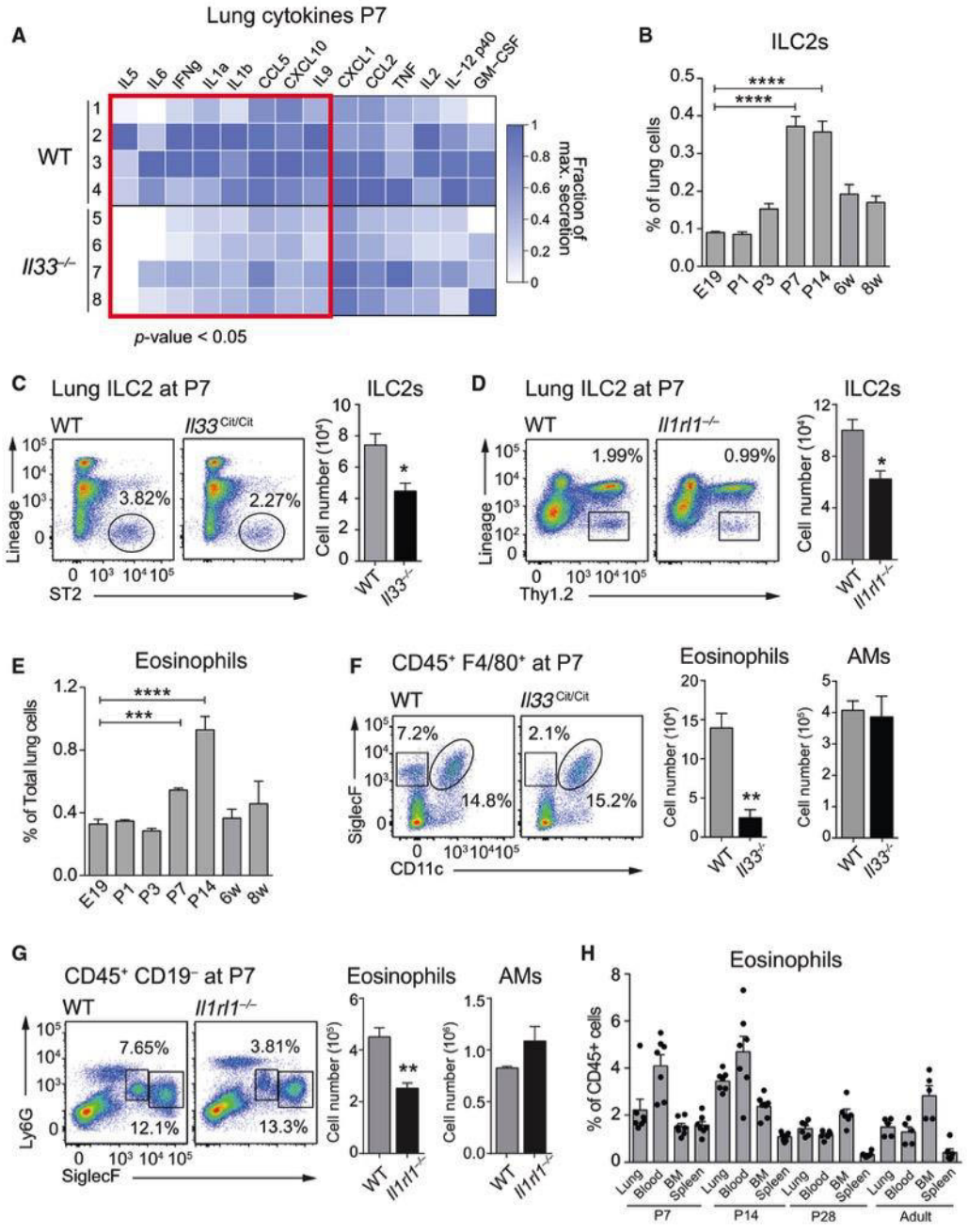

Figure 2. IL-33 Drives a Type 2 Immune Environment in Lungs of Newborns

(A) Heatmap representation of cytokine levels in whole lung homogenates comparing WT and *Il33*$^{Cit/Cit}$ mice at P7. Original values (see Figure S2A) were rescaled between zero and the maximum value detected for each cytokine and are presented as the fraction of maximum secretion.

(B) Percentage of lung ILC2s (Lin$^-$ ST2$^+$ Thy1.2$^+$ CD25$^+$ ICOS$^+$) analyzed by FACS at the indicated time points.

(C) FACS analysis of lung ILC2s (Lin$^-$ ST2$^+$) in WT and *Il33*$^{Cit/Cit}$ mice at P7, further gated for CD25$^+$ and ICOS$^+$ and quantified (right).

(D) FACS analysis of lung ILC2s (Lin$^-$ Thy1.2$^+$) in WT and *Il1rl1*$^{-/-}$ mice at P7, further gated for CD25$^+$ and ICOS$^+$ and quantified (right).

(E) Percentage of lung eosinophils (F4/80$^+$ CD11b$^+$SiglecF$^+$CD11c$^-$) analyzed by FACS at the indicated time points.

(F and G) FACS analysis of lung eosinophils (CD11b$^+$SiglecF$^+$CD11c$^-$) and AMs (CD11b$^-$SiglecF$^+$CD11c$^+$) at P7 in WT and *Il33*$^{Cit/Cit}$ mice (F) and WT and *Il1rl1*$^{-/-}$ mice (G).

(legend continued on next page)

AMs from *Il13*$^{-/-}$ mice continued to produce high levels of CXCL1 until P21 (Figure 3G). These data demonstrate that postnatal AMs exhibit an M1 phenotype and that IL-13 promotes the deactivation and M2 polarization of AMs over time.

IL-13 Maintains Adult Resident AMs in an M2 State

AMs are long-lived cells with local self-renewal capacity, which are, like other macrophages, strongly influenced by the environment they inhabit (Guilliams et al., 2013; Lavin et al., 2014; Murphy et al., 2008). We reasoned that the need for an unremittingly quiescent lung environment throughout life would favor an M2 AM phenotype and discovered that pulmonary IL-13 continued to affect the M2 polarization of AMs in adult mice (Figure 4A). Adult *Il13*$^{-/-}$ AMs stimulated with the respiratory pathogen *S. pneumoniae* or the TLR2 ligand lipoteichoic acid (LTA) consistently induced higher levels of CXCL1 than WT AMs (Figures 4B, 4C, and S4A). WT monocytes adoptively transferred to the lungs of WT or *Il13*$^{-/-}$ mice differentiated toward a SiglecF^{+} AM phenotype within 2 weeks (Figure S4B) and upregulated M2 markers in WT, but not *Il13*$^{-/-}$, recipient animals (Figures 4D and S4C). These results confirm that a tissue-derived source of IL-13 is required to polarize and maintain AMs in an M2 state in adult mice. Of note, IL-33 itself was not sufficient to shape the polarization and activity of AMs from adult mice, as *Il1rl*$^{-/-}$ AMs did not differ from WT AMs in their expression of M2 markers or response to *S. pneumoniae* (Figures S4D–S4F). In summary, endogenous IL-13 contributes to the M2 phenotype of resident and monocyte-derived AMs in healthy adult mice and is required to suppress potentially excessive inflammation.

Pulmonary IL-13 Is Detrimental upon Pneumococcal Infection

We hypothesized that the IL-13-driven M2 polarization of AMs might impact on innate defenses against *S. pneumoniae*. Upon infection of *Il13*$^{-/-}$ and WT mice with *S. pneumoniae*, we observed a more pronounced early (6 hr) influx of neutrophils in bronchoalveolar lavage fluid (BALF) and lung (Figures 4E and 4F) and enhanced amounts of lung CXCL1 (Figure 4G) in *Il13*$^{-/-}$ mice. This augmented early inflammatory response in the absence of *Il13* translated into an improved bacterial clearance from lungs 48 hr post-infection and completely prevented the systemic spread of bacteria (Figures 4H and 4I). In accordance with the reduced bacterial burden, we found decreased CXCL1 levels (Figure 4J), lower numbers of infiltrating monocytes (Figure S5A), and less pronounced lung infiltrates at 48 hr post-infection in *Il13*$^{-/-}$ as compared to WT animals (Figure 4K). To assess the broader relevance of these findings, we investigated the contribution of pulmonary IL-13 to host defense against *Staphylococcus aureus* as well as upon induction of lipopolysaccharide (LPS)-induced acute lung injury. Similar to our observations in pneumococcal pneumonia, we discovered an augmented early inflammatory response to LPS (Figures S5B and S5C) and an improved clearance of *S. aureus* associated with a reduced disease-associated temperature drop in *Il13*$^{-/-}$ animals (Figures S5D and S5E). Together, these results support the notion that pulmonary IL-13 shapes the immune environment in the lung, which upon infection delays the induction of innate defenses against pathogens.

We could not detect any baseline differences in immune cells involved in the defense against bacteria (NK, T, B, or PMN cells and monocytes; Figure S5F; data not shown) or in ILC2 levels (Figure S5G), except for an increased number of eosinophils in *Il13*$^{-/-}$ mice (Figure S5H). To exclude the possibility that eosinophils contributed to the phenotype, we repeated the infection studies in *Il5*$^{-/-}$ mice, which have severely reduced pulmonary eosinophilia (Figure S5I), and could not identify any differences in bacterial counts (Figure S5J) or the inflammatory response elicited by AMs in vitro (Figure S5K).

A short-term in vivo exposure to rmIL-13 was sufficient to "repolarize" resident AMs from IL-13-deficient mice toward an M2 phenotype (Figure 5A) and reduce CXCL1 releases induced by *S. pneumoniae* (Figures 5B and 5C). Finally, the intranasal administration of rmIL-13 to *Il13*$^{-/-}$ mice impaired bacterial clearance in lungs and blood, with bacterial counts being comparable to WT controls (Figures 5D and 5E). In summary, these data demonstrate that the lung immune environment at homeostasis is profoundly shaped by IL-13 at the expense of impaired anti-bacterial defenses.

Resident ILC2s Are the Sole Source of IL-13 in Healthy Adult Lungs

To determine the potential contribution of ILC2s to the AM phenotype, we evaluated the activity of lung ILC2s in adult mice using *Il13*$^{Tom/+}$ reporter mice and intracellular cytokine staining. We found that ~7%–8% of ILC2s in the lungs of naive adult mice (~3 × 10^3 cells) produced IL-13 (Figures 6A–6C). Notably, we excluded Th2 cells, eosinophils, mast cells, macrophages, NK cells, natural killer T (NKT) cells, and invariant natural killer T (iNKT) cells, which have all been shown to produce IL-13 in different lung pathological conditions (Kim et al., 2008; Price et al., 2010; Rijavec et al., 2011) as the source of IL-13 at steady state in healthy adult lungs (Figures 6D and S6A). In fact, ILC2s were the only cells expressing *Il13* in healthy adult lungs at homeostasis (Figure 6D), a finding we confirmed by intracellular staining for IL-13 (Figure S6B).

Constitutive IL-13 production by lung resident ILC2s did not depend on T or B cells in adult mice (Figures S6C–S6G). However, homeostatic IL-13 production depended on ST2 (Figure 6E) and less so on IL-25, another cytokine capable of inducing IL-13 production by ILC2s via IL17rb (Roediger and Weninger, 2015) (Figure S6H). The absolute number of lung ILC2s did not change in the absence of ST2 or IL17rb (Figure S6I). In summary, lung resident ILC2s are a constant and unique source of pulmonary IL-13 in healthy adult lungs at steady state.

To test if IL-13-producing ILC2s alone were sufficient to determine the responsiveness of AMs to *S. pneumoniae*, we

(H) Lung, blood, bone marrow, and spleen cells were analyzed by FACS for eosinophils (CD11b^{+}SiglecF^{+}F480^{+}CD11c^{-}) in P7, P14, P28, and adult (6–8 weeks) *Il5*$^{Cer/+}$ mice.

Data are representative of one (A and H) or two (B–G) independent experiments with four mice per group. Graph bars represent mean ± SEM. *$p < 0.05$, **$p < 0.01$, ***$p < 0.001$, and ****$p < 0.0001$. For flow cytometry, all cells were pre-gated on viable, single, CD45^{+}. E, embryonic; p, postnatal; w, week.

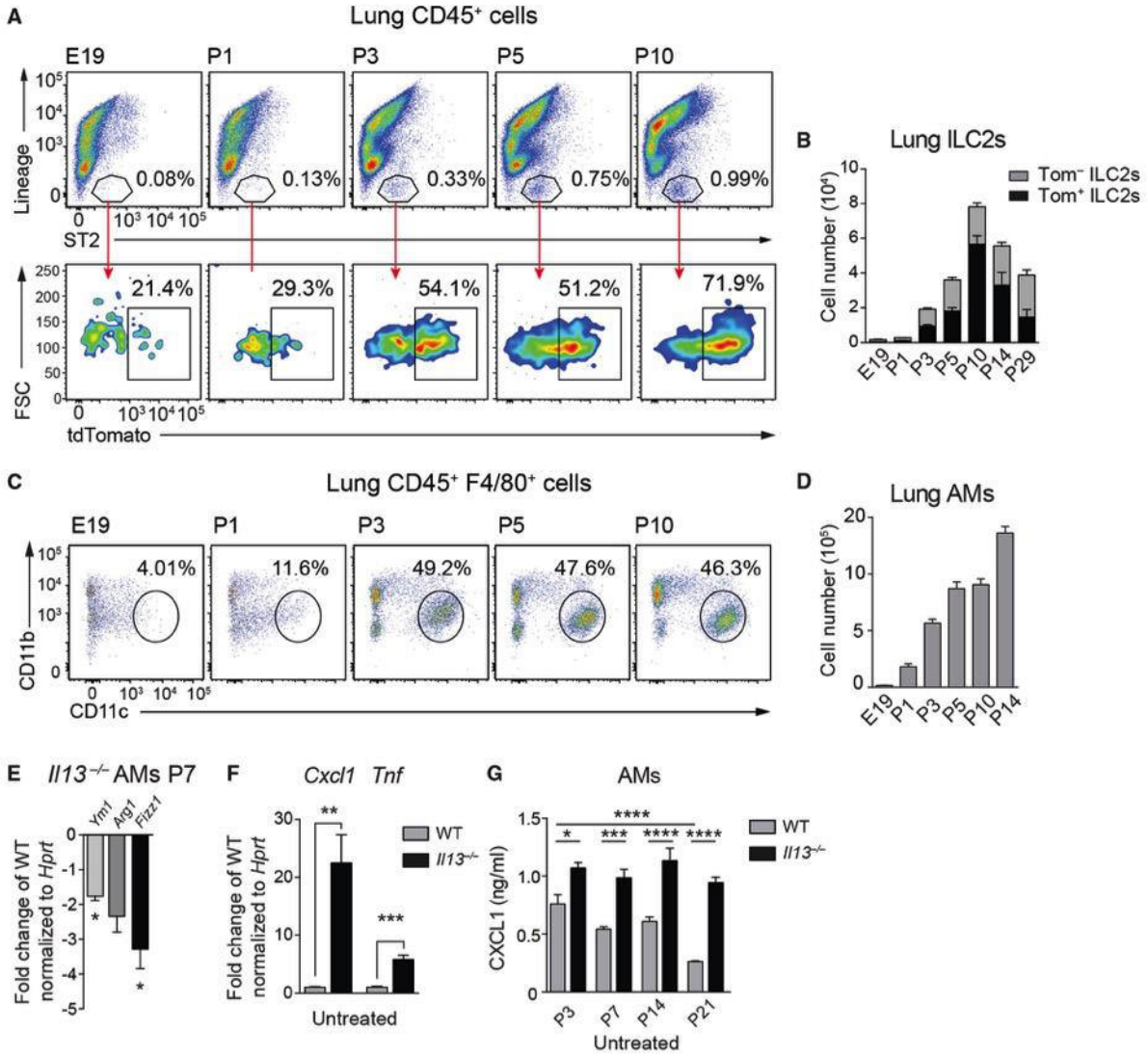

Figure 3. Lung ILC2s Expansion and Activation Coincides with AM Differentiation and M2 Polarization

(A) Representative FACS profiles of expanding lung ILC2s (Lin^- $ST2^+$) (top) and proportion of *Tom*$^+$ cells (bottom) in *Il13*$^{Tom/+}$ mice between E19 and P10.

(B) Quantification of absolute numbers of lung Lin^- $ST2^+$ $Thy1.2^+$ $Tom^{+/-}$ cells at the indicated time points.

(C) FACS plots illustrating percentages of AMs ($F4/80^+CD11b^-CD11c^+$) at the indicated time points.

(D) Absolute numbers of AMs gated as in (C) between E19 and P14.

(E) AMs ($F4/80^+CD11b^-CD11c^+SiglecF^+$) were sorted on P7 from WT and *Il13*$^{Tom/Tom}$ mice and M2 markers were assessed by RT-PCR.

(F) AMs from WT and *Il13*$^{Tom/Tom}$ (IL-13 deficient) mice on P7 were isolated as in (E) and cultured for 6 hr, and *Cxcl1* and *Tnf* gene induction was assessed by RT-PCR. Values were normalized to *Hprt* and are expressed as fold change versus WT.

(G) AMs from WT and *Il13*$^{Tom/Tom}$ (IL-13 deficient) mice on P3, P7, P14, and P21 were isolated as in (E) and cultured for 6 hr, and spontaneous CXCL1 secretion was quantified by ELISA.

Data are representative of three (A–D) or two (E–G) independent experiments with three or four mice per group. Values were normalized to *Hprt* and are expressed as fold change versus the indicated control. Bars represent mean ± SEM; $^*p < 0.05$, $^{**}p < 0.01$, $^{***}p < 0.001$, and $^{****}p < 0.0001$.

adoptively transferred IL-33-expanded lung Tom^+ ILC2s to WT and *Il13*$^{-/-}$ mice (Figure 6F). We observed a significant reduction of *S.-pneumoniae*-induced CXCL1 secretion by AMs isolated from *Il13*$^{-/-}$ recipients that received Tom^+ ILC2s (Figure 6G). Of note, adoptively transferred ILC2s were also able to reduce the responsiveness of WT AM to *S. pneumoniae* in vitro.

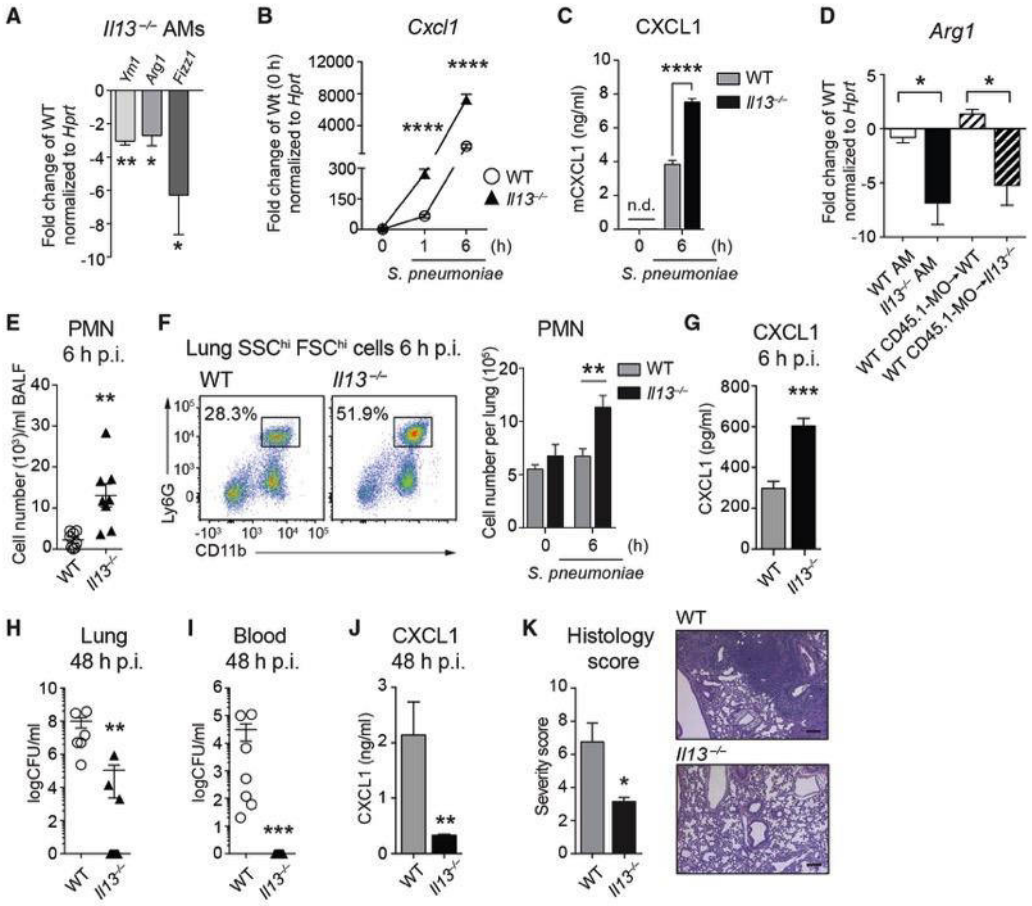

Figure 4. AMs from IL-13-Deficient Mice Present a Pro-inflammatory Phenotype and Improved Defenses against *S. pneumoniae*

(A) AMs from adult WT and *Il13*$^{-/-}$ mice were isolated by bronchoalveolar lavage and analyzed for expression of M2 polarization markers by RT-PCR.

(B and C) AMs isolated as in (A) were in vitro stimulated with *S. pneumoniae* (MOI 100). The induction of *Cxcl1* was quantified by RT-PCR (B), and supernatant protein levels were determined by ELISA (C).

(D) CD45.1 WT monocytes were intra-tracheally transferred to WT and *Il13*$^{-/-}$ CD45.2 recipients, and bronchoalveolar cells were harvested by lavage 2 weeks later. FACS-sorted recipient AMs and monocyte-derived AMs were analyzed for expression of M2 polarization markers by RT-PCR.

(E–G) WT and *Il13*$^{-/-}$ mice were i.n. infected with *S. pneumoniae* and sacrificed after 6 hr. PMN numbers in BALF were assessed on cytospins (E) and in lungs by FACS analysis (CD45^{+}SSC^{hi}FSC^{hi}CD11b^{+} Ly6G^{+}) (F). Lung CXCL1 was quantified by ELISA (G).

(H–K) WT and *Il13*$^{-/-}$ mice were i.n. infected with *S. pneumoniae* and sacrificed after 48 hr. CFU counts in lung homogenates (H) and blood (I). Lung CXCL1 was quantified by ELISA (J). H&E-stained lung sections were scored by a pathologist (see Experimental Procedures) (K, left). Representative H&E lung sections (K, right). Scale bars represent 180 μm.

Data are representative of at least three independent experiments with four (A–C) and seven or eight (E–K) mice per group. Data in (D) are from a single experiment with six mice per group. PCR values were normalized to *Hprt* and expressed as fold change versus indicated control. Mean ± SEM are depicted; $^{*}p < 0.05$, $^{**}p < 0.01$, $^{***}p < 0.001$, and $^{****}p < 0.0001$. BAL, bronchoalveolar lavage; CFU, colony-forming units; p.i., post-infection; PMN, polymorphonuclear cells.

Collectively, these data show that pulmonary ILC2-derived IL-13 maintains lung resident AMs in an M2 state in healthy adult mice.

ILC2s Maintain the M2 Polarization of AMs Early in Development and in Adult Lungs

We then asked if the congenital absence of ILC2s would mirror the phenotype observed in *Il13*$^{-/-}$ mice. AMs extracted from newborn (P7) and adult *Il7r*^{Cre}*Rora*$^{sg/fl}$ mice, congenitally deficient in lung resident ILC2s (Oliphant et al., 2014) (Figure 7A), showed a reduced expression of M2 markers (Figure 7B, 7C and S7A) and increased *Cxcl1* and *Tnf* expression when stimulated with *S. pneumoniae* (Figure 7D). Infection of *Il7r*^{Cre}*Rora*$^{sg/fl}$ mice with *S. pneumoniae* resulted in increased neutrophil influx and higher lung CXCL1 levels 6 hr post-infection (Figures 7E, 7F, and S7B). This translated into an improved bacterial clearance with reduced systemic dissemination of pneumococci (Figures 7G and 7H), lower pulmonary CXCL1 levels (Figure 7I), and less severe lung infiltrates in *Il7r*^{Cre}*Rora*$^{sg/fl}$

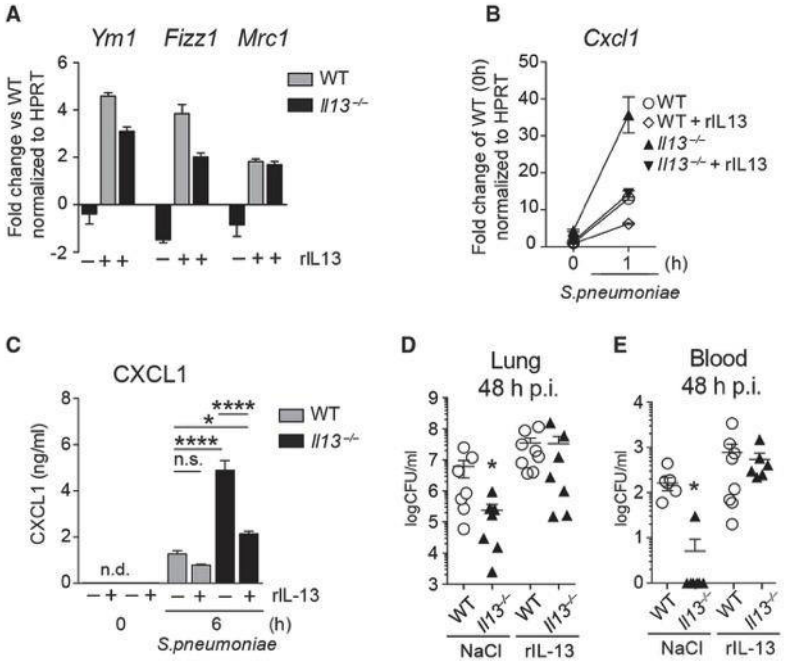

Figure 5. Intranasal rmIL-13 Treatment Reversed the Inflammatory Phenotype of AMs in *Il13*$^{-/-}$ Mice and the Responses to *S. pneumoniae*

(A–C) WT and *Il13*$^{-/-}$ mice were treated daily with rmIL-13 (6 ng in 50 μL NaCl) i.n., and AMs were isolated by bronchoalveolar lavage on day 3. M2 markers were assessed by RT-PCR (A). Cultured AMs were stimulated with *S. pneumoniae* (MOI 100), and fold induction of *Cxcl1* was measured by RT-PCR (B). AMs were treated as in (B), and CXCL1 protein was quantified by ELISA (C).

(D and E) WT and *Il13*$^{-/-}$ mice were treated with rmIL-13 as in (A)–(C), infected i.n. with *S. pneumoniae* on day 3, and sacrificed after 48 hr. CFU counts in lung homogenates (D) and blood (E) are shown.

Data in (A)–(C) are representative of two independent experiments with four mice per group. Data in (D) and (E) are from a single experiment with eight mice per group. Mean ± SEM are depicted; *p < 0.05 and ****p < 0.0001. BALF, bronchoalveolar lavage fluid; CFU, colony forming units; i.n., intranasal; p.i., post-infection.

mice 48 hr after infection (Figure 7J). We concluded that the congenital absence of ILC2s impacted on the M1 versus M2 polarization of AMs in neonatal and adult mice, with implications on the ability to fight bacterial lung infections.

We then asked to which degree ILC2s might contribute environmental signals to shape the functionality of bone-marrow-derived AMs (Lavin et al., 2014) and generated bone marrow chimeras using ILC2-deficient *Rora*$^{sg/sg}$ mice as donors (Wong et al., 2012) (Figures 7K and 7L). AMs isolated from WT/*Rora*$^{sg/sg}$ chimeras expressed lower levels of the M2 markers *Arg1* and *Fizz1* (Figure 7M) and higher levels of *Cxcl1* and *Tnf* in response to *S. pneumoniae* (Figure 7N). In vivo, WT/*Rora*$^{sg/sg}$ chimeras exhibited an augmented early inflammatory response upon pneumococcal infection (Figures 7O, 7P, and S7C). Collectively, lung ILC2s convey important cues that maintain quiescence by shaping the functional state of lung macrophages at homeostasis.

DISCUSSION

With the first breath, lungs are suddenly exposed to the external environment, therefore requiring regulatory forces in place to avoid continuous inflammatory reactions to environmental stimuli. Here, we show a perinatal wave of IL-33-mediated expansion and activation of ILC2s, resulting in an IL-13-driven polarization of newly differentiating AMs to an M2 phenotype. This exerts important homeostatic functions that contribute to a quiescent lung environment shortly after birth and throughout adult life.

AEC2 are the main source of IL-33, as shown earlier (Hardman et al., 2013; Pichery et al., 2012) and further confirmed by a recent study of developing AEC2 in embryonic lungs (Treutlein et al., 2014). Even though the mode of homeostatic IL-33 release remains to be elucidated, the mechanical stress induced by physiological ventilation possibly contributes to pulmonary IL-33 (Martin and Martin, 2016), and we discovered that exposing E19 lungs to negative pressure was sufficient to induce IL-33. Moreover, the release of bioactive IL-33 from living cells upon encounter of environmental allergens, extracellular ATP, or mechanical stress has been reported (Chen et al., 2015; Kakkar et al., 2012; Kouzaki et al., 2011; Sanada et al., 2007).

IL-33 and ILC2s are increasingly recognized as fundamental regulators of tissue homeostasis (Molofsky et al., 2015; von Moltke and Locksley, 2014). As such, recent reports described an IL-33-driven, ILC2-dependent mechanism for adipose tissue homeostasis, which involves the presence of eosinophils and M2 macrophages (Lee et al., 2015; Qiu et al., 2014). Excitingly, perinatal IL-33 induction was recently found to license adipocytes for uncoupled respiration and thermoregulation after birth (Odegaard et al., 2016).

The IL-33- and ILC2-dependent physiological type 2 milieu that we describe might play a role in the reportedly exaggerated airway hyperreactivity upon house dust mite exposure in newborns and strengthens the concept of a "window of immune development" (Gollwitzer et al., 2014). In fact, while this article was under revision, a report demonstrated a casual link between perinatal IL-33 induction and asthma (de Kleer et al., 2016). Here, we propose a unique and homeostatic role for ILC2s in shaping the lung immune environment in early life, as the appearance of activated ILC2s around P3 gradually de-activated AMs.

While type 2 responses, as seen upon helminth infections, are known to impair defenses against mycobacteria (Monin et al., 2015; Salgame et al., 2013), we now report that even homeostatic type 2 conditions impact on lung immunity, illustrated by

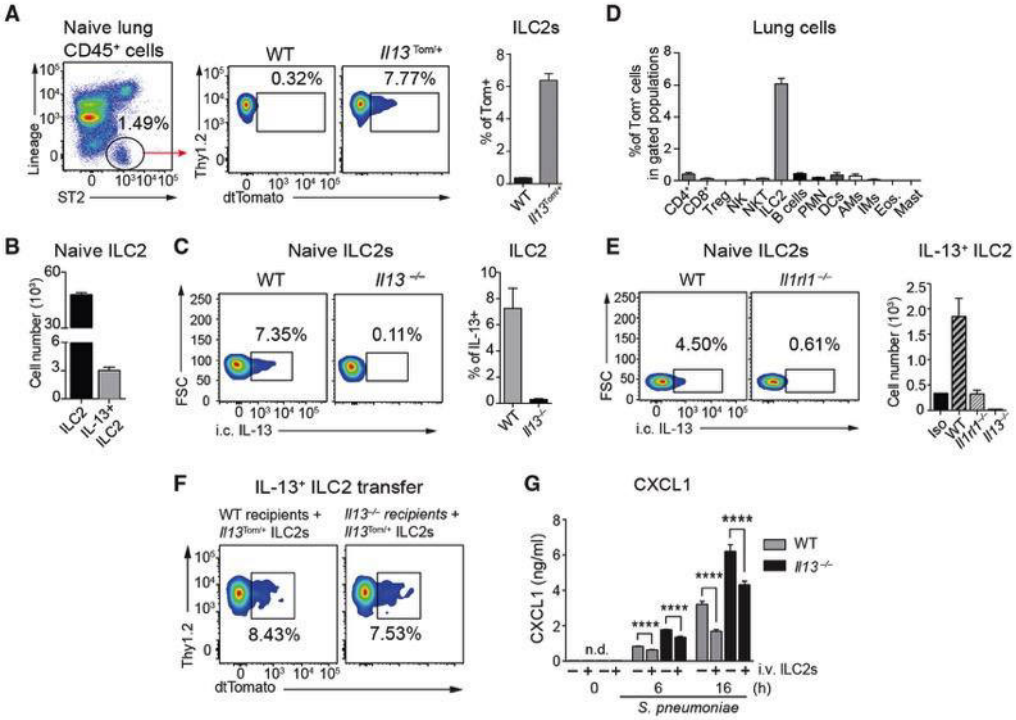

Figure 6. ILC2 Are the Only Cells Producing IL-13 in the Lung at Homeostasis

(A) IL-13 expression in ILC2s (Lin$^-$ ST2$^+$ ICOS$^+$ Thy1.2$^+$ CD25$^+$) assessed by flow cytometry in adult, naive *Il13*$^{Tom/+}$ mice. Representative plots and percentage of tdTomato$^+$ ILC2s are shown.

(B and C) ILC2s and IL-13$^+$ ILC2s were quantified by flow cytometry and intracellular staining for IL-13 in naive WT lungs. (B) Absolute numbers of total lung ILC2s (Lin$^-$ ST2$^+$ ICOS$^+$ Thy1.2$^+$ CD25$^+$) and IL-13$^+$ ILC2s. (C) Representative plots of IL-13$^+$ ILC2s gated as in (A) and percentage of IL-13-producing ILC2s (right).

(D) Lung cell populations were tested by FACS for IL-13 expression in healthy adult *Il13*$^{Tom/+}$ mice. Gating strategies are shown in Table S2.

(E) IL-13 production by lung ILC2s in WT, *Il1rl1*$^{-/-}$, and *Il13*$^{-/-}$ assessed by intracellular staining using flow cytometry (Iso, isotype control); representative plots and absolute numbers are depicted.

(F and G) ILC2s were first expanded in lungs of *Il13*$^{Tom/+}$ mice via i.n. administration of rmIL-33 (0.5 μg/50 μL for 5 days), and then sorted Tom$^+$ ILC2s were transferred intravenous to WT and *Il13*$^{-/-}$ mice. (F) Representative FACS plots showing the homing of *Il13*$^{Tom/+}$ ILC2s in lungs 5 days after adoptive transfer. (G) AMs were isolated by bronchoalveolar lavage from WT and *Il13*$^{-/-}$ recipients 5 days after adoptive transfer and in vitro stimulated with *S. pneumoniae* (MOI 100), and CXCL1 release was assessed by ELISA in supernatants.

Data are representative of three (A–C), two (E–G), and one (D) independent experiments with four mice per group. Mean ± SEM are depicted; ****$p < 0.0001$. BAL, bronchoalveolar lavage; i.c., intracellular; i.v., intravenous; FSC, forward scatter.

reduced lung inflammation upon LPS challenge and a delayed clearance of medically important lung pathogens such as *S. pneumoniae*.

Our experiments in mice congenitally deficient in ILC2s corroborated the concept that ILC2s affected the AM phenotype from birth until adult life. Analysis of bone marrow chimeras using *Rora*$^{sg/sg}$ mice further demonstrated that pulmonary ILC2s provided essential, tissue-specific signals to even polarize bone marrow precursors that arrive in lungs. Supporting our notion that ILC2s contribute to the in vivo phenotype of AMs, a recent publication identified tissue-specific transcriptional signatures of resident macrophages, and found AMs to be characterized by two IL-13- and IL-5-inducible genes, namely *Ym1* (*Chi3l3*) and *Car4*, respectively (Lavin et al., 2014).

In conclusion, we show that IL-33-driven ILC2 activation dominates the lung milieu early after birth by inducing a type-2 immune environment. Lung resident ILC2s are major contributors to the phenotype and function of tissue resident AMs at homeostasis, favoring a quiescent immune environment. While this effect might prove beneficial at steady state and upon sterile lung injury, it comes at the expense of a delayed response to the common lung pathogen *S. pneumoniae*.

EXPERIMENTAL PROCEDURES

Mice

Il13$^{-/-}$ (McKenzie et al., 1998), *Il13*$^{tdTomato/+}$ (Barlow et al., 2012) (referred as *Il13*$^{Tom/+}$), *Il1rl1*$^{-/-}$ (Townsend et al., 2000), *Il5*$^{-/-}$ (Kopf et al., 1996), *Rag2*$^{-/-}$ (Shinkai et al., 1992), *Il7r*^{Cre} (Schlenner et al., 2010), *Rora*$^{+/fl}$ (Oliphant et al., 2014), and Staggerer *Rora*$^{sg/+}$ mice (Jackson Laboratories) were on a C57BL/6 background. We obtained *Il7r*^{Cre}*Rora*$^{sg/fl}$ mice (experimental) or *Il7r*^{Cre}*Rora*$^{+/fl}$ littermate controls by crossing *Il7r*^{Cre} with *Rora*$^{+/fl}$ and *Rora*$^{sg/+}$. *Il33*$^{Cit/+}$ (Hardman et al., 2013) mice and *Il5*$^{Cerl/+}$ mice (Saunders et al., 2016)

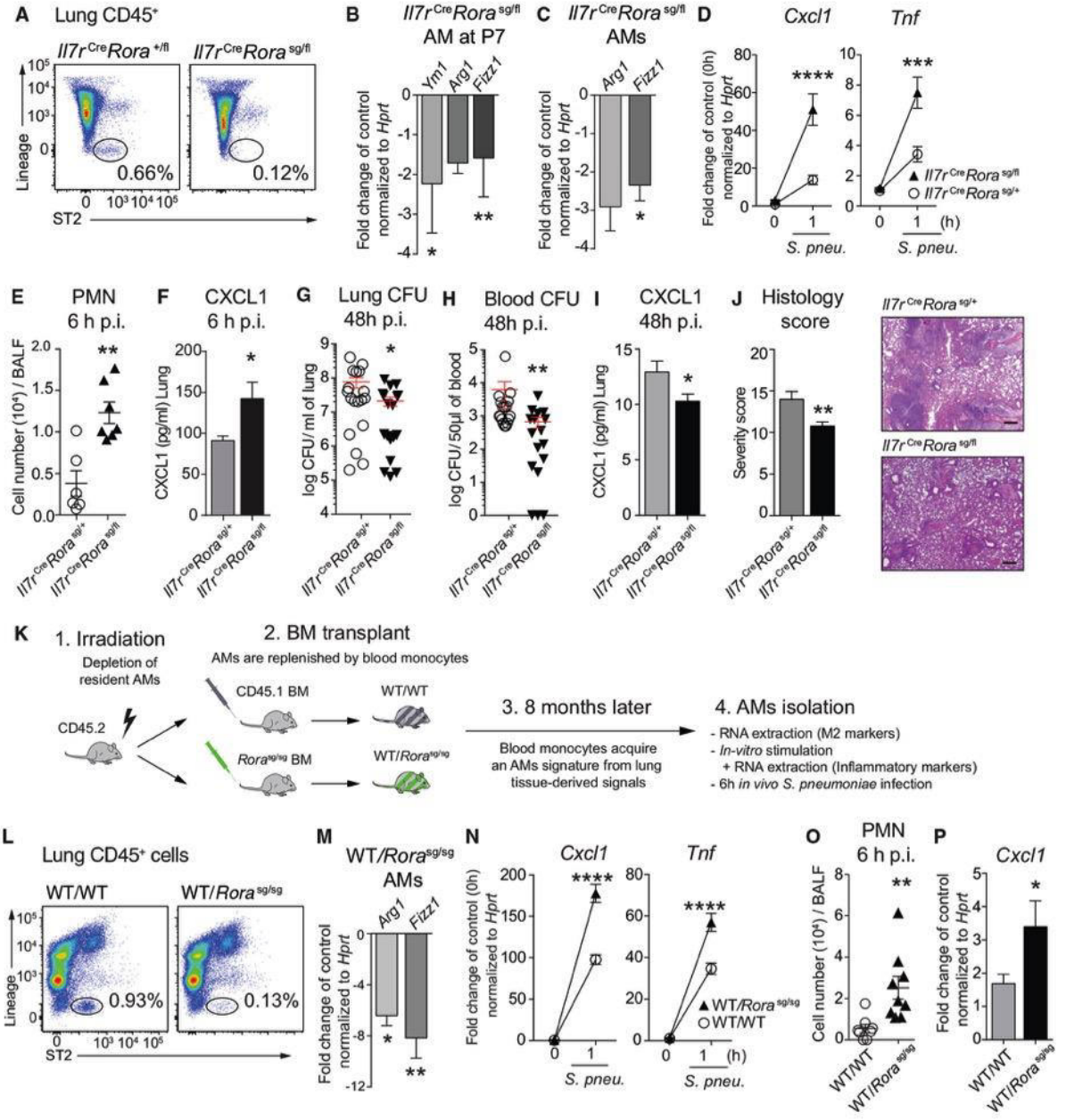

Figure 7. Lung Resident ILC2s Polarize Tissue Resident AMs toward an M2 Phenotype and Dampen Early Inflammatory Responses against Bacteria

(A) Flow cytometry plots of ILC2s in naive *Il7r*^{Cre}*Rora*$^{sg/fl}$ mice and *Il7r*^{Cre}*Rora*$^{+/fl}$ controls.

(B) AMs isolated by flow cytometry from healthy *Il7r*^{Cre}*Rora*$^{sg/fl}$ mice and controls at P7 and M2 markers evaluated by RT-PCR.

(C and D) AMs isolated by bronchoalveolar lavage from healthy adult *Il7r*^{Cre}*Rora*$^{sg/fl}$ mice and controls. (C) M2 markers evaluated by RT-PCR. (D) Primary AMs stimulated for 1 hr with *S. pneumoniae* (MOI 100) to assess the induction of *Cxcl1* and *Tnf*.

(E–J) *Il7r*^{Cre}*Rora*$^{sg/fl}$ mice and controls were i.n. infected with *S. pneumoniae* (10^5 CFUs) and sacrificed after 6 hr (E and F) or 48 hr (G–J). (E) PMN influx on BALF cytospins. (F) CXCL1 induction in whole-lung homogenate. (G and H) CFUs in lung (G) and in blood (H). (I) CXCL1 induction in whole-lung homogenate. (J) H&E-stained lung sections were scored by a pathologist (see Experimental Procedures) (J, left). Representative H&E lung sections (J, right). Scale bars represent 180 µm.

(legend continued on next page)

were on a BALB/c background. Mice were bred in a specific pathogen-free (SPF) facility and all mice were matched for age, gender and background in individual experiments. All animal experiments were approved by the Austrian Federal Ministry of Sciences and Research (BMWFW-66.009/0122-II/3b/2013) and the UK Home Office.

Isolation, Culture, and Stimulation of AMs

AMs from newborn mice were isolated by cell sorting using an FACSAria II (BD Biosciences) by gating on viable CD45$^+$F4/80$^+$CD11b^{low}CD11c$^+$ SiglecF$^+$ Ly6C$^-$ cells. In adult mice, AMs were isolated by bronchoalveolar lavage followed by cell adhesion. Purity of isolated AM with both methods was consistently >95%. AMs were stimulated in RPMI containing 3% fetal calf serum (FCS) with heat-inactivated *S. pneumoniae* at a MOI 100 or *S. aureus* LTA (10 μg/mL). In Figures 3E–3G, 4A–4D, 5A–5C, 7B–7D and 7M, and 7N, cells were pooled from three or four mice per group and analyzed in technical quadruplicates.

Cytokine Administration

Recombinant mouse IL-13 and IL-33 were purchased from BioLegend. Anesthetized mice were treated daily with rmIL-13 (6 ng/50 μL NaCl for 3 consecutive days) or rmIL-33 (0.5 μg/50 μL NaCl for 5 consecutive days). Mice were sacrificed 1 hr after the last administration.

Adoptive Transfer of ILC2s

Lung ILC2s were FACS purified as defined by lineage$^-$ (CD3a, CD4, CD8a, CD19, CD11c, CD11b, Gr1, FcεR1, CD49b), Thy1.2$^+$ ST2$^+$ ICOS$^+$ and Tom$^+$ from *Il13*$^{Tom/+}$ mice that had been treated intranasally (i.n.) with rmIL-33 for 5 days. Cells were transferred intravenously to *Il13*$^{-/-}$ or WT mice recipients (1×10^5 cells per mouse) and assessed for localization in lungs 5 days later.

Generation of Bone Marrow Chimeras

6-week-old CD45.2 *Rora*$^{sg/sg}$ or WT littermates served as bone marrow donors. CD45.1 recipients were irradiated (9 Gy) and reconstituted on the same day with 2×10^6 bone marrow cells per recipient by intravenous injection. Mice were analyzed for reconstitution and absence of lung resident ILC2s after 8 months.

Murine Pneumonia Model

Mice were infected i.n. with 10^5 CFUs *S. pneumoniae* serotype 3 (ATCC 6303) as described (Sharif et al., 2014; Warszawska et al., 2013), or with 5×10^7 CFUs *S. aureus* (USA300). Acute lung injury was induced by administration of 100 ng LPS i.n. (*E. coli* O55:B5). BALF was collected, cells were counted with an automated cell counter (Z2 Coulter Counter, Beckman), and Giemsa-stained cytospin preparations were used for differential cell counts. Lung tissues were homogenized in sterile saline using a Precellys 24TM (Peqlab), and lung colony-forming units (CFUs) were determined by 10-fold serial dilutions of homogenates on blood agar plates. An aliquot of lung homogenates was incubated in RA1 buffer (Macherey-Nagel) containing 10% of beta-mercaptoethanol (Calbiochem) and stored at −80° for RNA extraction. The remaining lung homogenates were incubated in Greenberger lysis buffer as described previously (Sharif et al., 2014), and supernatants were stored at −20°C until cytokines were assayed.

Pneumonia Severity Score

Paraffin-embedded lung sections were stained with H&E and scored by a trained pathologist who was blinded to experimental groups. The final pneumonia score was the sum of the following parameters: severity of pleuritis, interstitial inflammation, edema, and thrombi formation were scored as 0 = absent, 1 = mild, 2 = moderately severe, 3 = severe; bronchitis was scored as 1 if present; endotheliitis was scored as 0 = absent, 2 = present, 3 = present with endothelial wall necrosis; the existence of a lobar confluent infiltrate was scored as 1, and a score of 0.5 was added for every infiltrate covering 10% of the lung area.

Statistical Analysis

Data are expressed as mean ± SEM. Statistical significance in two-group comparisons was assessed with an unpaired Student's t test. When indicated, a Mann-Whitney *U* test was used for analysis of nonparametric data. For multivariable comparisons we performed a one-way ANOVA followed by Sidak's multiple comparison test. Results were analyzed with Graph Pad Prism software version 6, and a $p < 0.05$ was regarded as statistically significant.

SUPPLEMENTAL INFORMATION

Supplemental Information includes Supplemental Experimental Procedures, seven figures, and three tables and can be found with this article online at http://dx.doi.org/10.1016/j.celrep.2017.01.071.

AUTHOR CONTRIBUTIONS

S. Saluzzo and S.K. conceived the study. A.N.J.M. hosted S. Saluzzo, contributed to experimental design, and provided critical reagents. S. Saluzzo, A.-D.G., B.M.J.R., R.M., S. Scanlon, P.S., K.L., A.H., O.S., A.K., J.M.W., and H.J. performed the experiments or contributed to experimental design, reagents, and analysis. I.M. scored histological slides. S. Scanlon performed the immunofluorescence experiments. R.M. analyzed the newborns alveolarization. A.-D.G. and B.M.J.R. contributed equally to this work. S. Saluzzo and S.K. wrote the manuscript with contributions from A.N.J.M., B.M.J.R., O.S., and S. Scanlon. A.N.J.M and S.K. are joint senior authors.

ACKNOWLEDGMENTS

We thank Hans-Reimer Rodewald for providing us with *Il7Rα*^{Cre} mice. We thank the staff of the animal facility of the Medical University of Vienna (AT) and of the Ares facility in Cambridge (UK) for their technical assistance. We thank Timotheus Y.F. Halim for precious advice. This work was supported by the Austrian Science Funds (FWF) within the doctoral program Cell Communication in Health and Disease (W1205) and within the ERA-Infect framework (I1620) (to S.K.), the Vienna Science and Technology Fund (WWTF and LS11-008) (to S.K.), and grants from the MRC (U105178805) and Wellcome Trust (100963/Z/13/Z) (to A.N.J.M.).

Received: June 3, 2016
Revised: December 27, 2016
Accepted: January 26, 2017
Published: February 21, 2017

REFERENCES

Barlow, J.L., Bellosi, A., Hardman, C.S., Drynan, L.F., Wong, S.H., Cruickshank, J.P., and McKenzie, A.N.J. (2012). Innate IL-13-producing nuocytes arise during allergic lung inflammation and contribute to airways hyperreactivity. J. Allergy Clin. Immunol. *129*, 191–198.e4.

(K–N) CD45.2 recipients were lethally irradiated and transplanted with WT or *Rora*$^{sg/sg}$ bone marrow and sacrificed 8 months later. (K) Experimental setup. (L) Representative FACS plots of ILC2s in healthy WT/WT and WT/*Rora*$^{sg/sg}$ bone marrow chimeras. (M) AMs isolated via bronchoalveolar lavage and assessed for M2 markers by RT-PCR or (N) stimulated with *S. pneumoniae* (MOI 100) to evaluate *Cxcl1* and *Tnf* induction.
(O and P) WT/WT and WT/*Rora*$^{sg/sg}$ chimeras were infected with 10^5 CFUs *S. pneumoniae* and sacrificed after 6 hr to assess (O) PMN influx and (P) *Cxcl1* induction in lung tissue.
Data are representative of at least two independent experiments with four (A–D, M, and N) and seven or eight (E–J, O, and P) mice per group. Data in (G) and (H) are pooled from two independent experiments. Mean ± SEM are depicted; *$p \leq 0.05$, **$p < 0.01$, ***$p < 0.001$, and ****$p < 0.0001$. BALF, bronchoalveolar lavage fluid; CFU, colony-forming units; p.i., post-infection; PMN, polymorphonuclear cells.

Beers, M.F., and Morrisey, E.E. (2011). The three R's of lung health and disease: repair, remodeling, and regeneration. J. Clin. Invest. *121*, 2065–2073.

Brestoff, J.R., Kim, B.S., Saenz, S.A., Stine, R.R., Monticelli, L.A., Sonnenberg, G.F., Thome, J.J., Farber, D.L., Lutfy, K., Seale, P., and Artis, D. (2015). Group 2 innate lymphoid cells promote beiging of white adipose tissue and limit obesity. Nature *519*, 242–246.

Chang, Y.-J., Kim, H.Y., Albacker, L.A., Baumgarth, N., McKenzie, A.N., Smith, D.E., Dekruyff, R.H., and Umetsu, D.T. (2011). Innate lymphoid cells mediate influenza-induced airway hyper-reactivity independently of adaptive immunity. Nat. Immunol. *12*, 631–638.

Chen, W.H., Toapanta, F.R., Shirey, K.A., Zhang, L., Giannelou, A., Page, C., Frieman, M.B., Vogel, S.N., and Cross, A.S. (2012). Potential role for alternatively activated macrophages in the secondary bacterial infection during recovery from influenza. Immunol. Lett. *141*, 227–234.

Chen, W.-Y., Hong, J., Gannon, J., Kakkar, R., and Lee, R.T. (2015). Myocardial pressure overload induces systemic inflammation through endothelial cell IL-33. Proc. Natl. Acad. Sci. USA *112*, 7249–7254.

Chien, Y.-W., Klugman, K.P., and Morens, D.M. (2009). Bacterial pathogens and death during the 1918 influenza pandemic. N. Engl. J. Med. *361*, 2582–2583.

Chiu, C., and Openshaw, P.J. (2015). Antiviral B cell and T cell immunity in the lungs. Nat. Immunol. *16*, 18–26.

De Filippo, K., Dudeck, A., Hasenberg, M., Nye, E., van Rooijen, N., Hartmann, K., Gunzer, M., Roers, A., and Hogg, N. (2013). Mast cell and macrophage chemokines CXCL1/CXCL2 control the early stage of neutrophil recruitment during tissue inflammation. Blood *121*, 4930–4937.

de Kleer, I.M., Kool, M., de Bruijn, M.J.W., Willart, M., van Moorleghem, J., Schuijs, M.J., Plantinga, M., Beyaert, R., Hams, E., Fallon, P.G., et al. (2016). Perinatal activation of the interleukin-33 pathway promotes type 2 immunity in the developing lung. Immunity *45*, 1285–1298.

Gollwitzer, E.S., Saglani, S., Trompette, A., Yadava, K., Sherburn, R., McCoy, K.D., Nicod, L.P., Lloyd, C.M., and Marsland, B.J. (2014). Lung microbiota promotes tolerance to allergens in neonates via PD-L1. Nat. Med. *20*, 642–647.

Gordon, S., and Martinez, F.O. (2010). Alternative activation of macrophages: mechanism and functions. Immunity *32*, 593–604.

Guery, L., Benikhlef, N., Gautier, T., Paul, C., Jego, G., Dufour, E., Jacquel, A., Cally, R., Manoury, B., Vanden Berghe, T., et al. (2011). Fine-tuning nucleophosmin in macrophage differentiation and activation. Blood *118*, 4694–4704.

Guilliams, M., De Kleer, I., Henri, S., Post, S., Vanhoutte, L., De Prijck, S., Deswarte, K., Malissen, B., Hammad, H., and Lambrecht, B.N. (2013). Alveolar macrophages develop from fetal monocytes that differentiate into long-lived cells in the first week of life via GM-CSF. J. Exp. Med. *210*, 1977–1992.

Halim, T.Y.F., Steer, C.A., Mathä, L., Gold, M.J., Martinez-Gonzalez, I., McNagny, K.M., McKenzie, A.N.J., and Takei, F. (2014). Group 2 innate lymphoid cells are critical for the initiation of adaptive T helper 2 cell-mediated allergic lung inflammation. Immunity *40*, 425–435.

Hardman, C.S., Panova, V., and McKenzie, A.N.J. (2013). IL-33 citrine reporter mice reveal the temporal and spatial expression of IL-33 during allergic lung inflammation. Eur. J. Immunol. *43*, 488–498.

Hogan, B.L.M., Barkauskas, C.E., Chapman, H.A., Epstein, J.A., Jain, R., Hsia, C.C.W., Niklason, L., Calle, E., Le, A., Randell, S.H., et al. (2014). Repair and regeneration of the respiratory system: complexity, plasticity, and mechanisms of lung stem cell function. Cell Stem Cell *15*, 123–138.

Hussell, T., and Bell, T.J. (2014). Alveolar macrophages: plasticity in a tissue-specific context. Nat. Rev. Immunol. *14*, 81–93.

Kakkar, R., Hei, H., Dobner, S., and Lee, R.T. (2012). Interleukin 33 as a mechanically responsive cytokine secreted by living cells. J. Biol. Chem. *287*, 6941–6948.

Kearley, J., Silver, J.S., Sanden, C., Liu, Z., Berlin, A.A., White, N., Mori, M., Pham, T.-H., Ward, C.K., Criner, G.J., et al. (2015). Cigarette smoke silences innate lymphoid cell function and facilitates an exacerbated type I interleukin-33-dependent response to infection. Immunity *42*, 566–579.

Kim, E.Y., Battaile, J.T., Patel, A.C., You, Y., Agapov, E., Grayson, M.H., Benoit, L.A., Byers, D.E., Alevy, Y., Tucker, J., et al. (2008). Persistent activation of an innate immune response translates respiratory viral infection into chronic lung disease. Nat. Med. *14*, 633–640.

Kim, H.Y., Chang, Y.J., Subramanian, S., Lee, H.H., Albacker, L.A., Matangkasombut, P., Savage, P.B., McKenzie, A.N.J., Smith, D.E., Rottman, J.B., et al. (2012). Innate lymphoid cells responding to IL-33 mediate airway hyperreactivity independently of adaptive immunity. J. Allergy Clin. Immunol. *129*, 216–227.e6.

Kopf, M., Brombacher, F., Hodgkin, P.D., Ramsay, A.J., Milbourne, E.A., Dai, W.J., Ovington, K.S., Behm, C.A., Köhler, G., Young, I.G., and Matthaei, K.I. (1996). IL-5-deficient mice have a developmental defect in CD5+ B-1 cells and lack eosinophilia but have normal antibody and cytotoxic T cell responses. Immunity *4*, 15–24.

Kopf, M., Schneider, C., and Nobs, S.P. (2015). The development and function of lung-resident macrophages and dendritic cells. Nat. Immunol. *16*, 36–44.

Kouzaki, H., Iijima, K., Kobayashi, T., O'Grady, S.M., and Kita, H. (2011). The danger signal, extracellular ATP, is a sensor for an airborne allergen and triggers IL-33 release and innate Th2-type responses. J. Immunol. *186*, 4375–4387.

Lambrecht, B.N., and Hammad, H. (2015). The immunology of asthma. Nat. Immunol. *16*, 45–56.

Lamkanfi, M., and Dixit, V.M. (2009). IL-33 raises alarm. Immunity *31*, 5–7.

Lavin, Y., Winter, D., Blecher-Gonen, R., David, E., Keren-Shaul, H., Merad, M., Jung, S., and Amit, I. (2014). Tissue-resident macrophage enhancer landscapes are shaped by the local microenvironment. Cell *159*, 1312–1326.

Lee, M.W., Odegaard, J.I., Mukundan, L., Qiu, Y., Molofsky, A.B., Nussbaum, J.C., Yun, K., Locksley, R.M., and Chawla, A. (2015). Activated type 2 innate lymphoid cells regulate beige fat biogenesis. Cell *160*, 74–87.

Liew, F.Y., Pitman, N.I., and McInnes, I.B. (2010). Disease-associated functions of IL-33: the new kid in the IL-1 family. Nat. Rev. Immunol. *10*, 103–110.

Lu, J., Kang, J., Zhang, C., and Zhang, X. (2015). The role of IL-33/ST2L signals in the immune cells. Immunol. Lett. *164*, 11–17.

Mantovani, A., Sica, A., Sozzani, S., Allavena, P., Vecchi, A., and Locati, M. (2004). The chemokine system in diverse forms of macrophage activation and polarization. Trends Immunol. *25*, 677–686.

Martin, N.T., and Martin, M.U. (2016). Interleukin 33 is a guardian of barriers and a local alarmin. Nat. Immunol. *17*, 122–131.

McKenzie, G.J., Emson, C.L., Bell, S.E., Anderson, S., Fallon, P., Zurawski, G., Murray, R., Grencis, R., and McKenzie, A.N.J. (1998). Impaired development of Th2 cells in IL-13-deficient mice. Immunity *9*, 423–432.

Molofsky, A.B., Nussbaum, J.C., Liang, H.-E., Van Dyken, S.J., Cheng, L.E., Mohapatra, A., Chawla, A., and Locksley, R.M. (2013). Innate lymphoid type 2 cells sustain visceral adipose tissue eosinophils and alternatively activated macrophages. J. Exp. Med. *210*, 535–549.

Molofsky, A.B., Savage, A.K., and Locksley, R.M. (2015). Interleukin-33 in tissue homeostasis, injury, and inflammation. Immunity *42*, 1005–1019.

Monin, L., Griffiths, K.L., Lam, W.Y., Gopal, R., Kang, D.D., Ahmed, M., Rajamanickam, A., Cruz-Lagunas, A., Zúñiga, J., Babu, S., et al. (2015). Helminth-induced arginase-1 exacerbates lung inflammation and disease severity in tuberculosis. J. Clin. Invest. *125*, 4699–4713.

Monticelli, L.A., Sonnenberg, G.F., Abt, M.C., Alenghat, T., Ziegler, C.G., Doering, T.A., Angelosanto, J.M., Laidlaw, B.J., Yang, C.Y., Sathaliyawala, T., et al. (2011). Innate lymphoid cells promote lung-tissue homeostasis after infection with influenza virus. Nat. Immunol. *12*, 1045–1054.

Mund, S.I., Stampanoni, M., and Schittny, J.C. (2008). Developmental alveolarization of the mouse lung. Dev. Dyn. *237*, 2108–2116.

Murphy, J., Summer, R., Wilson, A.A., Kotton, D.N., and Fine, A. (2008). The prolonged life-span of alveolar macrophages. Am. J. Respir. Cell Mol. Biol. *38*, 380–385.

Neill, D.R., Wong, S.H., Bellosi, A., Flynn, R.J., Daly, M., Langford, T.K., Bucks, C., Kane, C.M., Fallon, P.G., Pannell, R., et al. (2010). Nuocytes represent a

new innate effector leukocyte that mediates type-2 immunity. Nature *464*, 1367–1370.

Nussbaum, J.C., Van Dyken, S.J., von Moltke, J., Cheng, L.E., Mohapatra, A., Molofsky, A.B., Thornton, E.E., Krummel, M.F., Chawla, A., Liang, H.-E., and Locksley, R.M. (2013). Type 2 innate lymphoid cells control eosinophil homeostasis. Nature *502*, 245–248.

Odegaard, J.I., Lee, M.-W., Sogawa, Y., Bertholet, A.M., Locksley, R.M., Weinberg, D.E., Kirichok, Y., Deo, R.C., and Chawla, A. (2016). Perinatal licensing of thermogenesis by IL-33 and ST2. Cell *166*, 841–854.

Okabe, Y., and Medzhitov, R. (2014). Tissue-specific signals control reversible program of localization and functional polarization of macrophages. Cell *157*, 832–844.

Oliphant, C.J., Hwang, Y.Y., Walker, J.A., Salimi, M., Wong, S.H., Brewer, J.M., Englezakis, A., Barlow, J.L., Hams, E., Scanlon, S.T., et al. (2014). MHCII-mediated dialog between group 2 innate lymphoid cells and CD4(+) T cells potentiates type 2 immunity and promotes parasitic helminth expulsion. Immunity *41*, 283–295.

Orr, A.W., Helmke, B.P., Blackman, B.R., and Schwartz, M.A. (2006). Mechanisms of mechanotransduction. Dev. Cell *10*, 11–20.

Peng, T., Frank, D.B., Kadzik, R.S., Morley, M.P., Rathi, K.S., Wang, T., Zhou, S., Cheng, L., Lu, M.M., and Morrisey, E.E. (2015). Hedgehog actively maintains adult lung quiescence and regulates repair and regeneration. Nature *526*, 578–582.

Pichery, M., Mirey, E., Mercier, P., Lefrancais, E., Dujardin, A., Ortega, N., and Girard, J.-P. (2012). Endogenous IL-33 is highly expressed in mouse epithelial barrier tissues, lymphoid organs, brain, embryos, and inflamed tissues: in situ analysis using a novel Il-33-LacZ gene trap reporter strain. J. Immunol. *188*, 3488–3495.

Price, A.E., Liang, H.-E., Sullivan, B.M., Reinhardt, R.L., Eisley, C.J., Erle, D.J., and Locksley, R.M. (2010). Systemically dispersed innate IL-13-expressing cells in type 2 immunity. Proc. Natl. Acad. Sci. USA *107*, 11489–11494.

Qiu, Y., Nguyen, K.D., Odegaard, J.I., Cui, X., Tian, X., Locksley, R.M., Palmiter, R.D., and Chawla, A. (2014). Eosinophils and type 2 cytokine signaling in macrophages orchestrate development of functional beige fat. Cell *157*, 1292–1308.

Rijavec, M., Volarevic, S., Osolnik, K., Kosnik, M., and Korosec, P. (2011). Natural killer T cells in pulmonary disorders. Respir. Med. *105* (*Suppl 1*), S20–S25.

Roediger, B., and Weninger, W. (2015). Group 2 innate lymphoid cells in the regulation of immune responses. Adv. Immunol. *125*, 111–154.

Salgame, P., Yap, G.S., and Gause, W.C. (2013). Effect of helminth-induced immunity on infections with microbial pathogens. Nat. Immunol. *14*, 1118–1126.

Sanada, S., Hakuno, D., Higgins, L.J., Schreiter, E.R., McKenzie, A.N.J., and Lee, R.T. (2007). IL-33 and ST2 comprise a critical biomechanically induced and cardioprotective signaling system. J. Clin. Invest. *117*, 1538–1549.

Saunders, S.P., Moran, T., Floudas, A., Wurlod, F., Kaszlikowska, A., Salimi, M., Quinn, E.M., Oliphant, C.J., Núñez, G., McManus, R., et al. (2016). Spontaneous atopic dermatitis is mediated by innate immunity, with the secondary lung inflammation of the atopic march requiring adaptive immunity. J. Allergy Clin. Immunol. *137*, 482–491.

Schlenner, S.M., Madan, V., Busch, K., Tietz, A., Läufle, C., Costa, C., Blum, C., Fehling, H.J., and Rodewald, H.R. (2010). Fate mapping reveals separate origins of T cells and myeloid lineages in the thymus. Immunity *32*, 426–436.

Schliehe, C., Flynn, E.K., Vilagos, B., Richson, U., Swaminathan, S., Bosnjak, B., Bauer, L., Kandasamy, R.K., Griesshammer, I.M., Kosack, L., et al. (2015). The methyltransferase Setdb2 mediates virus-induced susceptibility to bacterial superinfection. Nat. Immunol. *16*, 67–74.

Schmitz, J., Owyang, A., Oldham, E., Song, Y., Murphy, E., McClanahan, T.K., Zurawski, G., Moshrefi, M., Qin, J., Li, X., et al. (2005). IL-33, an interleukin-1-like cytokine that signals via the IL-1 receptor-related protein ST2 and induces T helper type 2-associated cytokines. Immunity *23*, 479–490.

Sharif, O., Gawish, R., Warszawska, J.M., Martins, R., Lakovits, K., Hladik, A., Doninger, B., Brunner, J., Korosec, A., Schwarzenbacher, R.E., et al. (2014). The triggering receptor expressed on myeloid cells 2 inhibits complement component 1q effector mechanisms and exerts detrimental effects during pneumococcal pneumonia. PLoS Pathog. *10*, e1004167.

Shinkai, Y., Rathbun, G., Lam, K.P., Oltz, E.M., Stewart, V., Mendelsohn, M., Charron, J., Datta, M., Young, F., Stall, A.M., et al. (1992). RAG-2-deficient mice lack mature lymphocytes owing to inability to initiate V(D)J rearrangement. Cell *68*, 855–867.

Talbot, T.R., Hartert, T.V., Mitchel, E., Halasa, N.B., Arbogast, P.G., Poehling, K.A., Schaffner, W., Craig, A.S., and Griffin, M.R. (2005). Asthma as a risk factor for invasive pneumococcal disease. N. Engl. J. Med. *352*, 2082–2090.

Townsend, M.J., Fallon, P.G., Matthews, D.J., Jolin, H.E., and McKenzie, A.N. (2000). T1/ST2-deficient mice demonstrate the importance of T1/ST2 in developing primary T helper cell type 2 responses. J. Exp. Med. *191*, 1069–1076.

Treutlein, B., Brownfield, D.G., Wu, A.R., Neff, N.F., Mantalas, G.L., Espinoza, F.H., Desai, T.J., Krasnow, M.A., and Quake, S.R. (2014). Reconstructing lineage hierarchies of the distal lung epithelium using single-cell RNA-seq. Nature *509*, 371–375.

van der Poll, T., and Opal, S.M. (2009). Pathogenesis, treatment, and prevention of pneumococcal pneumonia. Lancet *374*, 1543–1556.

von Moltke, J., and Locksley, R.M. (2014). I-L-C-2 it: type 2 immunity and group 2 innate lymphoid cells in homeostasis. Curr. Opin. Immunol. *31*, 58–65.

Warszawska, J.M., Gawish, R., Sharif, O., Sigel, S., Doninger, B., Lakovits, K., Mesteri, I., Nairz, M., Boon, L., Spiel, A., et al. (2013). Lipocalin 2 deactivates macrophages and worsens pneumococcal pneumonia outcomes. J. Clin. Invest. *123*, 3363–3372.

Wirtz, H.R., and Dobbs, L.G. (2000). The effects of mechanical forces on lung functions. Respir. Physiol. *119*, 1–17.

Woik, N., and Kroll, J. (2015). Regulation of lung development and regeneration by the vascular system. Cell. Mol. Life Sci. *72*, 2709–2718.

Wong, S.H., Walker, J.A., Jolin, H.E., Drynan, L.F., Hams, E., Camelo, A., Barlow, J.L., Neill, D.R., Panova, V., Koch, U., et al. (2012). Transcription factor RORα is critical for nuocyte development. Nat. Immunol. *13*, 229–236.

Cell Reports, Volume *18*

Supplemental Information

First-Breath-Induced Type 2 Pathways Shape the Lung Immune Environment

Simona Saluzzo, Anna-Dorothea Gorki, Batika M.J. Rana, Rui Martins, Seth Scanlon, Philipp Starkl, Karin Lakovits, Anastasiya Hladik, Ana Korosec, Omar Sharif, Joanna M. Warszawska, Helen Jolin, Ildiko Mesteri, Andrew N.J. McKenzie, and Sylvia Knapp

Supplemental Figures and Legends

Figure S1

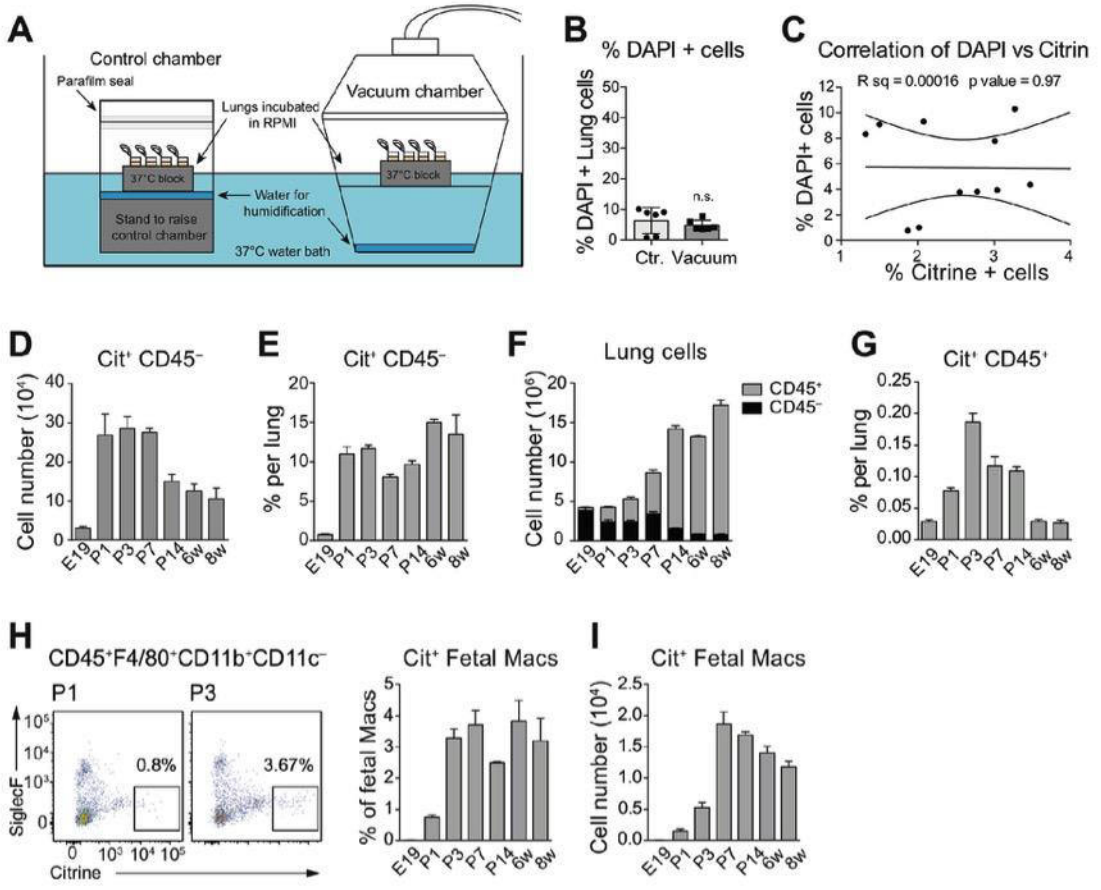

Figure S1. Integrated analysis of Citrine expression in lung cells of newborns and upon negative pressure. Related to Figure 1.

(A) Experimental set-up. Embryonic lungs (P19) were placed at 37°C and subjected to a negative pressure for 6h (see experimental procedures) (referring to Figure 1C, D, E).

(B) Viability of lung cells assessed by DAPI staining (referring to Figure 1C, D, E).

(C) Linear regression analysis of viability and IL-33 expression (Citrin) of embryonic lung cells subjected to negative pressure (vacuum) for 6h (referring to Figure 1C, D, E).

(D) Absolute numbers of $Cit^+ CD45^-$ lung cells (referring to Figure 1F lower panel and 1G).

(E) Proportion of $CD45^-$ cells that up-regulate Citrine at indicated time points (referring to Figure 1F lower panel)

(F) Relative contribution of $CD45^+$ and $CD45^-$ cells to total lung cell numbers from E19 to 8 weeks of age (referring to Figure 1F upper panel).

(G) Quantification of Citrine expression among CD45+ cells in newborn mice.

(H) Left: blots showing expression of Citrine among fetal macrophages gated as $CD45^+ F4/80^+ CD11b^+ CD11c^-$ $SiglecF^-$. Right: quantification of Citrine expression among fetal macrophages.

(I) Absolute numbers of lung fetal macrophages gated as in (H) at indicated time points.

Graph bars represent mean ± SEM. Data are representative of two independent experiments with 3-4 mice per time point.

Figure S2

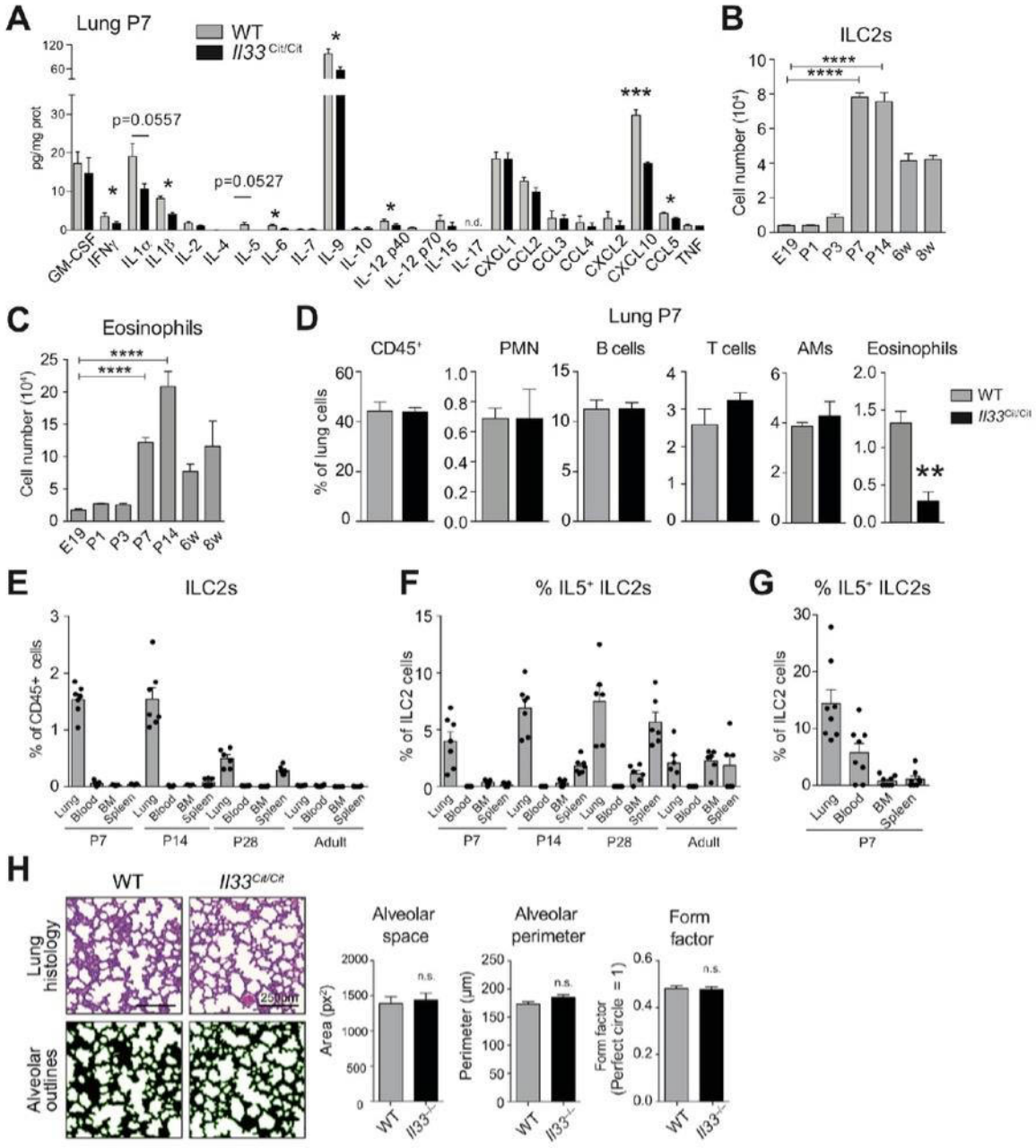

Figure S2. Integrated analysis of *Il33*$^{Cit/Cit}$ mice on P7, postnatal eosinophil expansion and perinatal alveolarization. Related to Figure 2.

(A) Absolute values of multiplex ELISA (referring to Figure 2A).

(B) Absolute numbers of lung ILC2s between E19 and week 8, (referring to Figure 2B).

(C) Absolute numbers of lung eosinophils between E19 and week 8, (referring to Figure 2E).

(D) Analysis of lung immune cell populations in WT and *Il33*$^{Cit/Cit}$ mice, depicted is the percentage of total lung cells, (referring to Figure 2F). PMN = polymorphonuclear cells gated as CD45$^+$ Ly6G$^+$; B cells = CD45$^+$ CD19$^+$; T cells = CD45$^+$ CD3$^+$; AMs = CD11b$^-$ SiglecF$^+$ CD11c$^+$; eosinophils = CD11b$^+$ SiglecF$^+$ CD11c$^-$.

(E, F) Proportion of ILC2s (among CD45$^+$cells) and IL5-expressing ILC2s (*Il5*$^{Cer/+}$ mice) in indicated body compartments between P7 and adulthood.

(G) Quantification of IL5 production by ILC2s assessed by i.c. cytokine stain, (referring to Figure 2H).

(H) Lung alveolarization was quantified on H&E stained lung sections from WT and *Il33*$^{Cit/Cit}$ mice at P7 using the automatic image analysis software CellProfiler. For details see Supplemental experimental procedures.

Figure S3

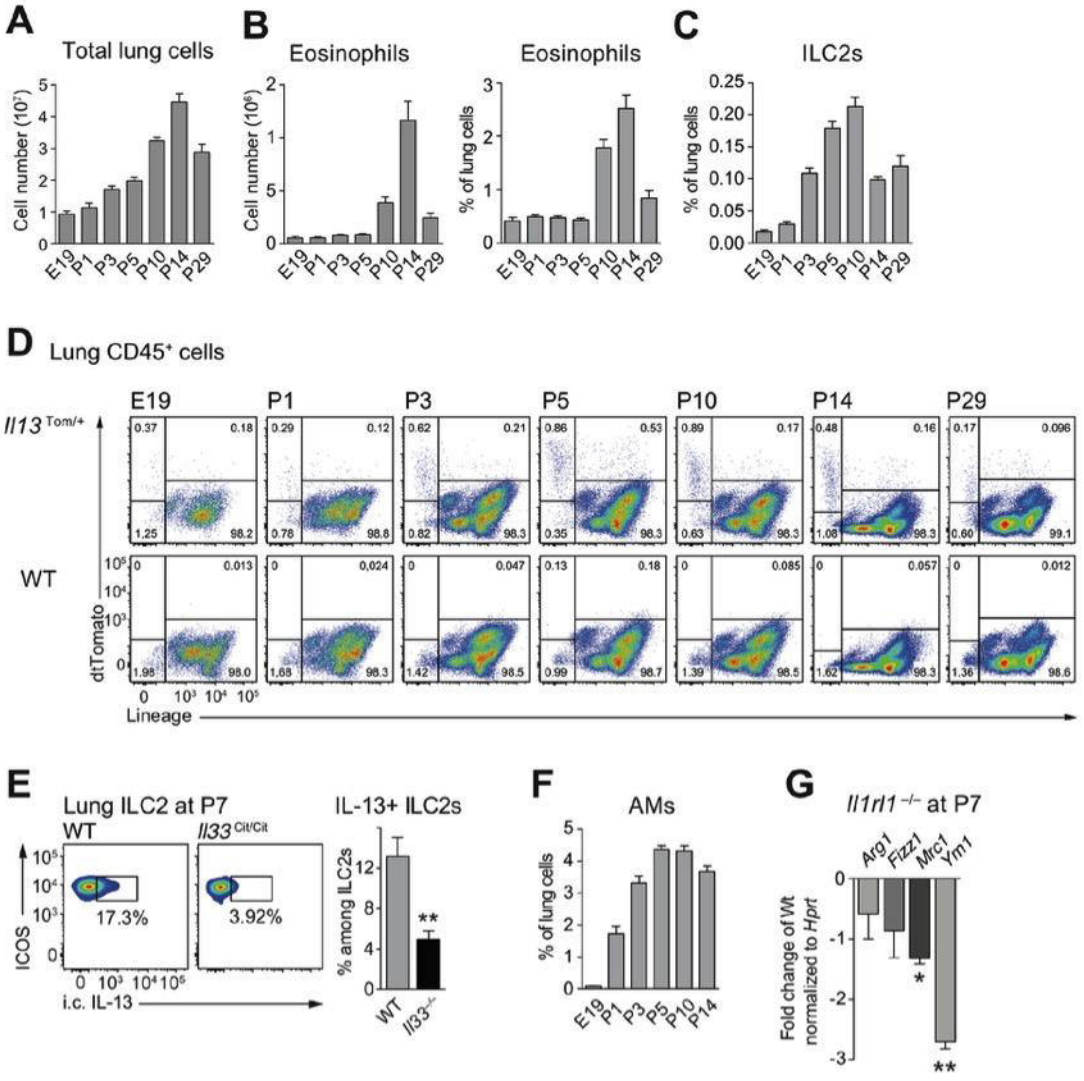

Figure S3. Lin⁻cells are the only IL-13 expressing cells in the first two weeks after birth. Related to Figure 3.

(A-C) Quantification of lung ILC2s and eosinophils at the indicated time points in *Il13*$^{Tom/+}$ mice. Of note, *Il13*$^{Tom/+}$ mice, which are on a C57BL/6 background, show the same cell influx dynamic as *Il33*$^{Cit/+}$ mice, which are on a Balb/c background, (referring to Figure 3A-D). (A) Absolute number of total lung cells. (B) Absolute numbers and percentages of eosinophils gated as in Figure 2E. (C) Percentage of ILC2s, gated as in Figure 2B. (D) FACS of lung cells gated for Lineage (CD3, CD4, CD8, CD19, F4/80, CD11b, CD11c, FceRI, NK1.1, Ly6C/G) and *Il13*^{dtTomato} expression at indicated time points.
(E) IL-13 expression in lung ILC2s at P7 quantified by i.c. cytokine stain.
(F) Percentage of AMs gated as in Figure 3C, (referring to Figure 3C-D).
(G) AMs (F4/80$^+$CD11b$^-$CD11c$^+$SiglecF$^+$) were sorted on P7 from WT and *Il1rl1*$^{-/-}$ mice and M2 markers were assessed by RT-PCR.
Data are representative of two (A-F) and one (G) independent experiments with 3-4 mice per group. Bars represent mean ± SEM; *p < 0.05; **p < 0.01.

Figure S4

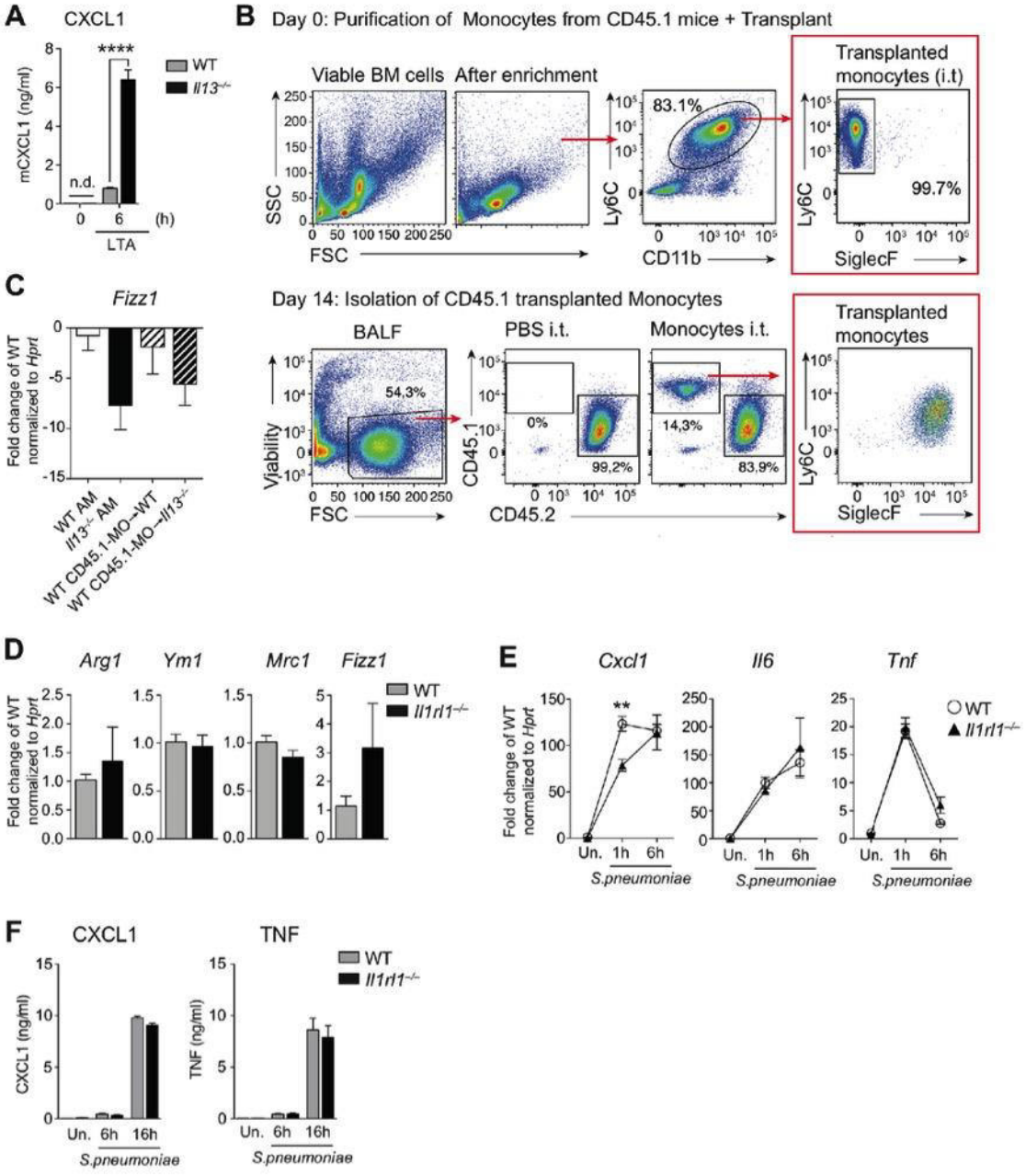

Figure S4. BM derived monocytes assume an AMs phenotype 2 weeks upon intratracheal transplant. *Il1rl1* alone plays no significant role in AM polarization in adult mice. Related to Fig 4.

(A) AMs from WT and *Il13*$^{-/-}$ mice were isolated by BAL and *in vitro* stimulated with LTA (10µg/ml). CXCL1 was quantified in supernatants, (refers to Figure 4B-C).

(B) FACS plots representing bone marrow derived monocytes isolated from WT CD45.1 mice and transferred i.t. into WT or *Il13*$^{-/-}$ mice. Two weeks later transferred monocytes showed upregulation of SiglecF, (refers to Fig 4D).

(C) *Fizz1* expression was quantified in FACS-sorted AMs upon monocytes transplant, (refers to Fig 4D.

(D, E) AMs isolated via BAL from WT and *Il1rl1*$^{-/-}$ mice analyzed for M2 markers by RT-PCR (D), or *in vitro* stimulated with *S. pneumoniae* (MOI 100) and analyzed for cytokine expression by RT-PCR (E). Values were normalized to HPRT and are expressed as fold-change versus WT at t = 0h.

(F) AMs were isolated as in (D), and stimulated *in vitro* with *S. pneumoniae* (MOI 100) and CXCL1 and TNF protein levels were quantified in supernatants by ELISA.

Data are representative of at least two independent experiments with four (A and D-F) and 6-7 (B, C) mice per group and/or time point. Mean ± SEM are depicted; **p < 0.01, ****p < 0.0001. I.t. = intra-tracheally; MOI = multiplicity of infection; BAL = bronchoalveolar lavage.

Figure S5

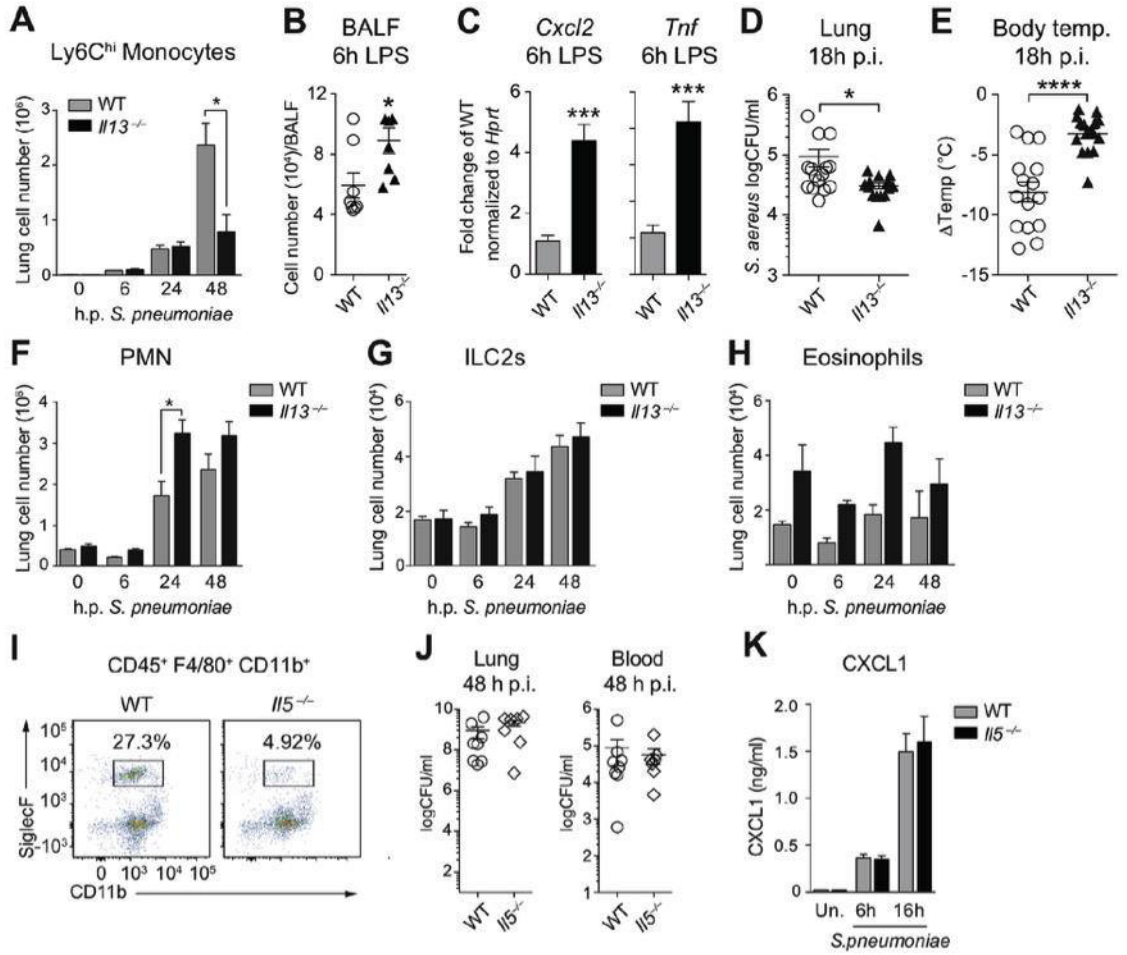

Figure S5. Broader role of IL-13 in the inflammatory response to LPS and *S. aureus*. Eosinophils do not impact on AM polarization, or responses to *S. pneumoniae*. Related to Fig 4.

(A) Numbers of lung Ly6C^{hi} monocytes (F4/80^{+} CD11b^{+} Ly6C^{hi}) during *S. pneumonia* infection, (refers to Figure 4E-K).

(B-C) Mice were treated i.n. with LPS (100ng/50µl) and harvested 6h later to assess cell influx in BALF (B) and cytokine expression in BALF (C).

(D-E) Mice were infected i.n. with *S. aureus* and assessed 18h later for body temperature (E), and harvested to quantify lung CFUs (D) .

(F-H) Absolute numbers of (F) PMN (SSC^{hi} FSC^{hi} CD11b^{+} Ly6G^{+}), (G) ILC2s (Lin^{-} ST2^{+} ICOS^{+} CD25^{+} Thy1.2^{+}), (H) eosinophils (CD11b^{+} F4/80^{+} SSC^{hi} CD11c^{-} SiglecF^{+}) during the course of *S. pneumoniae* infection; (refers to Figure 4E-K).

(I) FACS plots illustrating lung eosinophil numbers in healthy WT and *Il5*$^{-/-}$ mice.

(J) WT and *Il5*$^{-/-}$ mice were i.n. infected with 10^5 CFU *S. pneumoniae* and sacrificed after 48h. CFU counts were assessed in lung homogenates (left) and blood (right).

(K) BAL isolated AMs from WT and *Il5*$^{-/-}$ mice were *in vitro* stimulated with *S. pneumoniae* (MOI 100). CXCL1 was quantified in supernatants.

Graph bars represent mean ± SEM. *p < 0.05, ***p < 0.001, ****p < 0.0001. Data are representative of two independent experiments with 4 (A, I and K) and at least 8 (B-H, and J) mice per group and/or time point.

Figure S6

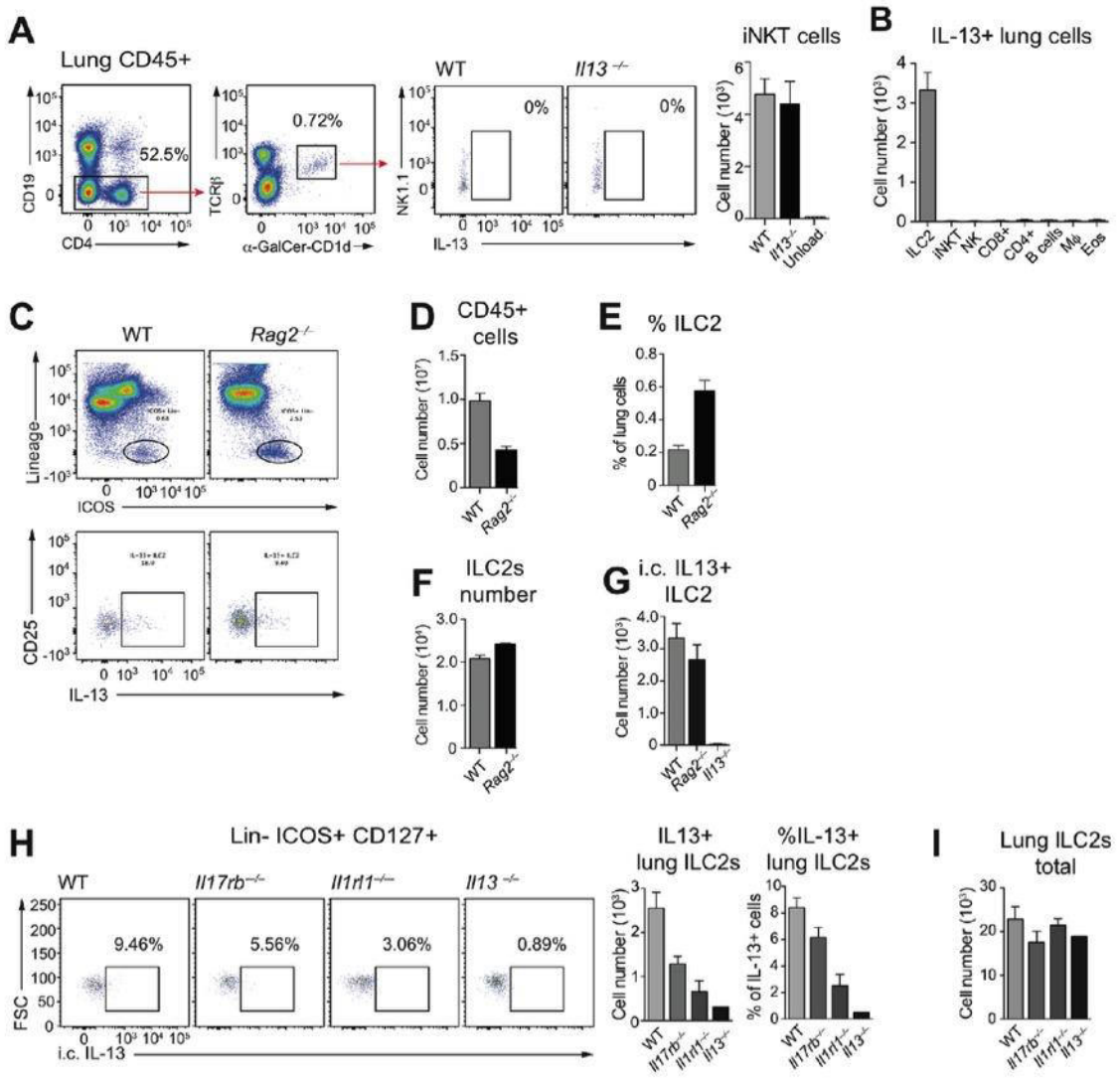

Figure S6. iNKT cells are not a source of IL-13 at homeostasis. Baseline ILC2-derived IL-13 expression does not depend or on B and T cells, but partially on *Il17rb*. Related to Figure 6.

(A) FACS gating strategy for iNKT cells ($CD19^-$ $CD4^{+/-}$ $TCR\beta^+$ α-GalCer-CD1d $dimer^+$ $NK1.1^+$). Unloaded CD1d dimer was used as negative control. Right panel: absolute number of iNKT cells in naive adult lungs. IL-13 production was assessed by i.c. staining.

(B) Absolute number of IL-13 secreting lung cells at homeostasis (cells gated as in Figure 6D). IL-13 production was assessed by i.c. staining. iNKT cells were gated as in Figure S6A.

(C-G) ILC2s were assessed for intracellular IL-13 production in naive WT and *Rag2*$^{-/-}$ mice at homeostasis. (C) Representative plots of ILC2s gating strategy. (D) Absolute lung cell number. (E) Percentage of ILC2s out of total lung cells. (F) Absolute number of ILC2s. (G) Absolute number of IL-13 expressing ILC2s.

(H) Representative FACS plots of ILC2s (Lin^- $ST2^+$ $ICOS^+$ $Thy1.2^+$ $CD25^+$) assessed for IL-13 expression via i.c. staining in indicated mouse strains at homeostasis. Right: Absolute number and percentage of IL-13 secreting ILC2s.

(I) Absolute number of lung ILC2s at steady state in indicated mouse strains.

Single cells were pre-gated for viability and CD45+ expression. Graph bars represent mean ± SEM. Data are representative of at least two independent experiments with 4 mice per group. i.c. = intracellular.

Figure S7

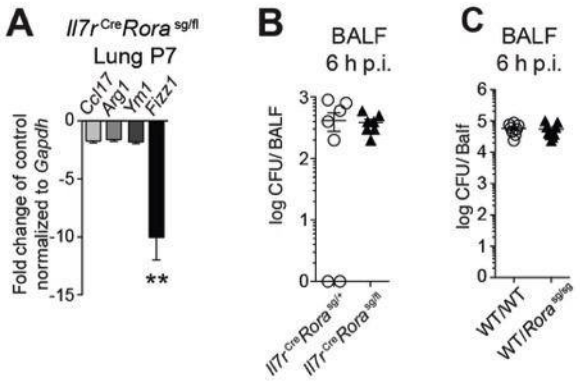

Figure S7. Reduced M2 marker expression in lungs of neonatal ILC2-deficient mice. Related to Fig 7.
(A) M2 markers were assessed by RT-PCR in whole lung homogenates of naive *Il7r*^{Cre}*Rora*$^{sg/fl}$ mice as compared to *Il7r*^{Cre}*Rora*$^{+/fl}$ controls on postnatal day 7 (P7), (refers to Figure 7B).
(B, C) BALF CFU in indicated mouse strains 6h post i.n. infection with *S. pneumoniae*, (refers to Figure 7E-J, and Figure 7O-P, respectively).
Graph bars represent mean ± SEM. **$p < 0.01$. Data are representative of at least two independent experiments with 4 mice per group (A) or 7-8 mice per group (B-C).

TABLES

Table S1. List of anti-mouse antibodies used in the study. Related to Figure 1-4 and 6-7.

Ab	Fluorochrome	Clone ID	Manufacturer	Isotype
B220	PerCP/Cy5.5	RA3-6B2	eBioscience	Rat IgG2a
CD45	V500	30-F11	BD Biosciences	Rat IgG2b
CD45	BV510	30-F11	Biolegend	Rat IgG2b
CD45.1	Pacific Blue	A20	Biolegend	Mouse IgG2a
CD45.2	PE	104	Biolegend	Mouse IgG2a
CD3	FITC, eFluor450	17A2	Biolegend	Rat IgG2b
CD3	PE/Cy7	145-2C11	Biolegend	Hamster IgG
CD4	FITC, PE/Cy7	GK1.5	eBioscience	Rat IgG2a
CD4	AF700, PE/Cy7, eFluor450	RM4-5	eBioscience	Rat IgG2a
CD8a	FITC, eFluor450, PE/Cy7	53-6.7	Biolegend or eBioscience	Rat IgG2a
CD11b	APC, FITC, AF700, PercP/Cy5.5, PE/Cy7, Pacific Blue	M1/70	Biolegend or eBioscience	Rat IgG2b
CD11c	FITC	HL3	BD Biosciences	Hamster IgG1
CD11c	AF700, PE/Cy7, BV421, AF647	N418	Biolegend or eBioscience	Hamster IgG
CD19	FITC, PE/Cy7	eBio1D3	eBioscience	Rat IgG2a
CD19	PE/Cy7, BV421, AF700	6D5	Biolegend	Rat IgG2a
CD31	PE/Cy7	390	eBioscience	Rat IgG2a
CD49b	FITC, Pacific Blue, PE/Cy7	DX5	Biolegend or eBioscience	Rat IgM
CD127	APC, PE/Cy7	A7R34	Biolegend	Rat IgG2a
CD138	APC	281-2	Biolegend	Rat IgG2a
c-Kit	AF700	ACK2	eBioscience	Rat IgG2b
EpCam	PE/Cy7	G8.8	Biolegend	Rat IgG2a
F4/80	BV421, BV785, FITC, PE/Cy7, APC, PerCp/Cy5.5	BM8	Biolegend or eBioscience	Rat IgG2a
FceRIa	FITC, Pacific Blue, PE/Cy7, PE	MAR-1	Biolegend or eBioscience	Hamster IgG
Foxp3	APC	FJK-16s	eBioscience	Rat IgG2a
Gr-1	FITC, BV421, PE/Cy7	RB6-8C5	Biolegend or eBioscience	Rat IgG2b
ICOS	APC, PE, PE/Cy7, BV421	C398.4A	Biolegend or eBioscience	Hamster IgG
IL5	APC	TRFK5	Biolegend	Rat IgG1
IL13	PE	eBio13A	eBioscience	Rat IgG1

Ly6C	BV605	HK 1.4	Biolegend	Rat IgG2c
Ly6G	PE, PE/Cy7	1A8	Biolegend	Rat IgG2a
MHCII	FITC	2G9	BD Biosciences	Rat IgG2a
MHCII	Pacific Blue, BV510	M5/114.15.2	Biolegend	Rat IgG2b
NK1.1	eFluor450	PK136	eBioscience	Rat IgG2a
RORγt	PE	AFKJS-9	eBioscience	Rat IgG2a
Siglec-F	APC, AF647	E50-2440	BD Biosciences	Rat IgG2a
Sca-1	APC	D7	Biolegend	Rat IgG2a
ST2	Biotin, PerCp/Cy5.5, FITC	DJ8	MD Bioproducts	Rat IgG1
ST2	eFluor710	RMST2-2	eBioscience	Rat IgG2a
Ter-119	BV421, PE/Cy7	Ter-119	Biolegend	Rat IgG2b
Thy1.2	eFluor450	53-2.1	eBioscience	Rat IgG2a

Table S2. Gating strategy for lung cells in the study. All cells were gated on viable CD45+ cells. Related to Figure 1-4 and 6-7.

Cell population	**Gating strategy**
B cells	CD19+ MHCII+
CD4+ T cells	CD3+/CD4+ CD8-
CD8+ T cells	CD3+/CD4- CD8+
T regs	CD3+ CD4+ /CD25+ Foxp3+
ILC2	Lin-(CD3-CD4-CD5-CD8-CD19-CD49b-FceRIa-CD11b-Cd11c-F4/80-Gr1-) Thy1.2+ICOS+ST2+CD25+
NK cells	CD3- /NK1.1+ CD49b+
NKT cells	CD3+ /NK1.1+CD49b+
DCs	CD8-/F4/80-CD11c^{hi} /CD11b^{lo} MHCII^{hi}
AMs	F4/80+ CD11c+ /CD11b^{lo} SiglecF+
PMN	CD19-F4/80- Ly6G+
Eosinophils	CD19-F4/80+ CD11b+ CD11c- SiglecF+ SSC^{hi}
Mast cells	CD19- CD11b+ cKit+ FceRIa+

Table S3. List of primers used in the study. Related to Figure 1, 3-5 and 7.

Gene target	**NM name**	**Fragment size**	**Sequence**
mArg1	NM_007482	158bp	F: CAGTGTGGTGCTGGGTGGAG R: ACACAGGTTGCCCATGCAGA
mYm1	NM_009892.1	191bp	F: TCTGGGTACAAGATCCCTGAACTG R: GCTGCTCCATGGTCCTTCCA

mMrc1	NM_008625	116bp	F: TCTGGGCCATGAGGCTTCTC R: CACGCAGCGCTTGTGATCTT
mFizz1	NM_020509	197bp	F: TCCAGCTGATGGTCCCAGTG R: AAAGCCACAAGCACACCCAGT
mIL33	NM_001164724.1	174bp	F: CCCTGGTCCCGCCTTGCAAAA R: AGTTCTCTTCATGCTTGGTACCCGA
mCXCL1	NM_008176	235bp	F: GACCATGGCTGGGATTCACC R: TCAGAAGCCAGCGTTCACCA
mTNF	NM_013693	200bp	F: GAACTGGCAGAAGAGGCACT R: GGTCTGGGCCATAGAACTGA
mHPRT	NM_013556	96bp	F: GTTAAGCAGTACAGCCCCAAAATG R: AAATCCAACAAAGTCTGGCCTGTA

Supplemental Experimental Procedures:

Vacuum-induced lung stress. Lungs were harvested, stored on ice and transferred to either a pre-heated 37°C humidified control chamber or a pre-heated humidified vacuum chamber (Vacuubrand model MZ2C) (see Fig S1A). The vacuum was initiated and both groups were incubated for 6hs. Lungs were then dissociated using scissors and digested in collagenase 1 (750U/ml Invitrogen) and DNase1 (0.31mg/ml Roche) in RPMI (Life technologies) for 45 mins at 37°C. Tissues were passed through a 70μM filter using PBS with 2% FCS and processed for flow cytometry.

Lung flow cytometry and cell sorting. Lung single cell suspensions were prepared by incubating finely minced lung tissue for 1h at 37°C in RPMI containing 5% FCS, collagenase I (ThermoFischer), and DNase I (Sigma-Aldrich), homogenized with a glass homogenizer and then passed through a 70μm strainer. Cells were incubated for 5 min on ice in red blood cell lysis buffer (Sigma-Aldrich), washed and finally passed through a 40μm cell strainer. Single cell suspensions were counted with a hemocytometer and $2x10^6$ cells/stain were incubated with anti-mouse Fc receptor blocking antibody CD16/CD32 (eBioscience) and stained with a mix of fluorochrome labeled antibodies (**Supplementary Methods Table 1**). The alpha-GalCer/CD1d loaded dimer and unloaded control were provided by the NIH tetramer core facility. DAPI or fixable viability dye (eBioscience 65-0865) was added to the surface antibody mix to allow dead cells exclusion by flow cytometry. For gating strategies see **Supplementary Methods Table 2**. For intra-cellular (i.c.) staining, lung cell suspensions were further purified using Percoll (Sigma), incubated with PMA (60ng/ml), ionomycin (500ng/ml) and 1x protein transport inhibitor (eBioscience), or with brefeldin A (GolgiPlug™, BD Biosciences) for 4h at 37°C. Cells were then stained with surface antibodies, fixed and permeabilized before addition of anti mouse IL-13 mAb or anti-IL-5 mAbs, respectively, or isotype control Abs (Fixation and Permeabilization Solution Kit, BD Biosciences). For nuclear staining, cells were permeabilized and processed using the Foxp3 / Transcription Factor Staining Buffer Set (eBioscience). Acquisition was performed with a LSRFortessa (BD Biosciences) and data were analyzed using the FlowJo software version vX.0.7 (TreeStar). Cell sorting was performed with BD FACSAria™ III.

Reagents for isolation, culture and stimulation of alveolar macrophages (AMs). AMs from newborn mice were isolated by cell sorting from lung single cell suspensions as described above. In adult mice, AMs were isolated by bronchoalveolar lavage (BAL) followed by cell adhesion. In brief, mice were lethally anesthetized using 100 mg/kg body weight ketamine (Ketaset) and 10 mg/kg body weight xylazine (Rompun, Bayer), administered in sterile PBS i.p. AMs were isolated by inserting a tracheal cannula (Venflon, BD Bioscience) and flushing the lungs 10 times with 1ml NaCl. Isolated cells were counted and allowed to adhere at 37°C for 2h in RPMI containing 10% FCS and 1% penicillin/streptomycin at a concentration of $5x10^4$ cells/well in a 96 well plate. Wells were washed twice with PBS and adherent cells were used for further experiments.

Real time PCR. Total mRNA was isolated using the NucleoSpin RNA XS kit (Macherey-Nagel) or the RNeasy Micro kit (Qiagen) according to the manufacturers' instructions. Real-time PCR was performed using either the SYBR Green Master Mix (Applied Biosystems), or the TaqMan universal PCR mix (Applied Biosystems) and the StepOnePlus™ Real-Time PCR System (Applied Biosystems) or using a ViiA 7 (Thermofisher). Commercially available Taqman probes were used for the expression of mCCL17 (Mm01244826_g1), mYm1 (Mm00657889_mH), mFizz1 (Mm00445109_m1), mArg1 (Mm00475988_m1) and GAPDH (Cat. 4352932E). Designed primers were purchased from Sigma-Aldrich and are listed in the **Supplementary Methods Table 3.** Gene expression was normalized to GAPDH or HPRT and expressed as fold change versus indicated controls.

Lung tissue homogenates and ELISA. Lungs were homogenized in the presence of protease inhibitors and total protein content was quantified by Pierce BCA Protein Assay Kit (Thermo Scientific). The Multiplex bead array (MILLIPLEX MAP Mouse Cytokine/Chemokine Magnetic Bead Panel - Premixed 25 Plex) was performed according to the manufacturer's instructions (Millipore), using MAGPIX multiplexing instrument and MILLIPLEX analysis 5.1 software (Millipore). Mouse IL-33 was measured using the eBioscience ELISA kit, according to the manufacturers' instructions. For protein quantification in *S. pneumoniae* infected lungs, CXCL1 and TNF were measured in lung homogenates using specific ELISA kits from RnD Systems, according to the manufacturers' instructions.

Analysis of alveolarization. H&E stained lung sections of newborn mice at postnatal day 7 were imaged using an Olympus FSX100 automated microscope and a 20X magnification (10 fields per lung). Lung alveolarization was quantified using the automatic image analysis software CellProfiler (Lamprecht et al., 2007) (http://www.cellprofiler.org/). Briefly, image masks for each field were generated by converting the images to grayscale and applying a binary threshold using the threshold function in ImageJ (version 1.49v; http://imagej.nih.gov/ij/). The original images were loaded into CellProfiler and alveoli were identified using the binary images generated in ImageJ (as described above), as the thresholding method using the *IdentifyPrimaryObjects* module. The shape and size features of the identified alveoli were then calculated using the *MeasureObjectSizeShape* module and exported to a spreadsheet format.

Immunofluorescence and analysis. Lungs from *Il33*$^{Cit/+}$ reporter mice were isolated at embryonic day 19 (E19) and postnatal days 1 (P1) and 3 and fixed overnight in 1% formaldehyde–PBS at 4 °C. After extensive washing with PBS, lungs were then incubated overnight in 30% sucrose solution at 4 °C. On the third day, lungs were embedded in 15% sucrose + 7.5% porcine skin gelatin (Sigma) in PBS and flash-frozen in isopentane chilled to −80 °C with liquid nitrogen. Lobes were sectioned to a 20-µm thickness onto Superfrost Plus slides (Thermo Scientific) and stored at −20 °C. Sections were air-dried for 1 h, rehydrated with PBS and then incubated in blocking buffer (3% goat serum (Jackson Immunoresearch) + 0.05% Triton-X in PBS) for 30 min. Sections were then incubated with a polyclonal rabbit anti-pro-surfactant protein-C antibody (Merck Millipore, AB3786) (1:500) in blocking buffer for 1 h. After washing, sections were then incubated with an Alexa Fluor 546-labeled polyclonal goat anti-rabbit antibody (4 µg/ml) (Thermo Fisher Scientific) and DAPI (300 nM) for 30 min in blocking buffer. After additional washes, Prolong Gold (Invitrogen) was added to slides plus a coverslip. Sections were imaged on a laser-scanning microscope (TCS SP8, Leica) with a 20×/ 20x/0.75NA HC PL APO CS2 air objective. Data were processed and analyzed using the open-source software ImageJ (Fiji package) (Schindelin et al., 2012).

Supplemental References:

Lamprecht, M.R., Sabatini, D.M., Carpenter, A.E., 2007. CellProfiler: Free, versatile software for automated biological image analysis. Biotechniques 42, 71–75. doi:10.2144/000112257

Schindelin, J., Arganda-Carreras, I., Frise, E., Kaynig, V., Longair, M., Pietzsch, T., Preibisch, S., Rueden, C., Saalfeld, S., Schmid, B., Tinevez, J.-Y., White, D.J., Hartenstein, V., Eliceiri, K., Tomancak, P., Cardona, A., 2012. Fiji: an open-source platform for biological-image analysis. Nat. Methods 9, 676–682. doi:10.1038/nmeth.2019

2.2. Lung single-cell signaling interaction map reveals basophil role in macrophage imprinting

In the second part of this chapter the publication “Lung single-cell signaling interaction map reveals basophil role in macrophage imprinting” will be presented. Using single-cell sequencing, transcription profiles of immune and non-immune cells are mapped across different time points of lung development. Cell-cell interaction analysis revealed a role for a lung-resident basophil population that was characterized by the expression of Il6, Il13 and Tnfa. This basophil population as well as the before mentioned ILC2 population were required to ensure alveolar macrophage maturation. This study not only provides a powerful tool for researchers worldwide but also brings us one step closer to unravel the complex mechanisms involved in lung development before and after birth.

Article

Cell

Lung Single-Cell Signaling Interaction Map Reveals Basophil Role in Macrophage Imprinting

Merav Cohen,[1,8] Amir Giladi,[1,8] Anna-Dorothea Gorki,[4,5,8] Dikla Gelbard Solodkin,[1] Mor Zada,[1] Anastasiya Hladik,[4,5] Andras Miklosi,[6] Tomer-Meir Salame,[2] Keren Bahar Halpern,[3] Eyal David,[1] Shalev Itzkovitz,[3] Tibor Harkany,[6,7] Sylvia Knapp,[4,5] and Ido Amit[1,9,*]

[1]Department of Immunology, Weizmann Institute of Science, Rehovot, Israel
[2]Flow Cytometry Unit, Department of Biological Services, Weizmann Institute of Science, Rehovot, Israel
[3]Department of Molecular Cell Biology, Weizmann Institute of Science, Rehovot, Israel
[4]CeMM Research Center for Molecular Medicine of the Austrian Academy of Sciences, 1090 Vienna, Austria
[5]Department of Medicine I, Laboratory of Infection Biology, Medical University of Vienna, 1090 Vienna, Austria
[6]Department of Molecular Neurosciences, Center for Brain Research, Medical University of Vienna, 1090 Vienna, Austria
[7]Department of Neuroscience, Karolinska Institutet, Retzius väg 8, 17177 Stockholm, Sweden
[8]These authors contributed equally
[9]Lead Contact
*Correspondence: ido.amit@weizmann.ac.il
https://doi.org/10.1016/j.cell.2018.09.009

SUMMARY

Lung development and function arises from the interactions between diverse cell types and lineages. Using single-cell RNA sequencing (RNA-seq), we characterize the cellular composition of the lung during development and identify vast dynamics in cell composition and their molecular characteristics. Analyzing 818 ligand-receptor interaction pairs within and between cell lineages, we identify broadly interacting cells, including AT2, innate lymphocytes (ILCs), and basophils. Using interleukin (IL)-33 receptor knockout mice and *in vitro* experiments, we show that basophils establish a lung-specific function imprinted by IL-33 and granulocyte-macrophage colony-stimulating factor (GM-CSF), characterized by unique signaling of cytokines and growth factors important for stromal, epithelial, and myeloid cell fates. Antibody-depletion strategies, diphtheria toxin-mediated selective depletion of basophils, and co-culture studies show that lung resident basophils are important regulators of alveolar macrophage development and function. Together, our study demonstrates how whole-tissue signaling interaction map on the single-cell level can broaden our understanding of cellular networks in health and disease.

INTRODUCTION

Mammalian tissues consist of diverse cell types that include fibroblasts, epithelial, endothelial, and immune lineages. Tissue formation during embryonic development requires the coordinated function and crosstalk between distinct cell types, in specific environmental contexts. Development of the lung into specialized cell types is a highly regulated process, characterized by unique pathways and functional properties. In parallel, cells of the immune system migrate from hematopoietic sites to the lung and establish an active immune compartment that interacts with stromal cells, influencing tissue differentiation, growth, and function.

Within a specific tissue, dominant signal transmitting cells determine the cellular quantities, composition, and characteristics by secretion of growth factors and cytokines (Camp et al., 2017; Lavin et al., 2014). Notably, growth factors and cytokines have pleiotropic effects critical for priming and maintaining tissue-specific microenvironments. Furthermore, the exact timing of tissue-specific cell circuits is critical in propagating successive developmental programs essential for proper tissue development (Matcovitch-Natan et al., 2016; Zhou et al., 2018). While tissue-specific crosstalk have been previously reported (Cohen et al., 2014; Guilliams et al., 2013; Rantakari et al., 2016), a system-wide approach to evaluate cellular communication during tissue development and the influence of specific cell types on the maturation and maintenance of their neighbors remains an active research field (Camp et al., 2017; Nabhan et al., 2018). Importantly, understanding cellular circuits during tissue development can potentially shed light on cellular crosstalk during pathologies.

The mammalian lung is the central respiratory organ, featuring a diverse set of specialized cell types. Gas exchange in the lung occurs in the alveoli, which are composed of specialized epithelial cells: the alveolar type (AT) 1 cells that mediate gas exchange, and AT2 cells that secrete surfactant and maintain the surface tension of the lungs (Whitsett and Alenghat, 2015). Alveolar epithelial cells branch from their mutual progenitor between the canalicular (E16.5) and saccular (E18.5) stages, resulting in changes in morphology and gene expression (Treutlein et al., 2014). Another major cell type is the alveolar macrophages (AM), which clear surfactant from the alveolar space and act as immune modulators, suppressing unwanted immune responses in the lungs (Hussell and Bell, 2014). AM originate from fetal liver embryonic precursors and are self-maintaining, with no

Cell

contribution from the adult bone marrow (Hashimoto et al., 2013; Shibata et al., 2001). The first wave of lung macrophages appears at embryonic day 12.5 (E12.5), followed by a second wave stemming from fetal liver-derived monocytes, which continues its differentiation axis during alveolarization into mature AM (Ginhoux, 2014; Kopf et al., 2015).

Every tissue is equipped with a unique signaling environment that interacts with the immune compartment and shapes the gene expression and chromatin landscapes of the cells (Cohen et al., 2014; Lavin et al., 2014; Panduro et al., 2016). However, it is still unknown whether this is a universal principal that applies to all immune cells or is limited to a few plastic cell types (Lavin et al., 2014). In the lung context, AM exhibit a tissue-specific phenotype and function (Gautier et al., 2012; Kopf et al., 2015; Lavin et al., 2014). There is a major gap in our understanding of the dynamic signaling during the alveolarization process, as attempts to grow AM *ex vivo* have not been successful. Lung macrophage development and maturation was shown to be dependent on different growth and differentiation cues transmitted from epithelial cells (mainly AT2), innate lymphocytes (ILC), and the AM themselves (de Kleer et al., 2016; Guilliams et al., 2013; Saluzzo et al., 2017; Yu et al., 2017). The function and crosstalk of other lung resident immune and non-immune cell types in the lung is currently much less understood.

Here, we report the extensive profiling of immune and non-immune lung cells by single-cell RNA sequencing (RNA-seq) of 50,770 cells along major time points of lung development. We observed a highly diverse set of cell types and states. Analysis of interacting ligands and receptors in our dataset revealed a highly connected signaling network and highlighted lung basophils as cells expressing major growth factors and cytokine signaling. We discovered that lung resident basophils localize in close proximity to alveoli and exhibit a lung-specific phenotype, highly diverged from peripheral circulating basophils. Using Il1rl1 (interleukin [IL]-33 receptor) knockout mice and *in vitro* cultures, we discovered that lung basophils' education is mediated by the combinatorial imprinting of granulocyte-macrophage colony-stimulating factor (GM-CSF) (Csf2) and IL-33 from the lung environment. Using different basophil depletion strategies and *in vitro* co-culture experiments, we demonstrate that basophils play an important role in guiding the maturation and function of AM in the lung. Our findings reveal an important role of lung resident basophils in lung development, and open new clinical strategies to macrophage manipulation and basophil-based therapeutics.

RESULTS

A Comprehensive Map of the Lung Cell Types during Development

To understand the contribution of different immune and non-immune cell types and states for lung development and homeostasis, we collected single-cell profiles along critical time points of lung development. In order to avoid biases stemming from cell-surface markers or selective tissue dissociation procedures, we combined a broad gating strategy and permissive tissue dissociation protocol, resulting in a comprehensive repertoire of the immune and non-immune cells located in the lung (Figures S1A–S1C; STAR Methods). We densely sampled cells from multiple time points of lung embryonic and postnatal development and performed massively parallel single-cell RNA-seq coupled to index sorting (MARS-seq) (Jaitin et al., 2014) (Figures 1A and S1D–S1G; Table S1). We collected cells from major embryonic developmental stages: early morphogenesis (E12.5), the canalicular stage (E16.5), and the saccular stage (E18.5–E19.5; Late E). We further collected cells from postnatal stages of alveolarization immediately after birth (1, 6, 7, and 10 hr postnatal; Early PN), 16 and 30 hr postnatal (Mid PN), as well as 2 days and 7 days postnatal (Figure 1A). To construct the lung cellular map, we profiled 10,196 $CD45^-$ (non-immune) and 10,904 $CD45^+$ (immune) single cells from 17 mice and used the MetaCell algorithm to identify homogeneous and robust groups of cells ("meta-cells") (STAR Methods) (Giladi et al., 2018), resulting in a detailed map of the 260 most transcriptionally distinct subpopulations (Figures S1H and S1I; Table S2; STAR Methods). A two-dimensional representation of immune and non-immune single cells revealed separation of cells into diverse lineages (Figures 1B, S1H, and S1I). In the immune compartment, lymphoid lineages were detected including natural killer (NK) cells (characterized by high expression of *Ccl5*), ILC subset 2 (*Il7r* and *Rora*), T cells (*Trbc2*), and B cells (*Cd19*) (Figure 1C), while granulocytes and myeloid cells separated into neutrophils (*Retnlg*), basophils (*Mcpt8*), mast cells (*Mcpt4*), DCs (*Siglech*), monocytes (*F13a1*), and three different subsets of macrophages (macrophage I–III; *Ear2*). Annotation by gene expression was further supported by conventional fluorescence-activated cell sorting (FACS) indices (Figure S1J). Despite its vast heterogeneity, clustering of the none-immune compartment ($CD45^-$) revealed the three major lineages, epithelium (marked by *Epcam* expression), endothelium (*Cdh5*), and fibroblasts (*Col1a2*). In concordance with previous characterizations of lung development (Treutlein et al., 2014), epithelial cells were separated into epithelium progenitors (high *Epcam*), AT1 cells (*Akap5*), AT2 cells (*Lamp3*), Club cells (*Scgb3a2*), and ciliated cells (*Foxj1*) subpopulations, while fibroblast subsets included fibroblast progenitors, smooth muscle cells (*Enpp2*), matrix fibroblasts (*Mfap4*), and pericytes (*Gucy1a3*) (Figures 1B and 1C). Overall, these data provide a detailed map of both the abundant and extremely rare lung cell types (>0.1% of all cells, Figure S1K) during important periods of development, which can be further used to study the differentiation, maturation, and cellular dynamics of the lung.

Lung Compartmentalization Is Shaped by Waves of Cellular Dynamics

During embryogenesis and soon after birth, the lung undergoes dramatic environmental changes with its maturation and abrupt exposure to airborne oxygen. Accordingly, our analysis shows that meta-cell composition varies widely at these time points (Figures 2A, S2A, and S2B). At the cell-type level, the most prominent cellular dynamics in the immune and non-immune compositions were observed during pregnancy (Figures 2B and 2C). Notably, because tissue dissociation protocols might affect cell type abundances, they can only be regarded as relative quantities (Figure S1B). At the earliest time point (E12.5), the immune compartment was composed mainly of macrophages (51% of $CD45^+$ cells), specifically related to subset I, monocytes

Cell

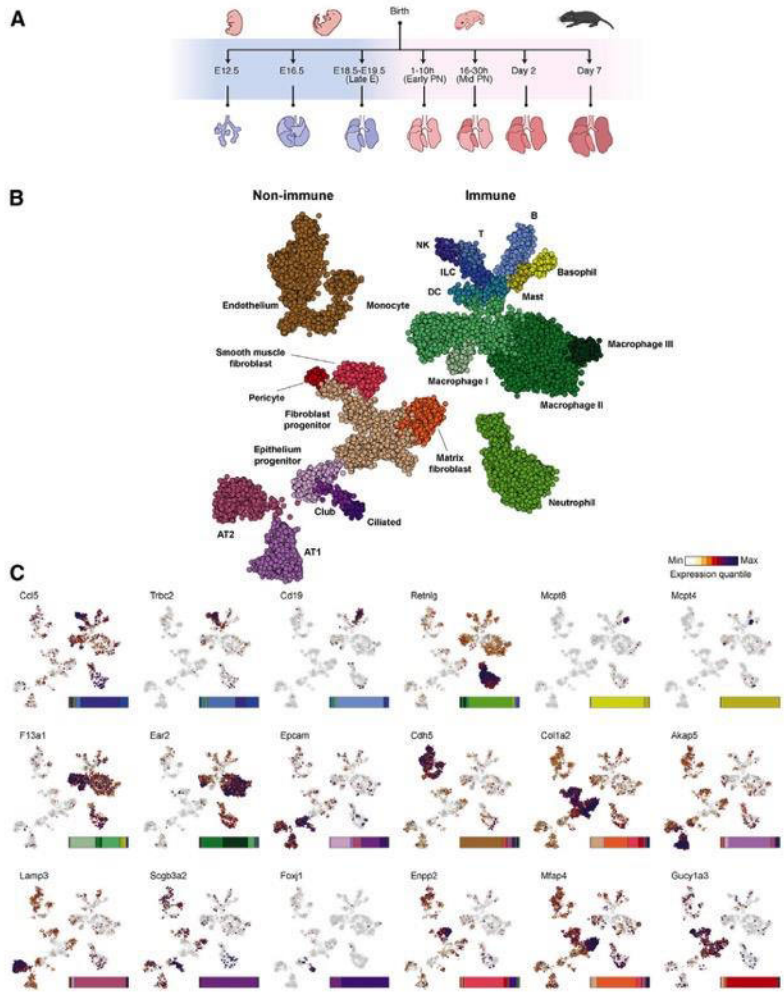

Figure 1. A Single-Cell Map of Lung Cells during Development

(A) Experimental design. Single cells were collected from various time points along lung development.

(B) Single-cell RNA-seq data from immune and non-immune compartments were analyzed and clustered by the MetaCell package (Figures S1H and S1I; Table S2) resulting in a two-dimensional projection of single cells onto a graph representation. 20,931 single cells from 17 mice from all time points were analyzed. 260 meta-cells were associated with 22 cell types and states, annotated, and marked by color code.

(C) Expression quantiles of key cell-type-specific marker genes on top of the 2D map of lung development. Bars depict unique molecular identifier (UMI) distribution of marker genes across all cell types, down-sampled for equal cell numbers. See also Table S1.

(10%), and mast cells (11%), whereas at the canalicular stage (E16.5) monocytes, macrophages (subset II), neutrophils, and basophils were dominant (58%, 13%, 7%, and 4% respectively) and the macrophage I subset was almost diminished. Starting from late pregnancy, all major immune cell populations were present, and later dynamics showed a steady increase in the lymphoid cell compartment (B and T cells), which reached up to 32% of the immune population on day 7 PN, and changes in the composition of the macrophage population (Figure 2B). Similar to the immune compartment, dynamics in non-immune cell composition were most pronounced during pregnancy (Figure 2C); E12.5 was composed mainly of undifferentiated fibroblasts (83%) and progenitor epithelial cells (10%). At E16.5, the progenitor epithelial subset continued to increase (30%) and a new epithelial cell subset of club cells (5%) appeared, in parallel to the appearance of pericytes, an increase in endothelium and the appearance of matrix fibroblasts. The cellular composition stabilized from late pregnancy onward, with the appearance of smooth muscle fibroblasts and branching of epithelium into AT1 and AT2 cells (Figure 2C). These cellular dynamics were consistent across biological replicates (Figures S2C and S2D).

In accordance to previous works (Kopf et al., 2015; Tan and Krasnow, 2016), we identified three distinct macrophage subsets, which we term macrophage I–III. These subsets appeared in waves during development, with macrophage I dominating in early pregnancy, macrophage II culminating around birth, and macrophage III steadily increasing since late pregnancy stage, and becoming the majority on day 7 PN (Figure 2D). Macrophage I cells are transcriptionally distinct from macrophage subsets II–III. Notably, macrophage subsets II–III form a continuous transcriptional spectrum with E16.5 monocytes (Figure 2E), suggesting that macrophages II and III differentiate from fetal liver monocytes, rather than from macrophage subset I, which might have a yolk sac origin (Ginhoux, 2014; Tan and Krasnow, 2016) (Figure 2E). To infer the most probable differentiation trajectory for monocytes and macrophage subsets, we used Slingshot for pseudo-time inference (Street et al., 2017) and characterized a gradual acquisition of macrophage genes from E18.5 onward (late E, Figure 2F). Slingshot trajectory suggests a linear transition of macrophage subsets along the developmental time points. Transcriptionally, macrophage I cells expressed high levels of *Cx3cr1* and complement genes (*C1qa*, *C1qb*) (Figures 2G and S2E). Macrophage II were molecularly reminiscent of monocytes, expressing *Ccr2*, *F13a1*, and *Il1b*, and intermediate levels of alveolar macrophage (AM)-hallmark genes, such as *Il1rn*, *Lpl*, *Pparg*, and *Clec7a* (Kopf et al., 2015; Schneider et al., 2014) (Figures 2G and S2E). Macrophage III expressed a unique set of AM hallmark genes, including; *Pparg*,

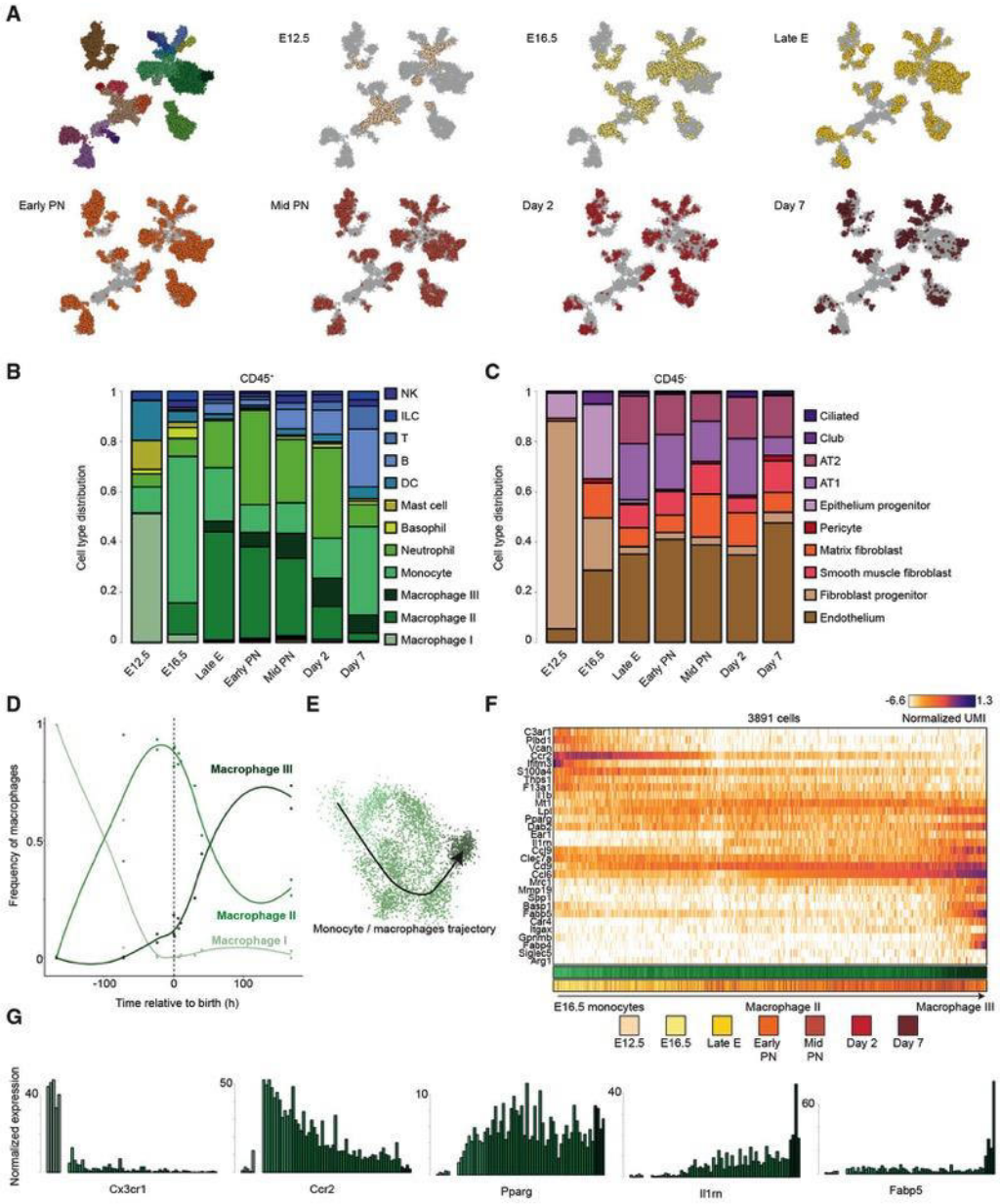

Figure 2. Dynamic Changes in Cellular Composition and Gene Expression during Lung Development

(A) Projection of cells from different time points on the 2D map.

(B and C) Cell type distribution of the immune ($CD45^+$) (B) and non-immune ($CD45^-$) (C) compartments across time points. Time points in (A)–(C) are pooled over several correlated biological replicates at close time intervals (Figures S2A and S2B; Table S1).

(D) Dynamic changes in macrophage compartment composition plotted before and after birth (hours; t_0 = birth). Dots represented biological samples (n = 15). Trend line is computed by local regression (Loess).

(E) Suggested trajectory from monocytes to macrophage II–III on the 2D map.

(F) Gene expression profiles of monocytes and macrophage II–III cells ordered according to Slingshot pseudo-time trajectory (STAR Methods). Lower color bars indicate annotation by cell type (middle) and time point of origin (bottom).

(G) Expression of hallmark monocyte and macrophage genes across meta-cells. Meta-cells are ordered by median pseudo-time; five leftmost meta-cells are macrophage I.

Fabp4, *Fabp5*, *Il1rn*, *Car4*, *Lpl*, *Clec7a*, and *Itgax* (Gautier et al., 2012; Lavin et al., 2014) (Figures 2F, 2G, S2E, and S2F). We similarly reconstructed the differentiation waves in the fibroblast and epithelial lineages, highlighting the main genes associated with the branching of smooth muscle and matrix fibroblasts (Figures S2G–S2K) and priming of epithelium progenitors into AT1 and AT2 cells (Figures S2L and S2M). Together, our data reveal tightly regulated dynamic changes in both cell type composition and gene expression programs along lung development. These cellular and molecular dynamics across different cell types suggest that these programs are orchestrated by a complex network of cellular crosstalk.

Lung Basophils Broadly Interact with the Immune and Non-immune Compartments

In multicellular organisms, tissue function emerges as heterogeneous cell types form complex communication networks, which are mediated primarily by interactions between ligands and receptors (LR) (Zhou et al., 2018). Examining LR pairs in single-cell maps can potentially reveal central cellular components shaping tissue fate (Camp et al., 2017; Zhou et al., 2018). In order to systematically map cellular interactions between cells and reveal potential communication factors controlling development, we characterized LR pairs between all lung cell types (Figure 3A). Briefly, we filtered all LR expressed in at least one meta-cell and associated each ligand or receptor with its expression profile across all cells and along the developmental time points, using a published dataset linking ligands to their receptors (STAR Methods) (Ramilowski et al., 2015).

In the developing lung, modules of LR mainly clustered by cell type (Figures S3A–S3C). However, for some LR, we could identify significant changes in expression levels in the same cell type during development (Figure S3D; Table S3). We projected ligands and receptors based on their correlation structure, resulting in a graphical representation of all LR and their interactions, which highlighted their separation into cell-type related modules (Figure 3B; STAR Methods). The lung LR map showed a clear separation between the communication patterns of the immune and non-immune compartments (Figures 3C and S3E), characterized by enrichment of LR interactions between the immune compartment (I) and itself and between the non-immune compartment (NI) and itself and depletion of interactions between compartments (I-I and NI-NI interactions, $p < 10^{-4}$, Figure S3F). Notably, whereas the majority of crosstalk occurs within each compartment, sporadic I-NI and NI-I interactions might include key signaling pathways for tissue development and homeostasis. We next classified specific ligand families and pathways into functional groups (STAR Methods). As expected, cytokines and components of the complement system were found mainly in the immune compartment, as well as the receptors recognizing them (Figures 3D and 3E). Complementarily, the non-immune compartment was enriched for growth factors, matrix signaling, and cell adhesion ligands and receptors (Figures 3D and 3E).

To identify important cellular communication hubs involved in a large number of interactions between and within compartments, we examined LR expression patterns across different cell types (Table S3). From the non-immune compartment, smooth muscle fibroblasts, expressing *Tgfb3* and the Wnt ligand *Wnt5a* (Nabhan et al., 2018), and AT2 cells, characterized by the exclusive expression of interleukin 33 (*Il33*) and surfactant protein (*Sfpta1*), were involved in complex NI-NI and NI-I signaling (Figures 3F and 3G) (Saluzzo et al., 2017). Within the immune compartment, we observed expression of hallmark receptors important for differentiation and maturation of unique cell subsets, such as *Csf2rb* and *Csf1r* in monocytes and macrophages (Ginhoux, 2014; Guilliams et al., 2013; Schneider et al., 2014) (Figures S3G–S3I). ILC, previously implicated to play an important role in the differentiation of AM (de Kleer et al., 2016; Saluzzo et al., 2017), were found here as the major cells expressing *Csf2* (GM-CSF, Figure 3H). Surprisingly, basophils, comprising a rare population of the immune compartment (1.5%), displayed a rich and complex LR profile, interacting with both the immune and the non-immune compartments. The interaction map highlighted basophils as the main source of many key cytokines and growth factors, such as *Csf1*, *Il6*, *Il13*, and *Hgf* (Figures 3I and S3J), and their counterpart receptors were expressed by unique resident lung cells. Overall, our analysis confirms important and established LR interactions in the process of lung development, while discovering potential novel crosstalk circuits between and within lung immune and non-immune cell types.

Lung Basophils Are Characterized by Distinct Spatial Localization and Gene Signature

In light of the rich interactive profile of basophils (Figure 3I), we hypothesized that these cells may have a central role in cellular communication within the lung, both by responding to lung cues and by modifying the microenvironment. In order to identify the spatial localization of lung basophils, we implemented a Mcpt8$^{YFP/+}$ transgenic mouse model and observed that YFP$^+$ basophils within the lung parenchyma were localized in close proximity to alveoli at 30 hr PN, on day 8.5 PN, and in 8-week-old mice (Figure S4A). We combined TissueFAXS images of whole lobe sections together with a semi-automated computational analysis to accurately identify basophils and quantify their spatial localization in the lung (STAR Methods). We observed that basophils were more likely to reside in proximity to alveoli than randomly selected cells, on day 8.5 PN, and to a lesser extent, in 8-week-old adult mice (Figures 4A and 4B; STAR Methods). In order to further measure basophil spatial organization in the lung parenchyma, we performed tissue clearing followed by left lung lobe imagining of Mcpt8$^{YFP/+}$ mice at different time points. Anti-GFP antibody staining further confirmed that basophils were distributed all over the lung lobes (Figure 4C; Videos S1, S2, and S3).

To molecularly characterize lung basophils, we sought to extensively isolate them by flow cytometry. We gated on basophil-specific markers identified in the data (CD45$^+$FceR1α^+cKit$^-$) and validated our sorting strategy using MARS-seq analysis (Figures S4B and S4C). Analysis of Mcpt8$^{YFP/+}$ transgenic mice showed that 84% of CD45$^+$FceR1α^+cKit$^-$ cells are YFP$^+$ cells, and 98% express the basophil marker CD49b (Figures S4D and S4E). Basophil quantification per whole lung tissue showed a gradual accumulation of this population along tissue development (Figure 4D), and its percentage within the immune population (CD45$^+$) remained stable (Figure 4SF). To inspect whether

Cell

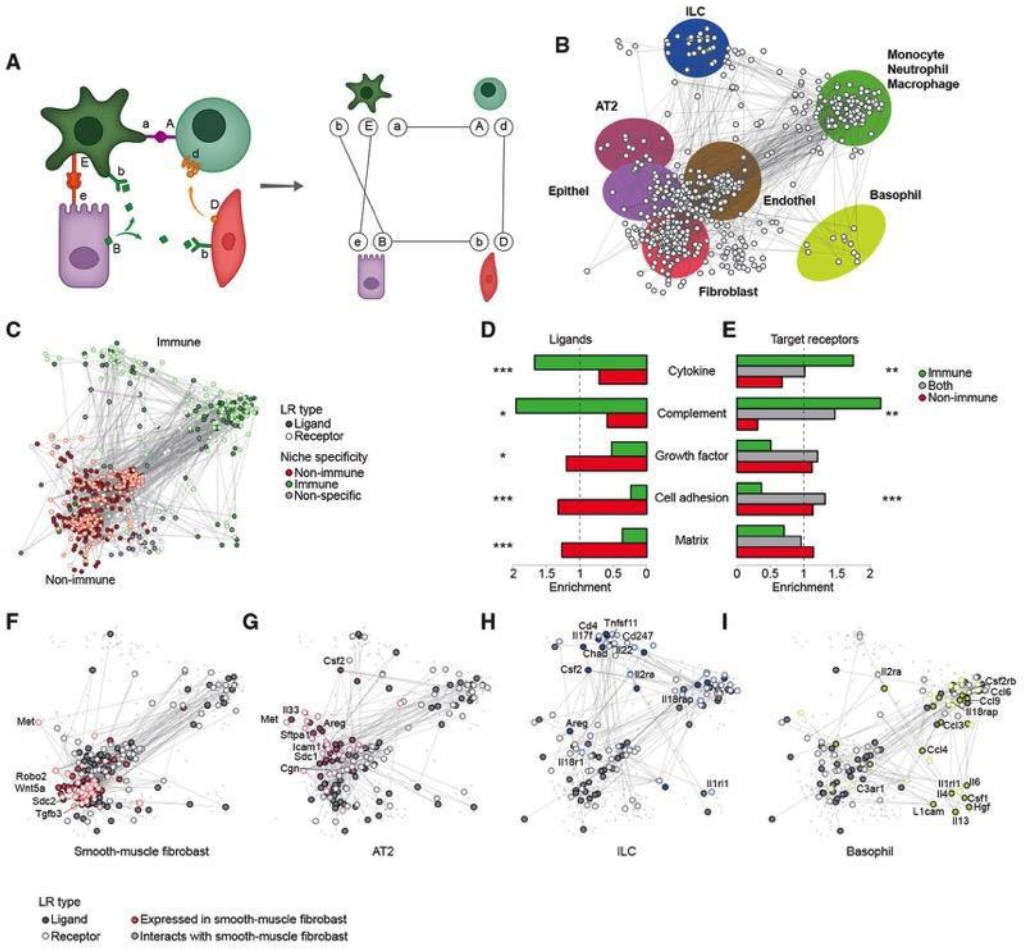

Figure 3. Lung-Resident Basophils Broadly Interact with the Immune and Other Compartments

(A) Illustration of ligand receptor map analysis. Each node is a ligand or receptor, and a line represents an interaction.

(B) The ligand-receptor map of lung development pooled across all time points. Genes (ligands and receptors) were projected on a 2D map based on their correlation structure (STAR Methods). Genes related to specific cells were marked by their unique colors according to Figure 1.

(C) Projection of genes activated in the immune (green) and non-immune (red) compartments (Figure S3D). Full and empty circles represent ligands and receptors, respectively. Gray circles represent ligand/receptors non-specific to one compartment.

(D and E) Ligands were classified to functional groups by GO-enrichment (STAR Methods).

(D) Enrichment of functional groups of ligands in the immune and non-immune compartments.

(E) Enrichment of receptors whose ligands are from different functional groups in the immune and non-immune compartments. False discovery rate (FDR) corrected Fisher exact test.

(F–I) LR interaction maps of smooth-muscle fibroblasts (F), AT2 cells (G), ILC (H), and basophils (I). Colored nodes represent genes upregulated in the cell type (>2 fold change), and gray nodes represent their interacting partners. Full and empty circles represent ligands and receptors, respectively. *$p < 0.05$, **$p < 0.01$, ***$p < 0.005$.

See also Table S3.

lung basophils have a unique resident expression program that is not observed in the circulation, we sorted time point-matched basophils from lung and peripheral blood for MARS-seq analysis (Figure S4F). The gene expression profile of lung basophils differed from blood-circulating basophils, characterized by a unique gene signature, that includes expression of *Il6*, *Il13*, *Cxcl2*, *Tnf*, *Osm*, and *Ccl4* (Figures 4E and 4F). This unique gene signature persisted in the adult lung resident basophils (Figures 4F, 4G, and S4G; Table S4). Notably, the ligands *Il6*, *Hgf*, and *L1cam* are exclusively expressed by lung basophils, compared to other lung immune and non-immune cells (Figures S4H and S4I). Together, we show that lung resident basophils reside within the tissue parenchyma, specifically localize near the alveoli, and acquire distinct and persistent

Cell

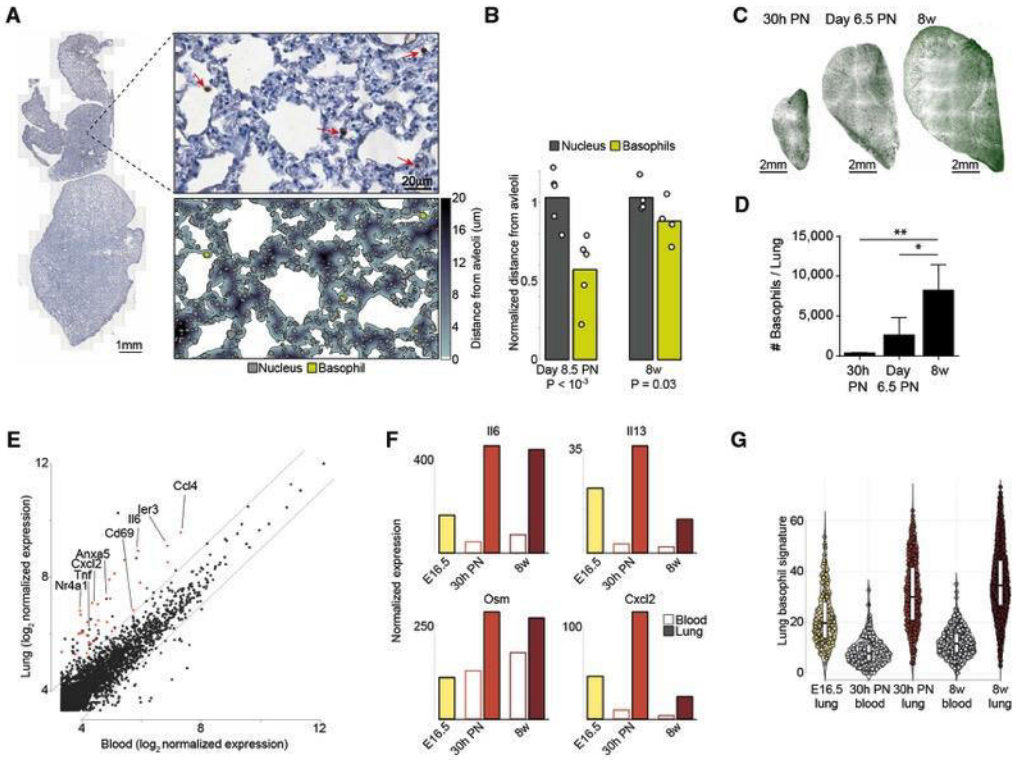

Figure 4. Spatial and Transcriptomic Characterization of Lung Basophils

(A) Detection of alveoli, nuclei, and basophils in whole lobe sections of Mcpt8$^{YFP/+}$ mice by TissueFAXS. Inset: red arrows point at YFP$^+$ basophils. Bottom: output of computational analysis showing alveoli (white), nuclei (gray), and basophils (yellow). Heat colors indicate distance from nearest alveoli (STAR Methods). Scale bars, 1 mm (whole lobe) and 20 μm (representative section).

(B) Quantification of basophil (yellow) distance from the alveoli compared to all other nuclei (gray) at day 8.5 PN and 8-week-old adult mice. Distances were normalized to median value across all nuclei. p values calculated by permutation test (STAR Methods). n = 4–5 mice per group.

(C) Representative images of Mcpt8$^+$ basophils (green) in cleared lungs derived from 30 hr PN, day 6.5 PN, and 8-week-old adult mice. Scale bar, 2 mm.

(D) Quantification of lung basophil numbers in whole lungs at different developmental time points by flow cytometry. n = 3–4 mice per group. One-way ANOVA; Student's t-test (two-tailed) between 8-week-old and day 6.5 PN and between 8-week-old and 30 hr PN.

(E) Differential gene expression of basophils derived from lung (y axis) and peripheral blood (x axis) at 30 hr PN.

(F) Expression of ligands specific to lung basophils across blood and lung basophils at E16.5, 30 hr PN, and 8- week-old. Values for (E) and (F) indicate normalized expression per 1,000 UMI scaled to number of cells.

(G) Distribution of lung basophil-specific signature (Figure S4G) across blood and lung basophils from time-matched developmental time points. Boxplots display median bar, 1st–3rd quantile box, and 5th–95th percentile whiskers. *p < 0.05, **p < 0.01.

See also Table S4 and Videos S1, S2, and S3.

lung- characteristic signaling and gene program compared to their circulating counterparts.

IL33 and GM-CSF Imprint the Lung-Alveolar Basophil Transcriptional Identity

Because lung-resident basophils showed a unique gene expression signature, we analyzed the data for lung-specific signals that can serve as differentiation cues for lung basophil receptors (Table S3). *Csf2* (GM-CSF) is a hematopoietic growth factor, whose role in shaping the lung microenvironment and specifically AM, has long been established (Ginhoux, 2014; Guilliams et al., 2013; Shibata et al., 2001). Interestingly, we found that the major source of *Csf2* expression in the lung stemmed from ILC and the basophils themselves, with only a small contribution from AT2 cells. Among all lung cells, basophils expressed the highest RNA and protein levels of *Csf2rb*, a major receptor for *Csf2* (Figures 5A and 5B). In addition, basophils and mast cells expressed the highest RNA and protein levels of the receptor *Il1rl1* (IL33R/ST2), which specifically binds *Il33* (Figures 5C and 5D). Previous reports identified IL-33 as a major driver for cellular differentiation and lung maturation, expressed mainly by AT2 cells. Specifically, lung ILC-2 were previously reported to depend on IL33-ST2 signaling for their function (de Kleer et al., 2016; Saluzzo et al., 2017). Single-molecule fluorescent *in situ* hybridization (smFISH) staining of post-natal lung tissue for *Il1rl1* and *Il33* genes, together with the basophil marker *Mcpt8*,

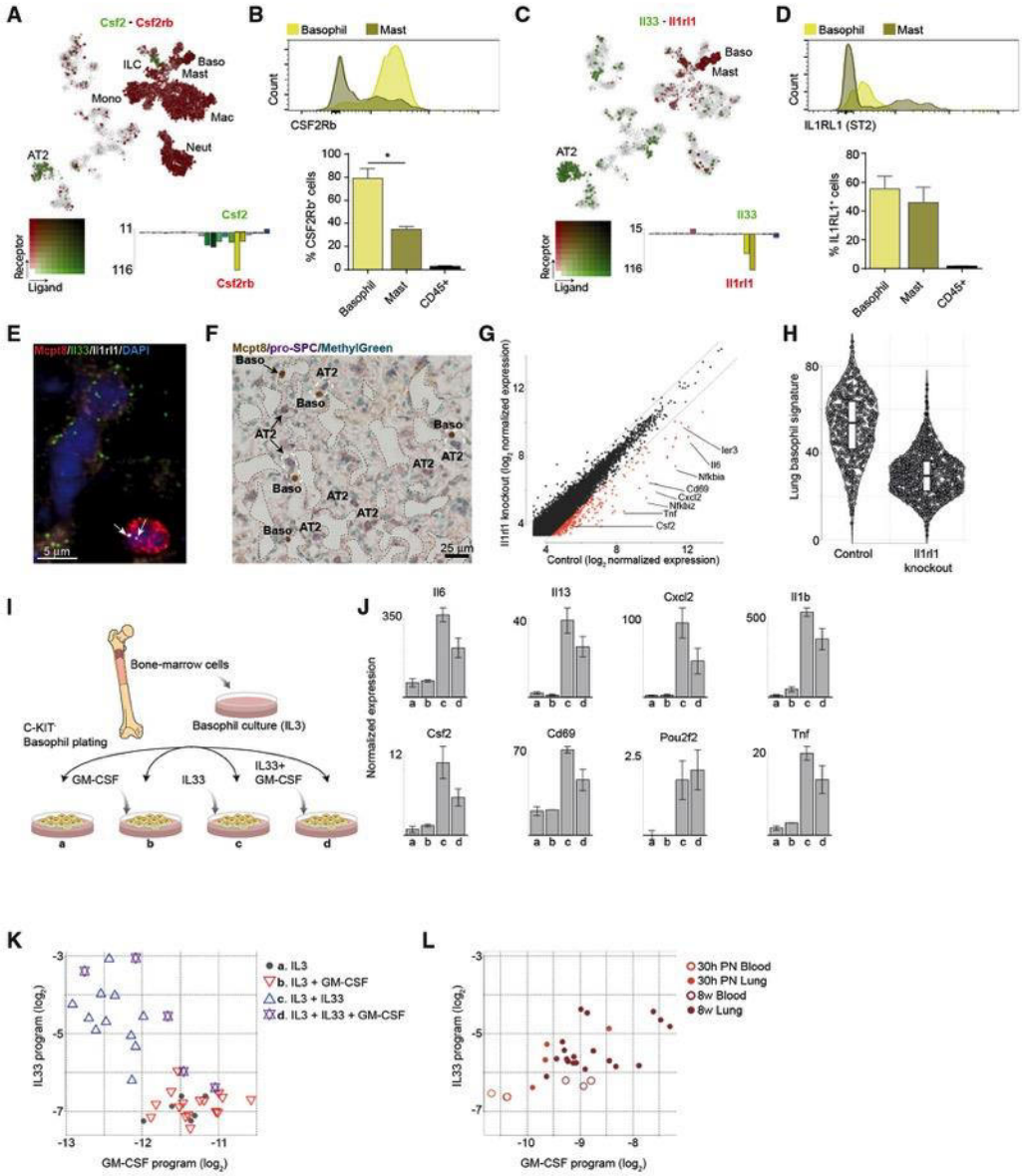

Figure 5. Lung-Resident Basophils Are Primed by IL33 and GM-CSF

(A) Dual projection of the ligand *Csf2* (green) and its unique receptor *Csf2rb* (red) on the single-cell map from Figure 1. Colors indicate expression quantiles. Bar plots indicate ligand and receptor normalized expression per 1,000 UMI across cell types.

(B) Quantification of CSF2Rb$^+$ lung basophils compared to mast cells and total CD45$^+$ cells at 30 hr PN by flow cytometry; n = 2 mice per group. One-way ANOVA: Student's t-test (two-tailed) between basophils and mast cells.

(C) As (A) but for the ligand *Il33* (green) and its unique receptor *Il1rl1* (red).

(D) As (B) but for IL1RL1$^+$ lung basophils; n = 3 mice per group.

(E) Representative smFISH image of mRNA molecules for *Mcpt8* (red), a marker for basophils, *Il33* (green), a ligand expressed by AT2 cells, and *Il1rl1* (white), the counterpart receptor expressed by basophils, together with DAPI staining (blue) to mark cell nuclei, in lung tissue derived from 8 days PN. Scale bar, 5 µm.

(F) Representative IHC image of Mcpt8$^+$ basophils (brown) and pro-SPC$^+$ AT2 cells (purple) together with methyl green staining for cell nuclei detection (green) in a lung section derived from adult (8-week-old) mice, showing their spatial proximity to each other and to the alveoli. Scale bar, 25 µm.

(G) Differential gene expression between 30 hr PN lung basophils from Il1rl1 (ST2) knockout (y axis) versus littermate controls (x axis). Values indicate $\log_2$ normalized expression per 1,000 UMI /cells.

(legend continued on next page)

Cell

showed co-expression of these genes in neighboring cells, suggesting that basophils and AT2 cells reside in spatial proximity in the lung tissue (Figure 5E). Immunohistochemistry (IHC) staining of AT2 and basophils at adult lung tissue further confirmed these results and localized this signaling in the alveoli niche (Figure 5F). To functionally validate the effects of IL-33 signaling on the lung-basophil gene expression profile, we purified basophils from the lungs of *Il1rl1* (IL33R) knockout mice for MARS-seq analysis. We found that Il1rl1-deficient lung basophils lacked expression of many of the genes specific to lung-resident basophils, and showed higher similarity to blood-circulating basophils (Figures 5G, 5H, and S5A), suggesting that IL-33 signaling is mediating a large part of the specific gene signature of lung basophils.

In order to test whether the lung environmental signals IL-33 and GM-CSF are directly responsible for inducing the lung basophil phenotype, we used an *in vitro* system where we cultured bone marrow (BM)-derived basophils in media supplemented with these cytokines. We differentiated BM-derived cells in IL3-supplemented medium, isolated basophils by negative selection of cKit (BM-basophils), and cultured them in the presence of growth media alone (IL3) or with different combinations of the lung cytokine milieu; GM-CSF and/or IL-33 (Figure 5I, S5B-C). We found that IL-33 and GM-CSF each induced a specific transcriptional program (Figure S5D). IL-33 induced a major part of the lung basophil gene signature including the ligands *Il6*, *Il13*, *Il1b*, *Tnf*, *Cxcl2*, and *Csf2*, as well as the transcription factor *Pou2f2* (Figures 5J and S5E), while GM-CSF induced a smaller set of the lung basophil gene program. Interestingly, we found that cells cultured with both GM-CSF and IL-33 activated both programs, suggesting a combinatorial effect of both cytokines on the BM-basophil signature (Figures 5K and S5F). Furthermore, revisiting the *in vivo* lung and blood basophils by projecting their gene expression profile on the GM-CSF/IL-33 differentiation programs revealed a time point-independent upregulation of both expression programs in lung-resident basophils compared to basophils from circulation (Figure 5L). Further support for two independent signaling programs was derived from the Il1rl1 knockout mice, which showed that Il1rl1-knockout basophils perturbed the IL-33 program without any change in expression of GM-CSF-induced genes (Figure S5G). Together, a combination of knockout data and *in vitro* assay demonstrate that the lung environment imprints a robust transcriptional program in basophils, which is mediated by at least two independent signaling pathways, dominated by IL-33, and with minor contribution of GM-CSF.

Lung Basophils Imprint Naive Macrophages with an Alveolar Macrophage Phenotype

The expression of critical lung signaling molecules by basophils prompted us to explore their signaling activity and contribution in shaping the unique phenotype of other lung resident cells. As lung-resident basophils highly express *Il6*, *Il13*, and *Csf1*, three important myeloid growth factors, we hypothesized that they may interact with other myeloid cells, particularly macrophages, via *Il6ra*, *Il13ra* and *Csf1r* (Figures 3, 6A–6D, and S6A). IHC of basophils (Mcpt8) and macrophages (F4/80) showed their spatial proximity within lung parenchyma during the alveolarization process (Figure 6E). In order to evaluate the impact of basophils on macrophage differentiation, we tested the effect of lung-basophil depletion on the maturation of lung myeloid cells. For this purpose, we administered anti-Fcεr1α (MAR1) antibody or isotype control intra-nasally to neonatal mice to induce local depletion of basophils (two injections at 12 hr and 16 hr PN; STAR Methods) and collected lung CD45$^+$ cells 30 hr PN for MARS-seq analysis (Figure S6B). The anti-Fcεr1α antibody efficiently and specifically depleted basophils in the lung, without perturbing the frequencies of other immune cells, determined both by FACS and MARS-seq (Figures 6F, S6C, and S6D). Lung basophil depletion was coupled with a reduction of the AM fraction (macrophage III) within the macrophage compartment (Figure 6G). Moreover, macrophages derived from basophil-depleted lungs showed a decrease in expression of genes reminiscent of mature AM, including an anti-inflammatory (M2) module (*Clec7a*, *Ccl17*) and an increase in genes related to macrophage II ($p = 10^{-4}$; Figures 6H, S6E, and S6F). Specifically, we observed downregulation in the levels of *Il1rn*, *Ear1*, *Lpl*, *Clec7a*, and *Siglec5*, hallmark genes of AM, concomitantly with the induction of *F13a1*, a gene shared by macrophage II and monocytes (Figure 6I). Because a proper AM maturation process is critical for their role in lung-immunomodulation and as phagocytic cells, we further characterized the effect of constitutive basophil depletion on AM function in adults. For this, we compared cells derived from bronchoalveolar lavage fluid (BALF) of adult Mcpt8$^{cre/+}$DTA$^{fl/+}$ mice, depleted specifically of basophils, to littermate controls. In both conditions, BALF cells consisted of 98% AM (Figure S6G). However, Mcpt8$^{cre/+}$DTA$^{fl/+}$ BALF had an overall lower cell count compared to control littermates (Figure 6J). Importantly, Mcpt8$^{cre/+}$DTA$^{fl/+}$-derived AM were impaired in the phagocytosis of inactivated bacteria compared to controls (Figure 6K). Together, our data show that the lung-basophil AM niche is

(H) Distribution of lung basophil-specific signature (Figure S4G) in Il1rl1 knockout and littermate controls. Boxplots display median bar, 1st–3rd quantile box, and 5th–95th percentile whiskers.

(I) Illustration of experimental paradigm for *in vitro* culture. BM-derived cells were grown with IL3 to induce basophils for 10 days and then cKit$^-$ cells were sorted for plating (Figure S4J). Basophils were plated for 16 hr with IL3 alone (a), IL3 and GM-CSF (b), IL3 and IL33 (c), and a combination of IL3, IL33, and GM-CSF (d). Gene expression of single-cell-sorted basophils was evaluated by MARS-seq.

(J) Expression of key genes across the four conditions. Values indicate normalized expression per 1,000 UMI per cell.

(K) Scoring meta-cells from the four conditions for their expression of the IL33-induced program (y axis) and the GM-CSF-induced program (x axis; Figure S4L). Meta-cell identity is determined by the majority of cells.

(L) Scoring meta-cells from 30 hr PN lung (filled red circles) and blood circulating (empty red circles) basophils, and adult (8-week-old) lung (filled brown circles) and blood circulating (empty brown circles) basophils projected on the gene-expression programs described in (K). (J–L) Samples were prepared in triplicates, and results are representative of three independent experiments. *$p < 0.05$, **$p < 0.01$. Data are represented as mean ± SEM.

See also Figure S5.

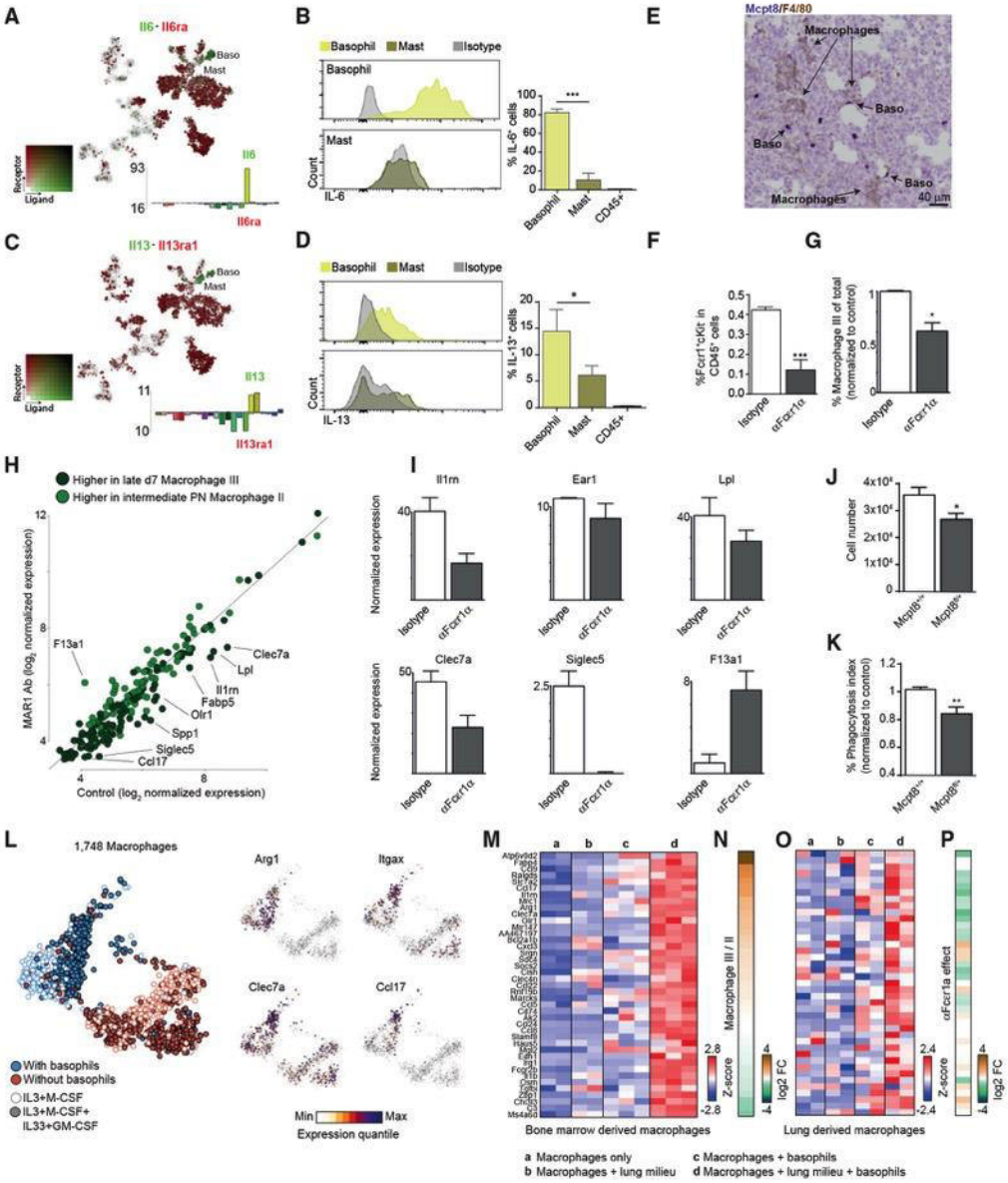

Figure 6. Lung Basophils Are Essential for Transcriptional and Functional Development of AM

(A) Dual projection of the ligand *Il16* (green) and its unique receptor *Il6ra* (red) on the single-cell map from Figure 1. Colors indicate expression quantiles. Bar plots indicate ligand and receptor normalized expression per 1,000 UMI across cell types.

(B) Histogram and quantification of intracellular staining of IL-6, compared to isotype control within lung basophils, mast cells, and total CD45$^+$ cells at 30 hr PN, by flow cytometry; n = 6 mice per group.

(C) As in (A) but for *Il13* (green) and its receptor *Il13ra1* (red).

(D) As in (B) but for IL-13; n = 6 mice per group. (A–D) One-way ANOVA; Student's t-test (two-tailed) between basophil and mast cells.

(E) Representative IHC image of Mcpt8$^+$ basophils (dark purple) and F4/80$^+$ macrophages (brown) on hematoxylin staining (light purple) in lung section derived from 8 days PN mice showing their spatial proximity. Scale bar, 40 μm.

(F–I) Newborn mice were injected intra-nasally with anti-Fcεr1α antibody for basophils depletion or with isotype control, and viable CD45$^+$ cells were sorted for MARS-seq processing and analysis at 30 hr PN. Each sample was pooled from three lungs, and results are representative of three replicates in two independent experiments.

(legend continued on next page)

important for differentiation, compartmentalization, and phagocytic properties of AM.

The effect of lung basophils on AM maturation *in vivo* led us to ask whether lung basophils can promote transition of monocytes or naive macrophages toward the AM signature directly. For this hypothesis, we performed an *in vitro* co-culturing assay. Naive BM-derived macrophages (BM-MΦ) were cultured alone or co-cultured with BM basophils in growth media supporting both cell types (M-CSF and IL-3, respectively), with or without a combination of GM-CSF and IL-33, the milieu signaling that primes basophils toward the lung-basophil phenotype (Figure S6H; STAR Methods). Co-culturing of BM-basophils with BM-MΦ did not change the previously characterized basophil phenotype in any condition (Figure S6I). However, meta-cell analysis showed a clear distinction between BM-MΦ that were cultured with and without basophils (Figure 6L). Importantly, only BM-MΦ grown in the presence of lung milieu-primed (GM-CSF + IL33) basophils upregulated genes associated to AM, including an anti-inflammatory (M2) module (*Cc17*, *Clec7a*, *Arg1*, and *Itgax*; Figures 6L, 6M, and S6J). Notably, this effect on BM-MΦ polarization was not seen when macrophages were cultured in a medium that was supplemented with lung environmental cytokines (GM-CSF and IL-33) alone, showing that these cytokines mediate the signaling effect via basophils (Figures 6L and 6M). We characterized a large and reproducible change in gene expression of BM-MΦ co-cultured with lung milieu-primed basophils compared to all other conditions, affecting many genes differentially expressed between macrophage subsets III (mature AM) and II, previously associated with the alternative anti-inflammatory (M2) polarization phenotype ($p < 10^{-10}$; Figures 6M, 6N, S6K, and S6L) (Gordon, 2003). To further examine the direct effect of lung milieu-primed basophils on AM maturation, we next purified $CD45^+CD115^+$ myeloid cells containing mainly monocytes and undifferentiated AM from 30 hr PN lungs, and performed the co-culture experiment (Figure S6G). Importantly, the same lung basophil program induced in naive BM-MΦ *in vitro* (Figure 6M) was also upregulated in monocytes and undifferentiated AM that were cultured with lung milieu-primed basophils (GM-CSF + IL-33) (Figure 6O), while it was downregulated in macrophages derived from basophil-depleted lungs (Figure 6P). These data suggest that the basophil phenotype might be imprinted by tissue environmental cues, and as a result, they mediate immunomodulating activities in tissue myeloid cells. We therefore compared gene expression profiles of basophils derived from lungs of 8-week-old mice to basophils isolated from the tumor microenvironment of B16 melanoma cell line injected mice and from spleen and liver of 8-week-old mice (Figure S6M). While all tissue basophils highly expressed basophil marker genes (e.g., *Mcpt8*, *Cpa3*, *Cd200r3*, *Fcer1α*), the lung signature was exclusive, with higher similarity to tumor-derived basophils, mainly in expression of immune suppression genes such as *Il4*, *Il6*, *Osm*, and *Il13* (Figures S6M and S6N). Taken together, our data indicate that the instructive signals from the lung environment imprint basophils with a unique signature of cytokines and growth factors, which subsequently propagate important signals to other lung resident cells, including the polarization of AM toward phagocytic and anti-inflammatory macrophages.

DISCUSSION

Despite their great promise, single-cell RNA-seq methods are still limited in their ability to reconstruct cellular signaling and location of unique niche structures, which are central to our understanding of molecular mechanisms involved in tissue development, homeostasis, and disease (Giladi and Amit, 2018). Recent efforts applied *ex vivo* and organoid assays to explore interactions between cells (Camp et al., 2017), but this has not

(F) Fraction of basophils ($Fc\varepsilon r1\alpha^+cKit^-$) from total $CD45^+$ cells in lungs derived from anti-$Fc\varepsilon r1\alpha$ and isotype control injected mice, as determined by FACS. Student's t-test (two-tailed) for percent of lung basophils; n = 3.
(G) Fraction of macrophage III from total macrophages in lungs derived from anti-$Fc\varepsilon r1\alpha$ and isotype control-injected mice. Numbers were scaled to match control levels between experiments. Student's t-test (two-tailed) for percent of AM.
(H) Expression of genes differentially expressed between macrophage II (light green) and macrophage III (dark green) cells in anti-$Fc\varepsilon r1\alpha$ (y axis)- and isotype control (x axis)-treated mice. Values indicate normalized expression per 1,000 UMI /cells.
(I) Median expression of hallmark AM and macrophage II (*F13a1*) genes in anti-$Fc\varepsilon r1\alpha$ versus isotype control-treated mice.
(J and K) AM derived from BALF of Mcpt8 knockout and their littermate controls were purified from adult, 8- to 12-week-old mice. Results are from four independent experiments; each of them consists of at least four replicates.
(J) BALF cell count of Mcpt8 knockout and their littermate control mice. Student's t-test for percent of AM.
(K) Phagocytosis capacity of AM derived from BALF of Mcpt8 knockout versus littermate control mice. Results are shown as fold change of phagocytosis index compared to averaged controls. Student's t-test for percent of AM.
(L–P) Co-culture experiment of BM-MΦ- and BM-derived basophils. BM-derived cells were split and grown into basophils (IL3) for 10 days and macrophages (M-CSF) for 8 days. Macrophages were then co-cultured with (a) M-CSF + IL3, (b) IL33 and GM-CSF, (c) naive basophils, and (d) lung milieu-primed basophils in the presence of IL33 and GM-CSF.
(L) A two-dimensional representation of the meta-cell analysis of co-cultured macrophages from the four conditions. Right: expression quantile of selected AM related genes onto the 2D projection.
(M) A lung milieu-primed basophil-induced program in co-cultured macrophages is associated with macrophage priming toward AM and immune suppression. Biological replicates are shown.
(N) Differential expression (log2 fold change) of the genes in M between macrophage III and II during development.
(O) Expression of the genes in M across $CD45^+CD115^+$ myeloid cells sorted from 30 hr PN lungs, grown under the same conditions as in (M). Biological replicates are shown.
(P) Differential expression (log2 fold change) of the genes in (M) between macrophages derived from lungs injected with anti-$Fc\varepsilon r1\alpha$ and isotype control. $^*p < 0.05$, $^{**}p < 0.01$, $^{***}p < 0.001$. Data are represented as mean ± SEM.
See also Figure S6.

been approached yet in the context of whole tissues *in vivo*. Here, we combined tissue developmental dynamics in the level of single-cell RNA-seq profiling, with an extensive screen for all ligand-receptor interactions between cell types, generating a comprehensive cellular network of all lung types.

Basophils are thought to be short-lived granulocytic cells, and their major function has been mainly attributed to induction of Th2 responses in allergy and IL-4 secretion after helminth infection (Min et al., 2004; Sokol et al., 2009). However, their role in tissue development and homeostasis is unclear. We found that lung basophils are characterized by expression of many cytokines and growth factors, critical for immune and non-immune cell functions. Historically, due to morphological and gene expression similarities, many functional features have been attributed, interchangeably, to both mast cells and basophils, mainly regarding their involvement in allergy responses (Varricchi et al., 2018). Nonetheless, unlike mast cells, which enter tissues as immature progenitors and finalize their development inside them, basophils were thought to reach full differentiation in hematopoietic tissues and circulate in the blood until they are eliminated or recruited into tissues under pathological conditions (Marone et al., 2002). Interestingly, the novel lung alveolar basophil subset we identified exists in the lung in early developmental stages, and also during adulthood, and exhibits tissue-specific characteristics dependent on lung-specific signals.

Lung basophils acquire their unique phenotype due to exposure to lung-specific signals, GM-CSF and IL33, both *in vivo* and *in vitro*. This is in accordance with *in vitro* studies showing elevation in IL-6 and IL-4 expression by basophils following exposure to IL33 and a combinatorial effect of both IL33 and GM-CSF on increased survival rate of the cytokine supplemented basophils (Chhiba et al., 2017; Schneider et al., 2009). Lung basophils form a complex signaling network through their exclusive ligands, such as *Il6* and *Hgf* (Ohmichi et al., 1998), by communicating with receptors expressed by a vast range of cell types. Notably, *Il6* expression, which is the most significant feature of lung basophils, was attributed previously to the induction of humoral memory immune responses and to the induction of Th17 differentiation in the context of basophils (Yuk et al., 2017). However, it may have other functions in the developing lung, because the lymphocyte compartment is only established in late stages of lung development.

Lung basophils polarize AM toward an anti-inflammatory state (M2), evident by the elevated expression of the hallmark anti-inflammatory genes *Arg1*, *Clec7a*, and *Itgax* (Gordon, 2003). The unique signaling of lung alveolar basophils, together with their gene expression resemblance to basophils derived from tumor microenvironment, suggest they may play a role in pathologies and have potential for generating new immunotherapies. In pathologies characterized by chronic inflammation, introduction of IL33-imprinted basophils (or the cytokines they secrete) may induce macrophages toward anti-inflammatory responses and promote inflammation resolution. Conversely, in pathologies that are exacerbated due to function of anti-inflammatory macrophages, as happens in many tumors and pulmonary fibrosis, basophil depletion may be beneficial in attenuating the detrimental immune response by suppression of tumor associated and the pro-fibrotic macrophage activity.

STAR★METHODS

Detailed methods are provided in the online version of this paper and include the following:

- KEY RESOURCES TABLE
- EXPERIMENTAL MODEL AND SUBJECT DETAILS
  - Mice
  - Tumor cell line
- METHOD DETAILS
  - Lung dissociation and single cell sorting
  - Isolation of peripheral blood cells
  - Tumor microenvironment dissociation
  - Spleen dissociation
  - Liver dissociation
  - Flow cytometry and sorting
  - BM derived cell cultures
  - MARS-seq Library preparation
  - Lung-resident basophil depletion
  - Phagocytosis assay
  - Single-molecule fluorescent *in situ* hybridization
  - Histology and immunohistochemistry
  - Tissue clearing
- QUANTIFICATION AND STATISTICAL ANALYSIS
  - Low level processing and filtering
  - Data processing and clustering
  - Trajectory finding
  - Interaction maps
  - Mapping cells to the lung cluster model
  - Basophil profiling, ex vivo and co-culture analysis
  - TissueFAXS quantification
  - Data and Software Availability

SUPPLEMENTAL INFORMATION

Supplemental Information includes six figures, five tables, and three videos and can be found with this article online at https://doi.org/10.1016/j.cell.2018.09.009.

ACKNOWLEDGMENTS

We thank Tal Bigdary for artwork. I.A. is supported by the Chan Zuckerberg Initiative (CZI), the HHMI International Scholar award, the European Research Council Consolidator Grant (ERC-COG; 724471-HemTree2.0), an MRA Established Investigator Award (509044), the Israel Science Foundation (703/15), the Helen and Martin Kimmel Award for Innovative Investigation, the SCA award of the Wolfson Foundation, and the Wolfson Foundation and Family Charitable Trust. S.K. is supported by the Austrian Science Fund (FWF), DK Cell Communication in Health and Disease (W 1205-B09), and the Special Research Program Chromatin Landscapes (L-Mac: F 6104-B21). T.H. is supported by the ERC-2015-AdG-695136. M.C. is supported by a postdoctoral fellowship in Applied and Engineering Science, Israeli Government, Ministry of Science and Technology. A.G. is supported by the Clore fellowship. A.D.G. received support from an EMBO short-term fellowship (#6879).

AUTHOR CONTRIBUTIONS

M.C. developed experimental protocols; conceived, designed, performed, and analyzed experiments; and wrote the manuscript. A.G. conceived, designed, and analyzed experiments; developed computational methods; performed bioinformatic analysis; and wrote the manuscript. A.-D.G. conceived, designed, performed, and analyzed experiments. D.G.S.

Cell

developed computational methods and performed bioinformatic analysis. M.Z., A.H., A.M., T.-M.S., K.B.H., E.D., S.I., and T.H. contributed to the experiments. S.K. conceived, designed, and supervised experiments. I.A. directed the project; conceived, designed, and analyzed experiments; and wrote the manuscript.

DECLARATION OF INTERESTS

A patent application has been filed related to this work.

Received: March 30, 2018
Revised: July 16, 2018
Accepted: September 7, 2018
Published: October 11, 2018

REFERENCES

Camp, J.G., Sekine, K., Gerber, T., Loeffler-Wirth, H., Binder, H., Gac, M., Kanton, S., Kageyama, J., Damm, G., Seehofer, D., et al. (2017). Multilineage communication regulates human liver bud development from pluripotency. Nature *546*, 533–538.

Chhiba, K.D., Hsu, C.L., Berdnikovs, S., and Bryce, P.J. (2017). Transcriptional heterogeneity of mast cells and basophils upon activation. J. Immunol. *198*, 4868–4878.

Cohen, M., Matcovitch, O., David, E., Barnett-Itzhaki, Z., Keren-Shaul, H., Blecher-Gonen, R., Jaitin, D.A., Sica, A., Amit, I., and Schwartz, M. (2014). Chronic exposure to TGFβ1 regulates myeloid cell inflammatory response in an IRF7-dependent manner. EMBO J. *33*, 2906–2921.

de Kleer, I.M., Kool, M., de Bruijn, M.J., Willart, M., van Moorleghem, J., Schuijs, M.J., Plantinga, M., Beyaert, R., Hams, E., Fallon, P.G., et al. (2016). Perinatal activation of the interleukin-33 pathway promotes type 2 immunity in the developing lung. Immunity *45*, 1285–1298.

Denzel, A., Maus, U.A., Rodriguez Gomez, M., Moll, C., Niedermeier, M., Winter, C., Maus, R., Hollingshead, S., Briles, D.E., Kunz-Schughart, L.A., et al. (2008). Basophils enhance immunological memory responses. Nat. Immunol. *9*, 733–742.

Fuzik, J., Zeisel, A., Máté, Z., Calvigioni, D., Yanagawa, Y., Szabó, G., Linnarsson, S., and Harkany, T. (2016). Integration of electrophysiological recordings with single-cell RNA-seq data identifies neuronal subtypes. Nat. Biotechnol. *34*, 175–183.

Gautier, E.L., Shay, T., Miller, J., Greter, M., Jakubzick, C., Ivanov, S., Helft, J., Chow, A., Elpek, K.G., Gordonov, S., et al.; Immunological Genome Consortium (2012). Gene-expression profiles and transcriptional regulatory pathways that underlie the identity and diversity of mouse tissue macrophages. Nat. Immunol. *13*, 1118–1128.

Giladi, A., and Amit, I. (2018). Single-cell genomics: a stepping stone for future immunology discoveries. Cell *172*, 14–21.

Giladi, A., Paul, F., Herzog, Y., Lubling, Y., Weiner, A., Yofe, I., Jaitin, D., Cabezas-Wallscheid, N., Dress, R., Ginhoux, F., et al. (2018). Single-cell characterization of haematopoietic progenitors and their trajectories in homeostasis and perturbed haematopoiesis. Nat. Cell Biol. *20*, 836–846.

Ginhoux, F. (2014). Fate PPAR-titioning: PPAR-γ 'instructs' alveolar macrophage development. Nat. Immunol. *15*, 1005–1007.

Gordon, S. (2003). Alternative activation of macrophages. Nat. Rev. Immunol. *3*, 23–35.

Guilliams, M., De Kleer, I., Henri, S., Post, S., Vanhoutte, L., De Prijck, S., Deswarte, K., Malissen, B., Hammad, H., and Lambrecht, B.N. (2013). Alveolar macrophages develop from fetal monocytes that differentiate into long-lived cells in the first week of life via GM-CSF. J. Exp. Med. *210*, 1977–1992.

Hashimoto, D., Chow, A., Noizat, C., Teo, P., Beasley, M.B., Leboeuf, M., Becker, C.D., See, P., Price, J., Lucas, D., et al. (2013). Tissue-resident macrophages self-maintain locally throughout adult life with minimal contribution from circulating monocytes. Immunity *38*, 792–804.

Huang, W., Sherman, B.T., and Lempicki, R.A. (2009). Systematic and integrative analysis of large gene lists using DAVID bioinformatics resources. Nat. Protoc. *4*, 44–57.

Hussell, T., and Bell, T.J. (2014). Alveolar macrophages: plasticity in a tissue-specific context. Nat. Rev. Immunol. *14*, 81–93.

Itzkovitz, S., Blat, I.C., Jacks, T., Clevers, H., and van Oudenaarden, A. (2012). Optimality in the development of intestinal crypts. Cell *148*, 608–619.

Jaitin, D.A., Kenigsberg, E., Keren-Shaul, H., Elefant, N., Paul, F., Zaretsky, I., Mildner, A., Cohen, N., Jung, S., Tanay, A., and Amit, I. (2014). Massively parallel single-cell RNA-seq for marker-free decomposition of tissues into cell types. Science *343*, 776–779.

Kim, D., Langmead, B., and Salzberg, S.L. (2015). HISAT: a fast spliced aligner with low memory requirements. Nat. Methods *12*, 357–360.

Kopf, M., Schneider, C., and Nobs, S.P. (2015). The development and function of lung-resident macrophages and dendritic cells. Nat. Immunol. *16*, 36–44.

Lavin, Y., Winter, D., Blecher-Gonen, R., David, E., Keren-Shaul, H., Merad, M., Jung, S., and Amit, I. (2014). Tissue-resident macrophage enhancer landscapes are shaped by the local microenvironment. Cell *159*, 1312–1326.

Marone, G., Galli, S.J., and Kitamura, Y. (2002). Probing the roles of mast cells and basophils in natural and acquired immunity, physiology and disease. Trends Immunol. *23*, 425–427.

Matcovitch-Natan, O., Winter, D.R., Giladi, A., Vargas Aguilar, S., Spinrad, A., Sarrazin, S., Ben-Yehuda, H., David, E., Zelada González, F., Perrin, P., et al. (2016). Microglia development follows a stepwise program to regulate brain homeostasis. Science *353*, aad8670.

Min, B., Prout, M., Hu-Li, J., Zhu, J., Jankovic, D., Morgan, E.S., Urban, J.F., Jr., Dvorak, A.M., Finkelman, F.D., LeGros, G., and Paul, W.E. (2004). Basophils produce IL-4 and accumulate in tissues after infection with a Th2-inducing parasite. J. Exp. Med. *200*, 507–517.

Nabhan, A.N., Brownfield, D.G., Harbury, P.B., Krasnow, M.A., and Desai, T.J. (2018). Single-cell Wnt signaling niches maintain stemness of alveolar type 2 cells. Science *359*, 1118–1123.

Ohmichi, H., Koshimizu, U., Matsumoto, K., and Nakamura, T. (1998). Hepatocyte growth factor (HGF) acts as a mesenchyme-derived morphogenic factor during fetal lung development. Development *125*, 1315–1324.

Panduro, M., Benoist, C., and Mathis, D. (2016). Tissue Tregs. Annu. Rev. Immunol. *34*, 609–633.

Paul, F., Arkin, Y., Giladi, A., Jaitin, D.A., Kenigsberg, E., Keren-Shaul, H., Winter, D., Lara-Astiaso, D., Gury, M., Weiner, A., et al. (2015). Transcriptional heterogeneity and lineage commitment in myeloid progenitors. Cell *163*, 1663–1677.

Ramilowski, J.A., Goldberg, T., Harshbarger, J., Kloppmann, E., Lizio, M., Satagopam, V.P., Itoh, M., Kawaji, H., Carninci, P., Rost, B., and Forrest, A.R. (2015). A draft network of ligand-receptor-mediated multicellular signalling in human. Nat. Commun. *6*, 7866.

Rantakari, P., Jäppinen, N., Lokka, E., Mokkala, E., Gerke, H., Peuhu, E., Ivaska, J., Elima, K., Auvinen, K., and Salmi, M. (2016). Fetal liver endothelium regulates the seeding of tissue-resident macrophages. Nature *538*, 392–396.

Saluzzo, S., Gorki, A.D., Rana, B.M.J., Martins, R., Scanlon, S., Starkl, P., Lakovits, K., Hladik, A., Korosec, A., Sharif, O., et al. (2017). First-breath-induced type 2 pathways shape the lung immune environment. Cell Rep. *18*, 1893–1905.

Schneider, E., Petit-Bertron, A.F., Bricard, R., Levasseur, M., Ramadan, A., Girard, J.P., Herbelin, A., and Dy, M. (2009). IL-33 activates unprimed murine basophils directly in vitro and induces their in vivo expansion indirectly by promoting hematopoietic growth factor production. J. Immunol. *183*, 3591–3597.

Schneider, C., Nobs, S.P., Kurrer, M., Rehrauer, H., Thiele, C., and Kopf, M. (2014). Induction of the nuclear receptor PPAR-γ by the cytokine GM-CSF is critical for the differentiation of fetal monocytes into alveolar macrophages. Nat. Immunol. *15*, 1026–1037.

Seglen, P.O. (1973). Preparation of rat liver cells. 3. Enzymatic requirements for tissue dispersion. Exp. Cell Res. *82*, 391–398.

Sharif, O., Gawish, R., Warszawska, J.M., Martins, R., Lakovits, K., Hladik, A., Doninger, B., Brunner, J., Korosec, A., Schwarzenbacher, R.E., et al. (2014). The triggering receptor expressed on myeloid cells 2 inhibits complement component 1q effector mechanisms and exerts detrimental effects during pneumococcal pneumonia. PLoS Pathog. *10*, e1004167.

Shibata, Y., Berclaz, P.Y., Chroneos, Z.C., Yoshida, M., Whitsett, J.A., and Trapnell, B.C. (2001). GM-CSF regulates alveolar macrophage differentiation and innate immunity in the lung through PU.1. Immunity *15*, 557–567.

Sokol, C.L., Chu, N.Q., Yu, S., Nish, S.A., Laufer, T.M., and Medzhitov, R. (2009). Basophils function as antigen-presenting cells for an allergen-induced T helper type 2 response. Nat. Immunol. *10*, 713–720.

Street, K., Risso, D., Fletcher, R.B., Das, D., Ngai, J., Yosef, N., Purdom, E., and Dudoit, S. (2017). Slingshot: Cell lineage and pseudotime inference for single-cell transcriptomics. bioRxiv. https://doi.org/10.1186/s12864-018-4772-0.

Sullivan, B.M., Liang, H.E., Bando, J.K., Wu, D., Cheng, L.E., McKerrow, J.K., Allen, C.D., and Locksley, R.M. (2011). Genetic analysis of basophil function in vivo. Nat. Immunol. *12*, 527–535.

Tan, S.Y., and Krasnow, M.A. (2016). Developmental origin of lung macrophage diversity. Development *143*, 1318–1327.

Townsend, M.J., Fallon, P.G., Matthews, D.J., Jolin, H.E., and McKenzie, A.N. (2000). T1/ST2-deficient mice demonstrate the importance of T1/ST2 in developing primary T helper cell type 2 responses. J. Exp. Med. *191*, 1069–1076.

Treutlein, B., Brownfield, D.G., Wu, A.R., Neff, N.F., Mantalas, G.L., Espinoza, F.H., Desai, T.J., Krasnow, M.A., and Quake, S.R. (2014). Reconstructing lineage hierarchies of the distal lung epithelium using single-cell RNA-seq. Nature *509*, 371–375.

Varricchi, G., Raap, U., Rivellese, F., Marone, G., and Gibbs, B.F. (2018). Human mast cells and basophils-How are they similar how are they different? Immunol. Rev. *282*, 8–34.

Voehringer, D., Liang, H.E., and Locksley, R.M. (2008). Homeostasis and effector function of lymphopenia-induced "memory-like" T cells in constitutively T cell-depleted mice. J. Immunol. *180*, 4742–4753.

Whitsett, J.A., and Alenghat, T. (2015). Respiratory epithelial cells orchestrate pulmonary innate immunity. Nat. Immunol. *16*, 27–35.

Yu, X., Buttgereit, A., Lelios, I., Utz, S.G., Cansever, D., Becher, B., and Greter, M. (2017). The cytokine TGF-beta promotes the development and homeostasis of alveolar macrophages. Immunity *47*, 903–912.

Yuk, C.M., Park, H.J., Kwon, B.I., Lah, S.J., Chang, J., Kim, J.Y., Lee, K.M., Park, S.H., Hong, S., and Lee, S.H. (2017). Basophil-derived IL-6 regulates T_H17 cell differentiation and CD4 T cell immunity. Sci. Rep. *7*, 41744.

Zhou, X., Franklin, R.A., Adler, M., Jacox, J.B., Bailis, W., Shyer, J.A., Flavell, R.A., Mayo, A., Alon, U., and Medzhitov, R. (2018). Circuit design features of a stable two-cell system. Cell *172*, 744–757.

Cell

STAR★METHODS

KEY RESOURCES TABLE

REAGENT or RESOURCE	SOURCE	IDENTIFIER
Antibodies		
eF780-conjugated Fixable viability dye	eBioscience	Cat#65-0865
eFluor450-conjugated TER-119	eBioscience	Cat#14-5921-81; RRID: AB_467728
APC-conjugated CD45	eBioscience	Cat#17-0451-82; RRID: AB_469392
FITC-conjugated CD117	eBioscience	Cat#11-1171-81; RRID: AB_465185
PerCPCy5.5-conjugated F4/80	eBioscience	Cat#45-4801-80; RRID: AB_914344
PerCP Cy5.5-conjugated FCεRa1	Biolegend	Cat#134320; RRID: AB_10641135
APC-Cy7-conjugated Ly6G	Biolegend	Cat#127624; RRID: AB_10640819
FITC-conjugated CD3	Biolegend	Cat#100204; RRID: AB_312661
PE-Cy7-conjugated CD19	Biolegend	Cat#115520; RRID: AB_313655
PE-Cy7-conjugated CD31	Biolegend	Cat#102417; RRID: AB_830756
APC-Cy7-conjugated CD326	Biolegend	Cat#118218; RRID: AB_2098648
APC/Cy7-conjugated TER-119	Biolegend	Cat#116223; RRID: AB_2137788
AF700-conjugated CD45	Biolegend	Cat#103128; RRID: AB_493715
Pacific blue-conjugated CD49b	Biolegend	Cat#108918; RRID: AB_2265144
PE-conjugated Fcer1a	Biolegend	Cat#134307; RRID: AB_1626104
PE/Cy7-conjugated CD117	Biolegend	Cat#105814; RRID: AB_313223
BV605-conjugated Ly6C	Biolegend	Cat#128035; RRID: AB_2562352
BV605-conjugated CD11b	Biolegend	Cat#101237; RRID: AB_11126744
PE-conjugated CD11c	Biolegend	Cat#117307; RRID: AB_313776
PE/Cy7-conjugated IL-33R	Biolegend	Cat#145315; RRID: AB_2687366
PE-conjugated IL-6	Biolegend	Cat#504504; RRID: AB_504504
PE-conjugated Rat IgG1	Biolegend	Cat#400408; RRID: AB_326514
FITC-conjugated Ly6C	Biolegend	Cat#128005; RRID: AB_1186134
FITC-conjugated CD11c	BD-PharMingen	Cat#557400; RRID: AB_396683
PE-conjugated IL-13	eBioscience	Cat#12-7133-82; RRID: AB_763559
Anti-Fcεr1α (Functional grade)	eBioscience	Cat#16-5898-85; RRID: AB_469138
Armenian Hamster IgG isotype control (Functional grade)	eBioscience	Cat#16-4888-81; RRID: AB_470171
PE-conjugated CD131	Miltenyi Biotech	Cat#130-118-456
Anti-proSP-C	Abcam	Cat#Ab40879
Goat-anti-rabbit IgG	Vector Laboratories	Cat#AI-1000; RRID: AB_2336193
Rat-anti-mouse F4/80	AbD Serotec	Cat#MCA497GA; RRID: AB_323806
Rabbit-anti-rat IgG	Vector Laboratories	Cat#AI-4000; RRID: AB_2336312
Anti-GFP	Abcam	Cat#Ab6556; RRID: AB_305564
Biotin rabbit anti goat IgG	Vector Laboratories	Cat#BA-5000; RRID: AB_2336126
AF555-donkey anti-goat	Invitrogen	Cat#A-21432; RRID: AB_2535853
Bacterial and Virus Strains		
Streptococcus pneumonia (klein) Chester	ATCC	Cat#6303
Chemicals, Peptides, Enzymes and Recombinant Proteins		
Hoechst 33342 (used for nuclear staining)	Invitrogen	Cat#H1399
Murine IL-33	Peprotech	Cat#210-33-50
Murine IL-3	Peprotech	Cat#213-13-100
Murine GM-CSF	Peprotech	Cat#315-03-100
Murine M-CSF	Peprotech	Cat#315-02-50

(*Continued on next page*)

Continued		
REAGENT or RESOURCE	SOURCE	IDENTIFIER
CD117 MicrBeads mouse	Miltenyi Biotech	Cat#130-091-224
Proteinase K	Sigma-Adrich	Cat#P6556
Elastase	Worthington	Cat#LS002279
DNase	Sigma-Adrich	Cat#11 284 932 001
Liberase DL research grade	Sigma-Aldrich	Cat#05 466 202 001
Collagenase IV	Worthington	Cat#LS004188
Dispase	Sigma-Adrich	Cat#42613-33-2
Ficoll-Paque PLUS	Sigma-Adrich	Cat#17-1440-03
Red blood lysis buffer	Sigma-Adrich	Cat#R7757
Accutase	Sigma-Adrich	Cat#A6964
Critical Commercial Assays		
Cytofix/CytoPerm with GolgiStop	BD bioscience	Cat#BD554715
lung dissociation kit	Miltenyi Biotec	Cat#130-095-927
Deposited Data		
Raw data files for single-cell RNA-seq	NCBI Gene Expression Omnibus	GSE119228
Experimental Models: Cell Lines		
B16F10 murine melanoma cell line	ATCC	Cat#6322
Experimental Models: Organisms/Strains		
Mouse: C57BL/6 WT	Harlan	N/A
Mouse: Mcpt8-Cre$^{+/-}$DTA$^{fl/+}$ B6.129P2-Gt(ROSA) 26Sortm1 (DTA)Lky/J	The Jackson Laboratory	Cat#009669
Mouse: YFP-expressing Mcpt8-Cre B6.129-Mcpt8tm1(Cre)Lksy/J	The Jackson Laboratory	Cat#017578
Mouse: IL1RL1$^{-/-}$	Generated in the Laboratory of Dr. Andrew N.J. McKenzie	N/A
Oligonucleotides		
See Table S5	N/A	N/A
Software and Algorithms		
MATLAB R2014b software	MathWorks	https://www.mathworks.com/
R 3.2.1	The R Foundation	http://www.r-project.org/
David 6.8	Laboratory of Human Retrovirology and Immunoinformatics	https://david.ncifcrf.gov/home.jsp
Hisat 0.1.6	Kim et al., 2015	http://www.ccb.jhu.edu/software/hisat/index.shtml
FlowJo software	FlowJo	https://www.flowjo.com/
Fiji-ImageJ	PMID 22743772	https://imagej.net/Fiji
Slingshot package	Street et al., 2017	https://www.bioconductor.org/packages/devel/bioc/html/slingshot.html
Other		
MARS-seq reagents	Jaitin et al., 2014	N/A

EXPERIMENTAL MODEL AND SUBJECT DETAILS

Mice

Sex- and age-matched Mcpt8-Cre$^{+/-}$DTA$^{fl/+}$ and Mcpt8-Cre$^{+/-}$DTA$^{+/+}$ littermate controls were used. YFP-expressing Mcpt8-Cre (B6.129-Mcpt8tm1(Cre)Lksy/J) (Sullivan et al., 2011) and DTA (B6.129P2-Gt(ROSA) 26Sortm1 (DTA)Lky/J) (Voehringer et al., 2008) mice were kindly provided by Stephen Galli, Stanford University, and originally obtained from the Jackson Laboratory. *Il1rl1*$^{-/-}$ (Townsend et al., 2000) mice were kindly provided by Andrew McKenzie, MRC Laboratory of Molecular Biology Cambridge. All these mice were bred and maintained at the animal facility of the Medical University of Vienna under specific pathogen free conditions. All

Cell

experiments were performed in accordance with Austrian law and approved by the Austrian Federal Ministry of Sciences and Research (BMWFW-66.009/0146-WF/V/3b/2015). C57BL/6 WT pregnant, neonate and adult mice were obtained from Harlan. Mice were housed under specific-pathogen-free conditions at the Animal Breeding Center of the Weizmann Institute of Science. All animals were handled according to the regulations formulated by the Institutional Animal Care and Use Committee.

Tumor cell line

B16F10 murine melanoma cells were maintained in DMEM, supplemented with 10% FCS, 100 U/mL penicillin, 100 mg/mL streptomycin and 1 mM l-glutamine (Biological Industries). Cells were cultured in a humidified 5% CO2 atmosphere, at 37°C.

METHOD DETAILS

Lung dissociation and single cell sorting

Single-cell experiments were performed on embryonic mouse lung at E12.5, E16.5, E18.5 and E19.5, on neonate lung at 1, 6, 7, 10, 16, 30h, 2 days, and 7 days PN, and on adult mouse lung (8-12 weeks). In general, embryonic experiments were performed on pooled sibling lungs of one litter (at E12.5 six lungs were pooled, at E16.5, E18.5 and E19.5 three lungs were pooled, at PN time points 2 lungs were pooled, and for adult lungs, samples were not pooled). Embryos were euthanized by laying on a frozen surface, while PN and adult mice were scarified by overdose of anesthesia. For all time points, except E12.5, mice were perfused by injection of cold PBS via the right ventricle prior to lung dissection. Lung tissue was dissected from mice and half tissues were homogenized using lung dissociation kit (Miltenyi Biotec), while enzymatic incubation was adapted to single cell protocol, and therefore was lasted 15min (for 8 week adult mice, enzymatic digestion was lasted 20min). The second half of the lung was dissociated as previously documented (Treutlein et al., 2014), briefly cells were supplemented with DMEM/F12 medium (Sigma-Aldrich) containing Elastase (3U/ml, Worthington) and DNase (0.33U/ml, Sigma-Adrich) incubated with frequent agitation at 37°C for 15min. Next, an equal volume of DMEM/F12 supplemented with 10%FBS, 1U/ml penicillin, and 1Uml streptomycin (Biological Industries) was added to single-cell suspensions. Following dissociations, single cell suspension of the same lung was merged and centrifuged at 400 g, 5min, 4°C. All samples were filtered through a 70 μm nylon mesh filter into ice cold sorting buffer (PBS supplemented with 0.2mM EDTA pH8 and 0.5% BSA).

For calibration of lung dissociation protocol, cells derived from adult mouse lungs were supplemented with 1). DMEM (Biological Industries) containing Liberase (50μg/ml, Sigma-Aldrich) and DNase (1μg/ml, Roche); 2). PBS $Ca^{+}Mg^{+}$ (Biological Industries) containing Collagenase IV (1mg/ml, Worthington) and Dispase (2.4U/ml, Sigma-Adrich); 3). DMEM/F12 (Sigma-Aldrich) containing Elastase and DNase, as described above; and 4). Enzymes derived from lung dissociation kit (Miltenyi biotec), as described above. Following enzymatic digestion with frequent agitation at 37°C for 20min, an equal volume of DMEM supplemented with 10%FBS, 1U/ml penicillin, and 1Uml streptomycin (Biological Industries), or sorting buffer was added to single-cell suspensions from liberase and collagenase-dispase treatments, respectively. All live cells were sorted, after exclusion of doublets and erythrocytes, for MARS-seq analysis. Single cell analysis of cells extracted by each dissociation technique showed differential distribution of cell types (Figure S1B). Next, we chose dissociation protocol for the study that extracted vast range of cell populations from the immune and the non-immune compartments, without any preference to specific cell type stemming from the dissociation enzymes. Therefore, lung digestions along the study were a combination of elastase digestion, which lead to the extraction of epithelial cells and AM, and miltenyi kit protocol, which led to the extraction of different cell populations from the immune compartment. Importantly, these digestions were not characterized in any cell type preference, like endothelium dominancy that we found following collagenase-dispase and liberase treatments (Figure S1B); however, the percentages of cells observed in the single cell maps are dependent on the different lung dissociation methods (Figures 1B, 2B, and 2C).

Isolation of peripheral blood cells

Peripheral blood cells were suspended with 20μl of heparin, and washed with PBS supplemented with 0.2mM EDTA pH8 and 0.5% BSA. Cells were suspended with ficoll-Paque PLUS (1:1 ratio with PBS, Sigma-Adrich) and centrifuged at 460 g, 20min, 10°C, with no-break and no-acceleration. The ring-like layer of mononuclear cells was transferred into new tube and washed twice with cold PBS, centrifuged at 400 g, 5min, 4°C, passed through a 40μm mesh filter, and then suspended in ice-cold sorting buffer.

Tumor microenvironment dissociation

For purification of basophils from tumor microenvironment, $1x10^{6}$ cells were suspended in 100μl PBS and injected subcutaneous (s.c.) into 8-week mice. Solid tumors were harvested 10 days post injection, cut into small pieces, and suspended with RPMI-1640 supplemented with DNase (12.5μg/ml, Sigma-Adrich) and collagenase IV (1mg/ml, Worthington). Tissues were homogenized by GentleMacs tissue homogenizer (Miltenyi Biotec), and incubated at 37°C for 10min. Following two times of mechanic and enzymatic dissociation, cells were washed and suspended in red blood lysis buffer (Sigma-Aldrich) and DNase (0.33U/ml, Sigma-Adrich), incubated for 5min at room temperature, washed twice with cold PBS, passed through a 40μm mesh filter, centrifuged at 400 g, 5min, 4°C and then resuspended in ice cold sorting buffer.

Cell

Spleen dissociation

Tissue was harvested from 8 week females, suspended with accutase solution (Sigma-Adrich), homogenized by GentleMacs tissue homogenizer (Miltenyi Biotec), and incubated with frequent agitation at 37°C for 10min. Cells were washed and suspended in red blood lysis buffer (Sigma-Aldrich) and DNase (0.33U/ml, Sigma-Adrich), incubated for 3min at room temperature, washed twice with cold PBS, passed through a 40μm mesh filter, centrifuged at 400 g, 5min, 4°C and then resuspended in ice cold sorting buffer.

Liver dissociation

Basophils from the liver were isolated by a modification of the two-step collagenase perfusion method of Seglen (1973). Digestion step was performed with Liberase (20μg/ml; Roche Diagnostics) according to the manufacturer's instruction. Liver was minced to small pieces, suspended with PBS and centrifuged at 30 g, 5min, 4°C. Supernatant was collected in new tube (to remove hepatocytes), suspended with PBS and centrifuged at 30 g, 5min, 4°C (this step was repeated twice). Following second wash, supernatant was collected in new tube, centrifuged at 500 g, 5min, 4°C, and then resuspended in ice-cold sorting buffer.

Flow cytometry and sorting

Cell populations were sorted with SORP-aria (BD Biosciences, San Jose, CA) or with AriaFusion instrument (BD Biosciences, San Jose, CA). Samples were stained using the following antibodies: eF780-conjugated Fixable viability dye, eFluor450-conjugated TER-119, APC-conjugated CD45, FITC-conjugated CD117 (cKit), and PerCPCy5.5-conjugated F4/80 were purchased from eBioscience, PerCP Cy5.5-conjugated FCεRa1 (MAR1), APC-Cy7-conjugated Ly6G, FITC-conjugated CD3, PE-Cy7-conjugated CD19, PE-Cy7-conjugated CD31, APC-Cy7-conjugated CD326, APC/Cy7-conjugated TER-119, AF700-conjugated CD45, Pacific blue-conjugated CD49b, PE-conjugated Fcer1a, PE/Cy7-conjugated CD117, FITC-conjugated Ly6C, PE-conjugated CD11c, BV605-conjugated CD11b and BV605-conjugated Ly-6C were purchased from Biolegend, and FITC-conjugated CD11C was purchased from BD-PharMingen.

Prior to sorting, cells were stained with DAPI or fixable viability dye for evaluation of live/dead cells, and then filtered through a 40 μm mesh. For the sorting of whole immune cell populations, samples were gated for $CD45^+$, for sorting of whole stromal cell samples were gated for $CD45^-$, and for the isolation of basophils, samples were gated for $CD45^+FC\varepsilon R1\alpha^+cKit^-$, after exclusion of doublets, dead cells and erythrocytes. To record marker level of each single cell, the FACS Diva 7 ''index sorting'' function was activated during single cell sorting. Following the sequencing and analysis of the single cells, each surface marker was linked to the genome-wide expression profile. This methodology was used to optimize the gating strategy. Isolated live cells were single-cell sorted into 384-well cell capture plates containing 2 μL of lysis solution and barcoded poly(T) reverse-transcription (RT) primers for single-cell RNA-seq (Jaitin et al., 2014; Paul et al., 2015). Four empty wells were kept in each 384-well plate as a no-cell control during data analysis. Immediately after sorting, each plate was spun down to ensure cell immersion into the lysis solution, and stored at −80°C until processed.

For evaluation of protein levels of receptors expressed by lung basophils, we performed cell surface staining of PE-conjugated CD131 (CSF2Rb, Miltenyi Biotec), PE/Cy7-conjugated IL-33R (Biolegend), and PacificBlue-conjugated CD49b (Biolegend). For evaluation of intracellular protein levels of ligands expressed by lung basophils, cells were incubated with RPMI-1640 supplemented with 10% FCS, 1mM l-glutamine, 100U/ml penicillin, 100 mg/ml streptomycin (Biological Industries) and GolgiStop (1:1000; for IL-13, BD bioscience, San Jose, CA), or Brefeldin A solution (1:1000, for IL-6, Biolegend), for 2h at 37°C, to enable expression of intracellular cytokines, and to prevent their extracellular secretion. Cells were washed, fixed, permeabilized and stained for surface and intracellular proteins using the Cytofix/Cytoperm kit, according to the manufacture's instructions (BD bioscience, San Jose, CA). For the intracellular experiments the following antibodies were used: PE-conjugated IL-6 (Biolegend), PE-conjugated IL-13 (eBioscience) and matched Isotype control PE-conjugated Rat IgG1 (Biolegend). Cells were analyzed using BD FACSDIVA software (BD Bioscience) and FlowJo software (FlowJo, LLC).

BM derived cell cultures

BM progenitors were harvested from C57BL/6 8 week old mice and cultured at concentration of 0.5×10^6 cells/ml. For BM-MΦ differentiation, BM cultures were cultured for 8 days in the presence of M-CSF (50ng/ml; Peprotech). On day 8, cells were scraped with cold PBS and replated on 96-well flat bottom tissue culture plates for 16h. For BM-derived basophils differentiation, BM cultures were cultured for 10 days in the presence of IL-3 (30 ng/ml; Peprotech). Basophils were enriched by magnetic-activated cell sorting for $CD117^-$ population (cKit; Miltenyi Biotec), and replated on 96-well flat bottom tissue culture plates for 16h. All BM cultures were done in the standard media RPMI-1640 supplemented with 10% FCS, 1mM l-glutamine, 100U/ml penicillin, 100 mg/ml streptomycin (Biological Industries). Every 4 days BM cultures were treated with differentiation factors M-CSF (50ng/ml) or IL-3 (30ng/ml). Following replating of BM-derived cells, co-cultured and mono-cultured cells were seeded in concentration of 0.5×10^6 cells/ml (1:1 ration in co-cultures), and supplemented with IL-3 (10ng/ml) and M-CSF (10ng/ml) for cell survival, IL33 (50ng/ml; Peprotech) or GM-CSF (50ng/ml; Peprotech) for cell activation.

For co-culture of BM-basophils with lung-derived monocytes and undifferentiated macrophages, we sorted $CD45^+CD115^+$ myeloid cells from 30h PN lungs and performed the *in vitro* experiment, as detailed above.

Cell

MARS-seq Library preparation

Single-cell libraries were prepared as previously described (Jaitin et al., 2014). In brief, mRNA from cell sorted into cell capture plates were barcoded and converted into cDNA and pooled using an automated pipeline. The pooled sample is then linearly amplified by T7 *in vitro* transcription, and the resulting RNA is fragmented and converted into a sequencing-ready library by tagging the samples with pool barcodes and illumina sequences during ligation, RT, and PCR. Each pool of cells was tested for library quality and concentration is assessed as described earlier (Jaitin et al., 2014).

Lung-resident basophil depletion

For depletion of basophils in neonate lungs, we calibrated a protocol based on previous studies (Denzel et al., 2008; Guilliams et al., 2013). Mice were injected i.n. with 7μl of 100 μg anti-Fcεr1α (MAR1; eBioscience) or IgG isotype control (Armenian hamster, eBioscience) twice, at 10h and 15h following birth. Lungs were purified from injected neonates 30h following birth and $CD45^+$ cells were sorted for RNA-seq analysis.

Phagocytosis assay

Phagocytosis assays were performed as described earlier (Sharif et al., 2014). AM were isolated by bronchoalveolar lavage (BAL). In brief, the trachea of mice was exposed and cannulated with a sterile 18-gauge venflon (BD Biosciences) and 10ml of sterile saline were instilled in 0.5ml steps. Total cell numbers in the retrieved BAL fluid (comprising > 95% AM) were counted using a Neubauer chamber. To assess bacterial phagocytosis, $1–2.5 \times 10^5$ AM were plated and allowed to adhere for 3h in RPMI containing 10% fetal calf serum (FCS), 1% penicillin and 1% streptomycin. Next, AM were incubated with FITC-labeled heat-inactivated S. pneumoniae (MOI 100) for 45min at 37°C or 4°C (as a negative control). Cells were washed and incubated with proteinase K (50 μg/ml) for 10min on ice to remove adherent bacteria. Uptake of bacteria was assessed via flow cytometry and the phagocytosis index was calculated as (MFI × % positive cells at 37°C) minus (MFI × % positive cells at 4°C).

Single-molecule fluorescent *in situ* hybridization

Neonates in the age of 7 days were perfused with PBS. Lung tissues harvested and fixed in 4% paraformaldehyde for 3h at 4°C, incubated overnight with 30% sucrose in 2% paraformaldehyde at 4°C and then embedded in OCT. Cryo-sections (6μm) were used for hybridization. Probe libraries were designed and constructed as previously described (Table S5) (Itzkovitz et al., 2012). Single molecule FISH probe libraries consisted of 48 probes of length 20 bps. smFISH probe libraries of Il1rl1, Il33, and Mcpt8 probes were coupled to Cy3, AF594, and cy5, respectively. Hybridizations were performed overnight in 30°C. DAPI dye for nuclear staining was added during the washes. Images were taken with a Nikon Ti-E inverted fluorescence microscope equipped with a x60 and x100 oil-immersion objective and a Photometrics Pixis 1024 CCD camera using MetaMorph software (Molecular Devices, Downington, PA). smFISH molecules were counted only within the DAPI staining of the cell.

Histology and immunohistochemistry

For histologic examination, paraffin-embedded lung sections were taken at indicated time-points. To stain for proSP-C, endogenous peroxidase activity was quenched and antigen was retrieved with Antigen Unmasking Solution (Vector Laboratories, H-3300). Blocking was done in donkey serum and the slides were then stained with anti-proSP-C (Abcam), followed by secondary goat-anti-rabbit IgG antibody (Vector Laboratories), and signal amplification using the Vectastain ELITE kit (Vector Laboratories). For F4/80 staining, antigen was retrieved using protease type XIV (SIGMA), followed by blocking with rabbit serum and staining with rat-anti-mouse F4/80 mAb (AbD Serotec). A secondary rabbit-anti-rat IgG Ab (Vector Laboratories) was applied and the signal was amplified with Vectastain ELITE kit (Vector Laboratories). For Mcpt8 staining, an anti-GFP Ab (Abcam) was used followed by a secondary biotinylated rabbit-anti-goat IgG Ab (Vector Laboratories). For detection, Peroxidase Substrate kit (Vector) or Vector VIP Peroxidase Kit (Vector Laboratories) was applied. Cell structures were counter-stained with hematoxylin or methylgreen and pictures were taken on an Olympus FSX100 Microscope.

For whole lobe analysis, slides were scanned using a TissueFAXS imaging system (TissueGnostics GmbH) equipped with a Zeiss Axio Imager.Z1 microscope (Carl Zeiss, Jena, Germany). Images were taken using a PCO PixelFly camera (Zeiss).

Tissue clearing

Tissue clearing protocol was performed as described earlier (Fuzik et al., 2016). In short, lungs at indicated time-points were perfused once with PBS and afterward with 7.5% formaldehyde in PBS. Lung lobes were fixed in 7.5% formaldehyde in PBS at room temperature overnight. Lung lobes were cleared using CUBIC reagent 1 (25 wt% urea, 25 wt% *N,N,N',N'*-tetrakis(2-hydroxypropyl) ethylenediamine and 15 wt% Triton X-100) for 4 days (30h PN, day 8.5) or 7 days (8-weeks) at 37°C. After repeated washes in PBS, lung lobes were incubated in blocking solution (PBS, 2.5% BSA, 0.5% Triton X-100, 3% normal donkey serum) and afterward placed in primary antibody solution (1:100; goat anti-mouse GFP, abcam) for 4 days (30h PN, day 8.5) or 5 days (8-weeks) at 37°C. After washing the secondary antibody solution (1:500; donkey anti-goat AF555, Invitrogen) was added for 4 days (30h PN, day 8.5) or 5 days (8-weeks) at 37°C. After re-washing with PBS and a fixing step for 2h at room temperature in 7.5% formaldehyde, washing steps were repeated and lung lobes were incubated in CUBIC reagent 2 (50 wt% sucrose, 25 wt% urea, 10 wt% 2,20,20'-nitrilotriethanol and 0.1% v/v% Triton X-100) for another 4 days (30h PN, day 8.5) or 7 days (8-weeks). Cleared lung lobes were imaged in

CUBIC reagent 2 with a measured refractive index of 1.45 using a Zeiss Z1 light sheet microscope through 5x detection objective, 5x illumination optics at 561 laser excitation wavelength and 0.56x zoom. Z stacks were acquired in multi-view tile scan mode by dual side illumination with light sheet thickness of 8.42 μm and 441.9ms exposure. Stitching, 3D reconstruction, visualization and rendering was performed using Arivis Vision4D Zeiss Edition (v.2.12).

QUANTIFICATION AND STATISTICAL ANALYSIS

Low level processing and filtering

All RNA-Seq libraries (pooled at equimolar concentration) were sequenced using Illumina NextSeq 500 at a median sequencing depth of 58,585 reads per single cell. Sequences were mapped to mouse genome (mm9), demultiplexed, and filtered as previously described (Jaitin et al., 2014), extracting a set of unique molecular identifiers (UMI) that define distinct transcripts in single cells for further processing. We estimated the level of spurious UMIs in the data using statistics on empty MARS-seq wells (median noise 2.7%; Figure S1). Mapping of reads was done using HISAT (version 0.1.6) (Kim et al., 2015); reads with multiple mapping positions were excluded. Reads were associated with genes if they were mapped to an exon, using the UCSC genome browser for reference. Exons of different genes that shared genomic position on the same strand were considered a single gene with a concatenated gene symbol. Cells with less than 500 UMIs were discarded from the analysis. After filtering, cells contained a median of 2,483 unique molecules per cell. All downstream analysis was performed in R.

Data processing and clustering

The Meta-cell pipeline (Giladi et al., 2018) was used to derive informative genes and compute cell-to-cell similarity, to compute K-nn graph covers and derive distribution of RNA in cohesive groups of cells (or meta-cells), and to derive strongly separated clusters using bootstrap analysis and computation of graph covers on resampled data. Default parameters were used unless otherwise stated.

Clustering of lung development was performed for the immune ($CD45^+$) and non-immune ($CD45^-$) compartments combined. Cells with high (> 64) combined expression of hemoglobin genes were discarded (*Hba-a2*, *Alas2*, *Hba-a1*, *Hbb-b2*, *Hba-x*, *Hbb-b1*). We used bootstrapping to derive robust clustering (500 iterations; resampling 70% of the cells in each iteration, and clustering the co-cluster matrix with minimal cluster size set to 20). No further filtering or cluster splitting was performed on the meta-cells.

In order to annotate the resulting meta-cells into cell types, we used the metric $FP_{gene,mc}$ (Table S2), which signifies for each gene and meta-cell the fold change between the geometric mean of this gene within the meta-cell and the median geometric mean across all meta-cells. The FP metric highlights for each meta-cell genes which are robustly overexpressed in it compared to the background. We then used this metric to "color" meta-cells for the expression of lineage specific genes such as *Clic5* (AT1), *Ear2* (macrophages), and *Cd79b* (B cells), etc. Each gene was given a FP threshold and a priority index – such that coloring for AT1 by *Clic5* is favored over coloring for general epithelium by *Epcam*. The selected genes, priority, and fold change threshold parameters are as follows:

group	gene	priority	fold change
Epithel	Epcam	1	2
AT1	Clic5	3	5
AT2	Sftpc	3	40
Endothel	Cdh5	4	4
Fibro	Col1a2	1	2
Pericytes	Gucy1a3	3	5
Club	Scgb3a2	3	2
Matrix	Mfap4	3	10
Smooth	Tgfbi	2	8
Ciliated	Ccdc19	3	2
Ciliated	Foxj1	3	2
B	Cd79b	1	2
Baso	Mcpt8	5	2
DC	Flt3	4	2
MacI	Cx3cr1	4	6
MacII	Ear2	3	2
MacIII	Ccl6	5	20
MacIII	Cd9	5	7

(Continued on next page)

Continued

group	gene	priority	fold change
Mast	Mcpt4	4	2
Mast	Gata2	3	3
Mon	Ccr2	2	2
Mon	F13a1	3	4
Mon	Fcgr4	5	3.5
Mon	Csf1r	3	4
Neut	S100a8	1	20
Neut	Csf3r	4	5
NK	Gzma	3	5
T	Trbc2	2	2
ILC	Rora	4	2

Trajectory finding

To infer trajectories and align cells along developmental pseudo-time, we used the published package Slingshot (Street et al., 2017). In short, Slingshot is a tool that uses pre-existing clusters to infer lineage hierarchies (based on minimal spanning tree, MST) and align cells in each cluster on a pseudo-time trajectory. Since our data is complex and contains many connected components and time points, we chose to apply Slingshot on subsets of interconnected cells type, namely E16.5 monocytes and macrophage II and III (dataset a), and the fibroblast lineage (dataset b).

For dataset a, we performed Slingshot on all macrophages II-III and on monocyte meta-cells with low relative expression of *Ly6c2* (excluding differentiated monocytes and retaining E16.5 monocytes). For each dataset we chose a set of differential genes between the cell types (FDR corrected chi^2 test, $q < 10^{-3}$, fold change > 2). We performed PCA on the log transformed UMI normalized to cell size. We ran Slingshot on the seven top principal components, with monocytes and fibroblast progenitors as starting clusters.

We first observe strong AT1 and AT2 signatures on day E18.5. This is parallel to disappearance of progenitor epithelium cells. From this we hypothesized that the precise branching point is not sampled with high temporal resolution in our developmental cohort, rendering Slingshot inefficient for this particular case. Instead, we examined whether progenitor epithelial cells on day E16.5 may be already primed toward either AT1 or AT2. To detect AT1 AT2 priming in epithelium progenitors, we used published gene lists of AT1 and AT2 (Treutlein et al., 2014) and computed two scores by the following term: $\sum_{gene} \log(1 + 7 * UMI_{gene}^{cell})$. We then examined score distribution in epithelium progenitors.

Interaction maps

To visualize all lung interactions, we used a published dataset of ligand and receptor pairs (Ramilowski et al., 2015). We applied a lenient filtering, including all LR with > 13 UMI in at least one meta-cell (normalized to meta-cell size). We computed the Spearman correlation between the log transformed UMI (down-sampled to 1000 UMI), and used hierarchical clustering to identify LR modules (cutree with K = 15). We built a scaffold of an interaction graph by computing the Spearman correlation between LR modules and connecting edges between modules with $\rho > 0.4$, generating a graph with the Rgraphviz package. We projected single LR on the graph scaffold by computing the mean *x,y* coordinates across all LR with $\rho > 0.05$ (Figure 3B).

To determine enrichment of non-immune-non-immune and immune-immune interactions we determined for each LR whether it's mainly expressed in the non-immune or the immune compartments (log_2 fold change > 1, Figure S3C). We computed the number of NI-NI and I-I interactions and compared to 10,000 randomly generated graphs. Importantly, as the interaction graph is not regular, we preserved nodes' degrees for each randomly generated graph. Ligand functional groups were extracted from David GO annotation tool (Huang et al., 2009), and curated manually.

For projections in Figures 3E–3H, a cell type was determined to express a LR if its expression was more than two fold higher than in all other cells.

Mapping cells to the lung cluster model

Given an existing reference single cell dataset and cluster model, and a new set of single cell profiles, we extract for each new cell the K (K = 10) reference cells with top Pearson correlation on transformed marker gene UMIs as described above. The distribution of cluster memberships over these K-neighbors was used to define the new cell reference cluster (by majority voting).

Basophil profiling, ex vivo and co-culture analysis

We used the MetaCell pipeline to analyze and filter the following datasets: (a) lung and blood derived basophils (Figures 4E–4G); (b) Il1rl1 knockout and control (Figures 5G and 5H); (c) *ex vivo* grown basophils (Figures 5J–5L and S5D); (d) and *ex vivo co*-culture of macrophages and basophils (Figures 6L, 6M, and S6J). Meta cell analysis was performed with default settings. In each dataset we

identified basophils and filtered contaminants by selecting meta-cells with increased mean expression of *Mcpt8* against the median. In the co-culture experiment (d), meta-cells were determined as macrophages by increased mean expression of *Csf1r*.

To compute the combined expression of genes in single cells (Figures S5E and S5K), we computed the following term: $\sum_{gene} \log(1 + 7 * UMI_{gene}^{cell})$. This allows pooling of gene at different expression levels.

TissueFAXS quantification

TissueFAXS images were processed by MATLAB (R2014b). Segmentation of alveoli was performed by a custom-made pipeline. Images were converted to grayscale and enhanced, opened and closed with a disk size of 15 pixels. Alveoli were determined by intensity threshold of 200. Areas larger than 300,000 pixels were discarded. Segmentation of nuclei was performed by a similar pipeline (disk size = 5 pixels), followed by applying a watershed algorithm, and detection of local minima. Images were converted to L*A*B color-space, and mean values of each nucleus were collected. Nuclei at the edges of the section were discarded. Nuclei with area < T_{area}, mean luminance > T_l or high circularity score (> T_{circ}) were discarded. Nuclei distances to alveoli (in pixels) were calculated with the bwdist method. Basophils (which are YFP$^+$) are distinguished from other nuclei by their dark brownish hue (Figure 4A). Therefore, we identified basophils by having low mean luminance and high mean b color channel (mean(b) – mean(l) > T_{baso}). For day 8.5 PN lobes we used the following parameters: $T_{area} = 50$; $T_l = 60$; $T_{circ} = 5$; $T_{baso} = -40$. For 8 weeks lobes we used the following parameters: $T_{area} = 20$; $T_l = 60$; $T_{circ} = 5$; $T_{baso} = -40$. To validate that our results are not affected by low quality sections, we randomly selected subsections from each TissueFAXS lobe, and manually inspected them for image clarity. We repeated until we obtained at least 200 basophils per lobe, or until no more basophils existed in lobe. We tested for significance of distances to alveoli as follows: For each lobe we rank-transformed all nuclei distances separately. We then randomly selected N_{baso} nuclei from each lobe (where N_{baso} stand for the number of basophils in that lobe), and calculated the median ranked distance. We repeated this permutation process 10^5 times for each time point and compared them to the observed median ranked distances.

Data and Software Availability

The accession number for the raw and processed scRNA-seq data reported in this paper is GEO: GSE119228. Software and custom code will be available by request.

Cell

Supplemental Figures

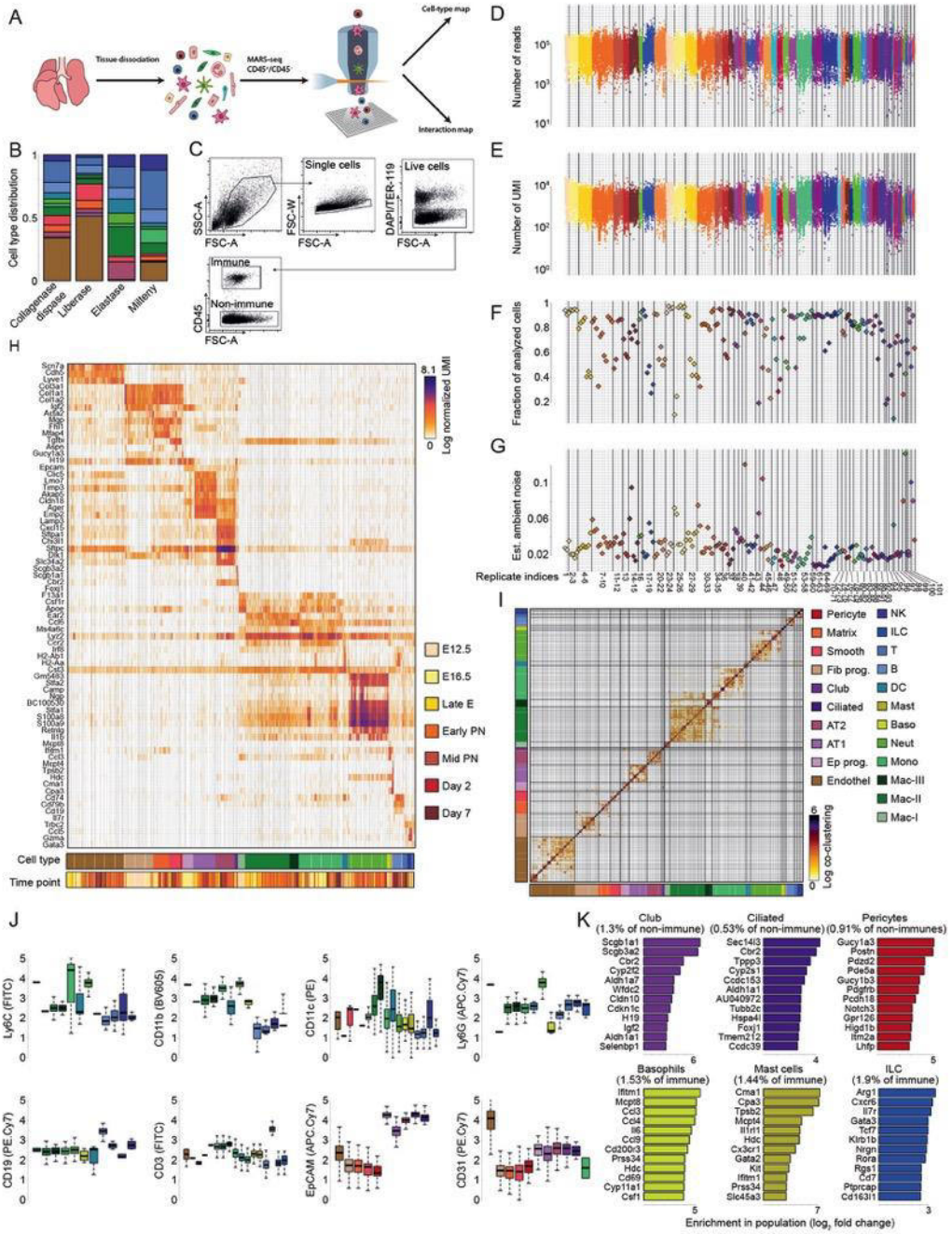

Figure S1. A Single-Cell Map of Lung Cells during Development, Related to Figure 1

(A) Illustration of tissue dissociation and MARS-seq analysis for lung development.

(B) Comparison of cell type distribution between different cell dissociation protocols. Adult lung tissues were digested with collagenase and dispase, liberase, elastase, and Miltenyi kit protocol. All live single cells were sorted and analyzed by MARS-seq. Colors represent cell types, as in Figure 1. C. Gating strategy for immune ($CD45^+$) and non-immune ($CD45^-$) cells, after erythrocyte (marked by TER-119) and doublets exclusion.

(D–G) Single cell quality control of 50,770 analyzed single cells from the entire study.

(D and E) Number of Illumina reads (D) and total UMI (E) per single cell.

(legend continued on next page)

(F and G) Fraction of analyzed cells after filtering (F) and estimated ambient noise (G, STAR Methods) per amplification batch (182 total). Cells are grouped and colored by experimental procedure. Lower indices indicate biological replicates as in Table S1.
(H) Gene expression of key markers across single cells from both immune and non-immune compartments. Lower panels indicate association to cell type (color bars represent cell type as in Figure 1), and developmental time-point of each single cell.
(I) Log values of the co-clustering structure of both compartments, as assessed by bootstrapping analysis. Color bars represent cell types as in Figure 1.
(J) Distribution of FACS indices (measured by index-sorting, STAR Methods) across different cell types. Values are in log10. Each panel shows indices from $CD45^+$ or $CD45^-$ sorting. Colors represent cell types as in Figure 1.
(K) Twelve top highly differentiated genes of six rare populations. Values represent log2 fold change between each rare population compared to all other cells. Brackets indicate estimated population frequencies out of $CD45^-$ (upper panel) or $CD45^+$ (lower panel).

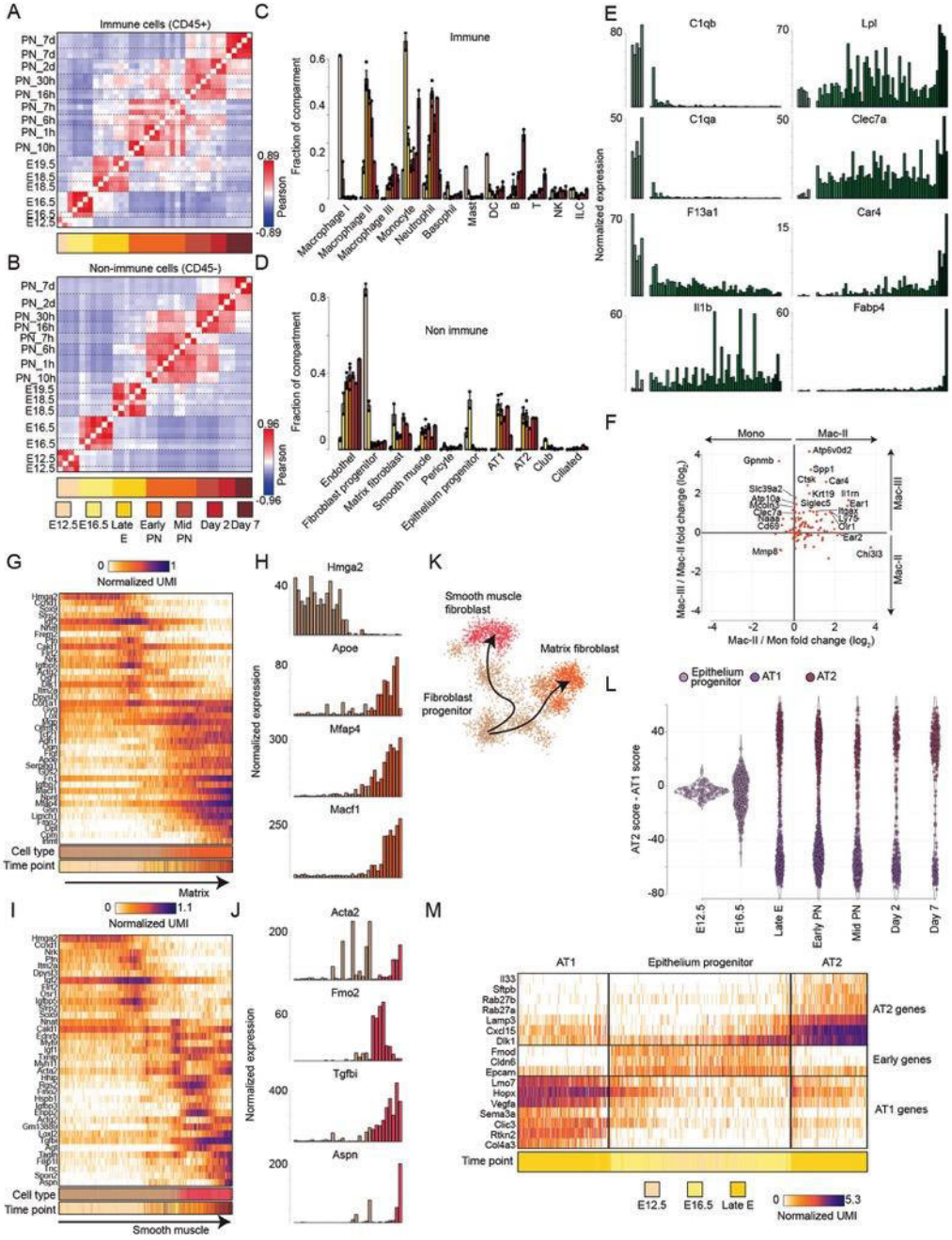

Figure S2. Cellular Dynamics during Lung Development, Related to Figure 2

(A and B) Pearson correlation of meta-cell distribution in biological replicates along different time points for the immune (A) and non-immune (B) compartments. Lower panel indicates grouping of samples into seven developmental groups, merging close time points according to the correlation, as in Figure 1A.

(C and D) Cell type levels at different time points in the immune (C) and non-immune (D) compartments. Error bars represent SEM across biological replicates.

(E) Expression of hallmark monocyte and macrophage genes across meta-cells. Meta-cells are ordered by median pseudo-time (Figure 2F); five leftmost meta-cells are macrophage I. Colors represent cell type as in Figure 1.

(legend continued on next page)

Cell

(F) Differential expression of lung macrophage genes across the transition from monocytes to macrophage II and to macrophage III. Axes represent fold change between macrophage-II and monocytes (x axis), and between macrophage-III and macrophage-II (y axis). Gene list was taken from Gautier et al. (2012).
(G) Gene expression profiles along the trajectory of fibroblast progenitors toward matrix fibroblasts. Cells are ordered by Slingshot inferred pseudo-time. Lower panels indicate annotation by cell type (middle) and time point of origin (bottom).
(H) Expression of fibroblast progenitors and matrix fibroblast genes across meta-cells. Meta-cells are ordered by median pseudo-time.
(I and J) As in G-H but for the trajectory from fibroblast progenitors to smooth muscle fibroblasts.
(K) Suggested trajectory of the fibroblast progenitors branching to matrix and smooth muscle fibroblasts on the 2D map.
(L and M) Scoring cells on expression of AT1 and AT2 genes reveal early priming in epithelium progenitors.
(L) The distribution of the difference between the AT2 and the AT1 scores in cells at different time points. Cells are colored by their lineage annotation. AT1 and AT2 gene lists were taken from Treutlein et al. (Treutlein et al., 2014).
(M) Expression of AT1 and AT2 genes in epithelium cells from E12.5, E16.5 and E18.5 time points. Lower panel indicates annotation by time point of origin.

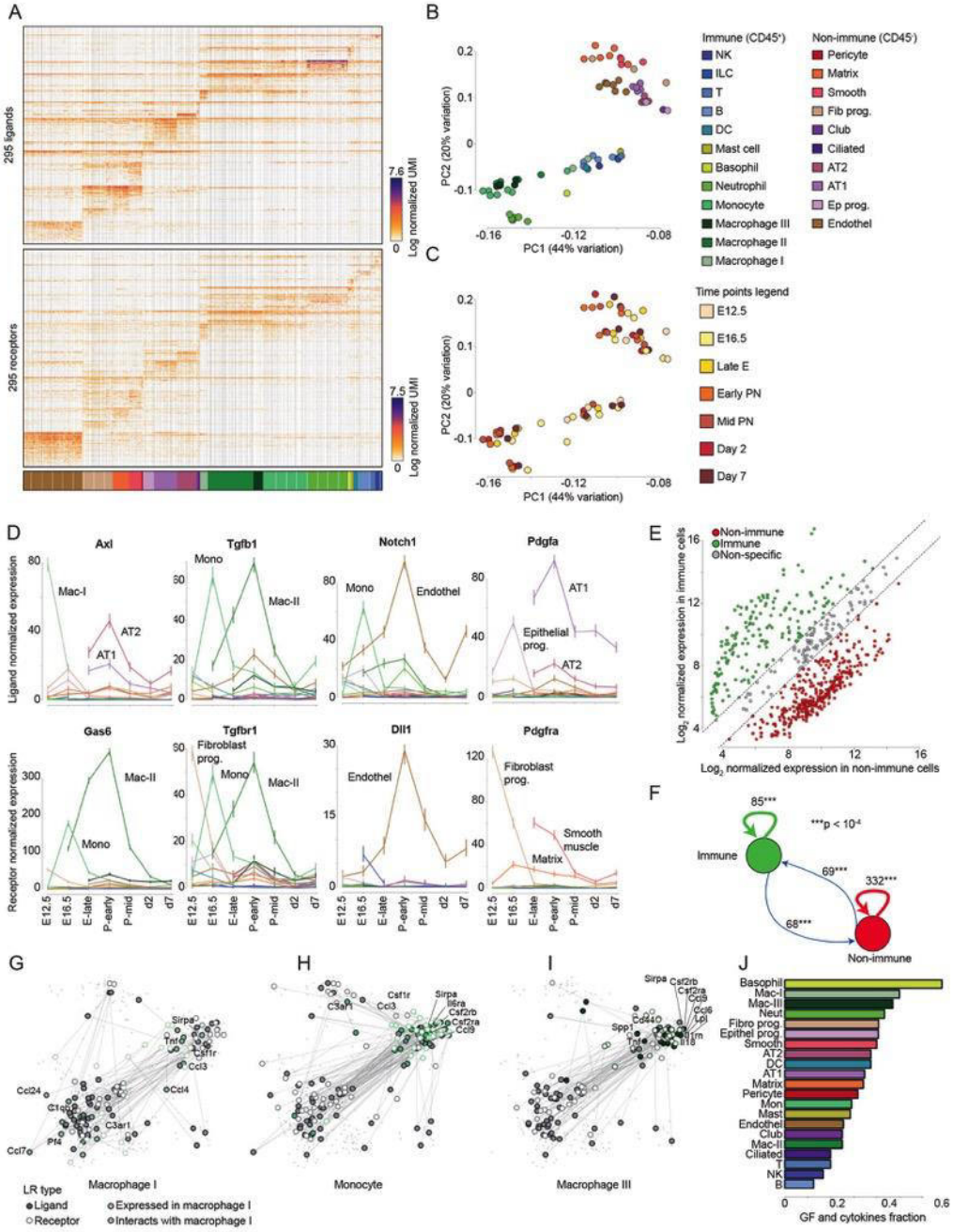

Figure S3. Ligand-Receptor Interaction Map during Lung Development, Related to Figure 3

(A) Expression profiles of 295 ligands and 295 receptors across all lung cells, ordered by cell type. Lower panel indicates annotation by cell type as in Figure 1.

(B and C) Principal component analysis of all 590 LR expression profiles of cell types in different time points. Data points are colored by cell type as in Figure 1 (B) or by time point (C). Data points with less than 50 cells were discarded.

(D) Dynamic expression of important ligand (top) - receptor (bottom) pairs along developmental time points. Each line represents dynamic expression by a cell type, colored as in Figure 1. Error bars represent 95% binomial confidence intervals.

(E) Differential expression of 590 LR genes between the non-immune (red, x axis) and immune (green, y axis) compartments. Compartment specificity is determined by two-fold change threshold. LR which are not specific for immune or stromal compartment are marked in gray circles.

(legend continued on next page)

(F) Quantification of interactions between and within immune and non-immune compartments. Thick and thin edges represent enriched and depleted interactions, respectively. Significance is determined by comparison to 10^4 randomly generated interaction graphs with preserved node degrees; $p < 10^{-4}$.
(G–I) LR interaction maps of macrophage I (G), monocyte (H), and macrophage III (I). Colored nodes represents genes upregulated in the cell type (> 2 fold change), and gray nodes represent their interacting partners. Full and empty circles represent ligands and receptors, respectively.
(J) Fraction of ligands classified as cytokines and growth factors out of expressed ligands in each cell type. Colors represent cell types, as in Figure 1. ***$p < 0.001$.

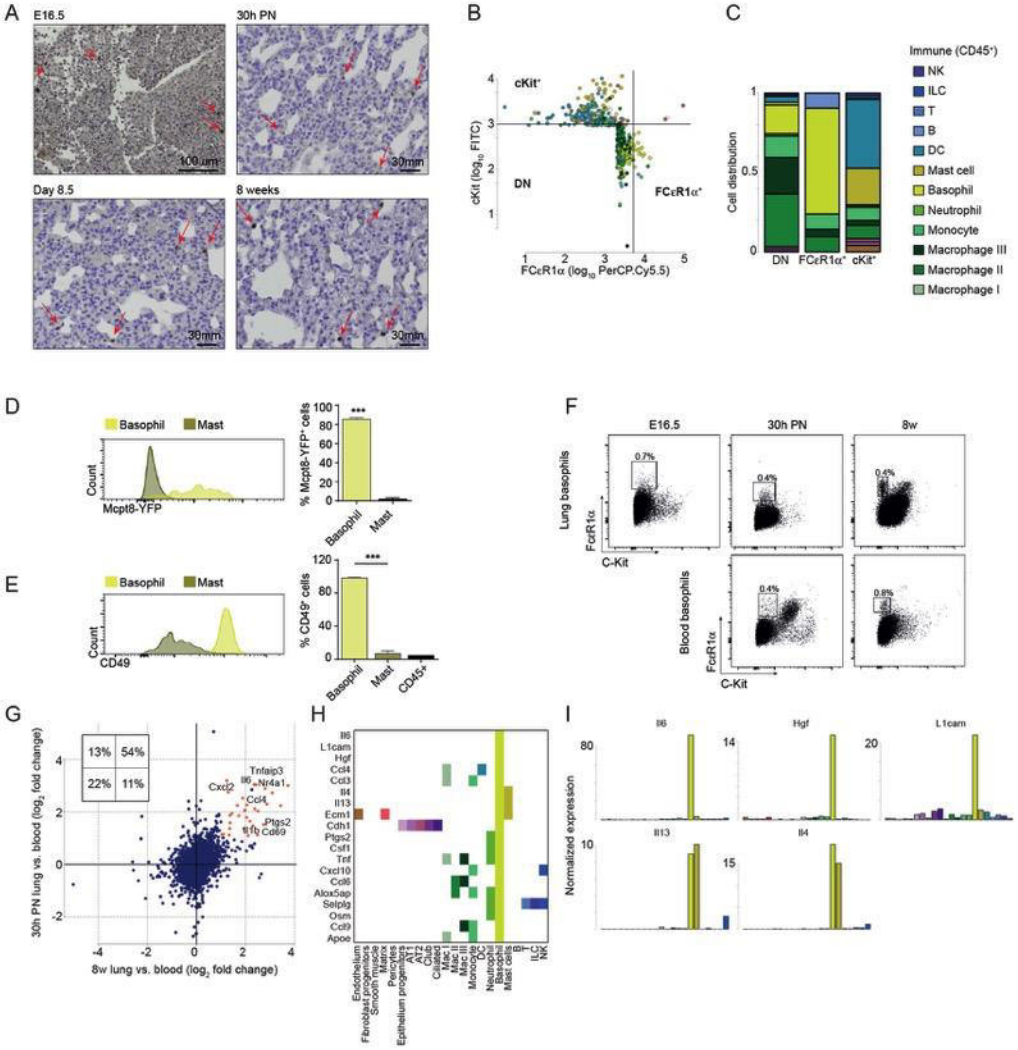

Figure S4. Spatial and Transcriptional Characterization of Lung Basophils, Related to Figure 4

(A) Representative IHC images of Mcpt8$^+$ basophils (brown; red arrows) with hematoxylin background in lung section derived from E16.5, 30h PN, day 8.5 PN and 8 week adult mice n = 3-5 for each time point.

(B) Lung cells derived from day 2 PN mice were enriched for basophils, by single cell sorting according to specific cell-surface markers. Protein levels of cKit and Fcεr1α of CD45$^+$ cells were determined by FACS index sorting. Cells are colored by association to cell type as in Figure 1, by transcriptional similarity (STAR Methods).

(C) Cell type distribution of the cKit$^+$, Fcεr1α$^+$ and double negative (DN) gates as in (B).

(D) Quantification of YFP$^+$ fraction in lung cells derived from Mcpt8$^{YFP/+}$ transgenic neonates at 30h PN, and enriched for basophils (CD45$^+$cKit$^-$Fcεr1α$^+$), compared to mast cells (CD45$^+$cKit$^+$) and the CD45$^+$ compartment; n = 6. Student's *t*-test (two tailed): ***p < 0.001.

(E) Quantification of CD49b$^+$ lung basophils compared to mast cells and total CD45$^+$ cells at 30h PN by flow cytometry; n = 6. One-way ANOVA: ***p < 0.001; Student's *t*-test (two tailed) between basophil and mast cells: ***p < 0.001; Data are represented as mean ± SEM

(F) Gating strategy for basophils derived from blood circulation (low panel) and lung parenchyma (upper panel) at E16.5, 30h PN and 8 weeks old mice, according to Fcεr1α$^+$cKit$^-$ expression.

(G) Differential gene expression between lung and blood basophils in 30h PN (y axis) and adult (8 weeks, x axis) mice. Inlet displays percentages of differentially expressed genes (fold change > 1) in each quartile. Red genes were selected for the definition of the lung basophil signature (Figures 4 and 5).

(H) Specificity of basophils expressed ligands across all lung cell types. Expression threshold is 2-fold change (Table S3). Colors represent cell types, as in Figure 1.

(I) Expression of ligands exclusively expressed by basophils compared to all cell types. ***p < 0.001. Data are represented as mean ± SEM.

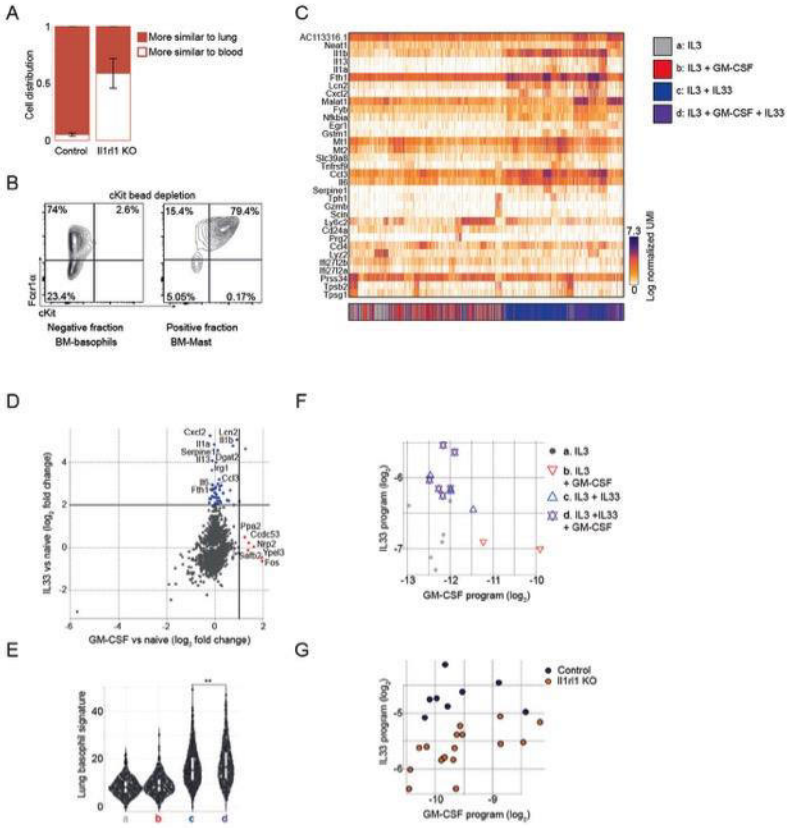

Figure S5. Lung Resident Basophils Are Primed by IL33 and GM-CSF, Related to Figure 5

(A) Gene expression similarity of Il1rl1 knockout, or its littermate control, lung basophils to lung or blood basophils derived from mice at 30h PN. Each Il1rl1 KO cell was assigned to either blood or lung by k nearest neighbor majority voting (STAR Methods).

(B–E) BM-derived cells were grown with IL3 to induce basophils for 10 days and then cKIT$^+$ cells were sorted for plating. Basophils were plated for 16h with IL3 alone (a), IL3 and GM-CSF (b) IL3 and IL33 (c) and a combination of IL3, IL33 and GM-CSF (d).

(B) BM-derived cells were enriched for BM-basophils by negative selection using cKit beads. Percentage of pure BM-basophil population out of total BM cells was evaluated by FACS.

(C) Heat-map represents gene expression profiles of basophils that were grown with different combinations of cytokines. Color bar indicates a-d cytokine combinations.

(D) Differential gene expression between basophils grown with one cytokine (*x axis* - GM-CSF; *y axis* - IL33) and naive basophils (grown with IL3 alone). Horizontal and vertical intercepts indicate thresholds for IL33 and GM-CSF induced gene programs, respectively.

(E) Distribution of lung basophil specific signature (Figure S4G) in BM-derived basophils grown under the four conditions. Boxplots display median bar, first–third quantile box and 5th–95th percentile whiskers. **p = 0.009; Kolmogorov–Smirnov test.

(F) Scoring biological replicates from the a-d cytokine conditions for their expression of the IL33 induced program (*y axis*) and the GM-CSF induced program (*x axis*). Conditions a and d are from three independent experiments.

(G) Scoring meta-cells from the Il1rl1 knockout lung basophils and their littermate controls at 30h PN, for their expression of the IL33 induced program (*y axis*) and the GM-CSF induced program (*x axis*).

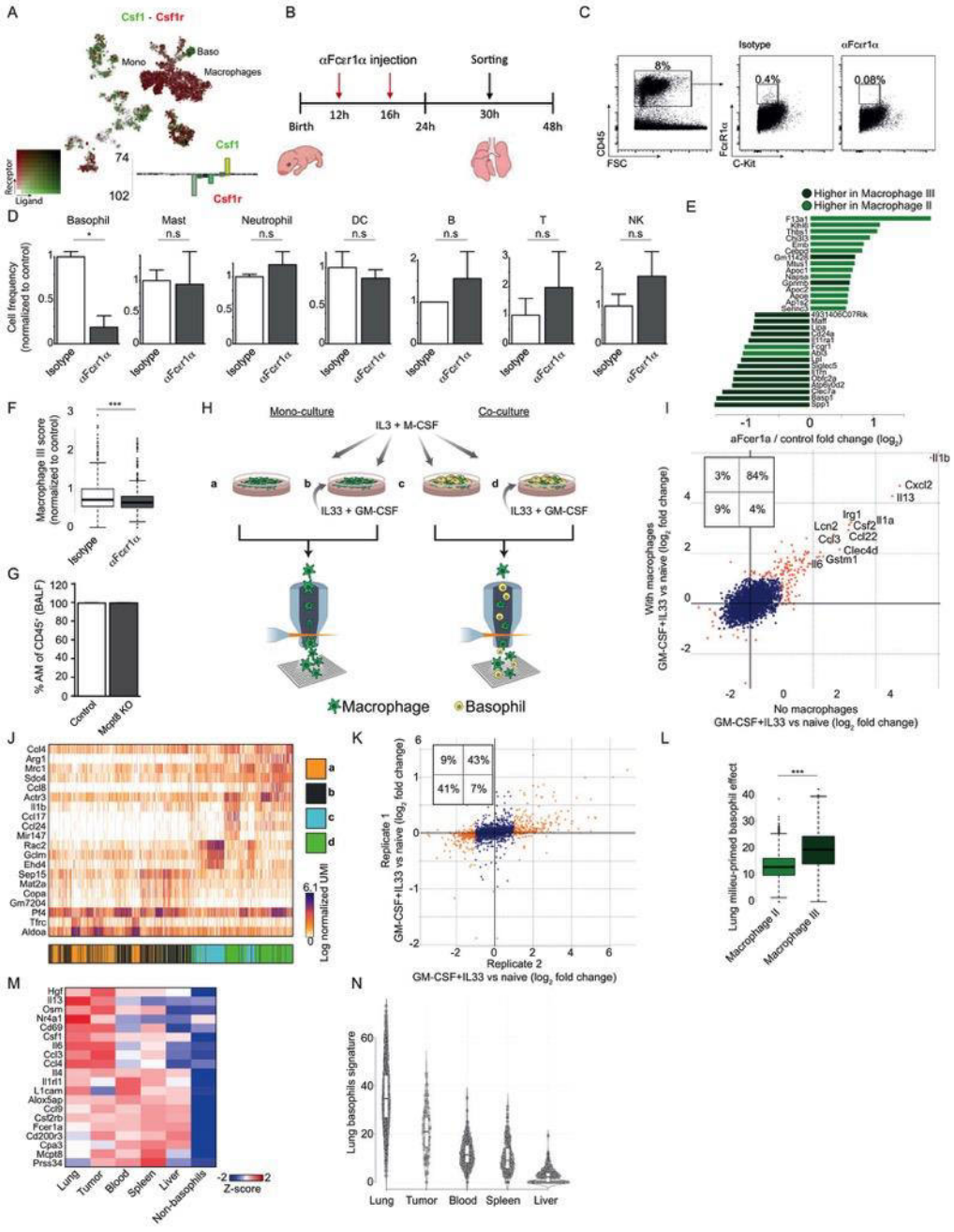

Figure S6. Lung Basophils Are Essential for Transcriptional and Functional Development of AM, Related to Figure 6

(A) Dual projection of the ligand *Csf1* (green) and its unique receptor *Csf1r* (red) on the single cell map from Figure 1. Colors indicate expression quantiles. Bar plots indicate ligand and receptor normalized expression per 1,000 UMI across cell types.

(B) Illustration of the basophil depletion experiment. Newborn mice were injected intra-nasally with anti-Fcεr1α antibody for basophils depletion or with isotype control twice, at 12h and 16h PN, and viable CD45$^+$ cells were sorted for MARS-seq processing and analysis at 30h PN.

(C) Gating strategy for CD45$^+$Fcεr1α$^+$cKit$^-$ lung basophils derived from anti-Fcεr1α or isotype control injected neonates.

(D) Frequency of different cell types from total CD45$^+$ cells in lungs derived from anti-Fcεr1α and isotype control injected mice, as determined by mapping single cells to the lung model (Figure 1; STAR Methods). Numbers were scaled to match control levels between experiments. Student's t-test (two tailed): *p = 0.02; n = 3.

(legend continued on next page)

(E) Expression difference of the most differentially expressed genes between macrophages subsets II (light-green) and III (dark-green), when comparing lung macrophages derived from anti-Fcεr1α and isotype control injected mice. Shown are the top 15 differentially expressed genes on both sides. Values represent log_2 fold change.
(F) Distribution of macrophage III specific gene expression across macrophages derived from anti-Fcεr1α and isotype control injected mice. Expression level was scaled to match control levels between experiments. Kolmogorov–Smirnov test; ***$p < 10^{-4}$.
(G) Percentage of AM out of $CD45^+$ cells derived from BALF of Mcpt8 knockout and their littermate controls at adult, 8-12 weeks old mice.
(H) BM derived cells were split and grown into basophils (IL3) for 10 days, and macrophages (M-CSF) for 8 days. Macrophages were then co-cultured with (a) M-CSF+IL3, (b) IL33 and GM-CSF, (c) BM-derived basophils and (d) lung milieu-primed basophils (in the presence of IL33 and GM-CSF).
(I) Differential gene expression between basophils grown with GM-CSF and IL33 and naive basophils. Basophils were grown alone (*x axis*), or in the presence of macrophages (*y axis*). Inlet displays fraction of differentially expressed genes (fold change > 1) in each quartile.
(J) Heat-map represents gene expression profiles of BM-MΦ grown with and without basophils as in Figure 6L. Color bar indicates a-d growth conditions.
(K) Differential gene expression between macrophages grown with or without lung basophils (conditions a and d). Axes represent two independent experiments. Inlet displays fraction of differentially expressed genes (fold change > 1) in each quartile.
(L) Distribution of the immune-modulating specific gene expression induced by lung resident basophils across Macrophage II and III in lung development. Kolmogorov–Smirnov test; ***$p < 10^{-10}$.
(M and N) Comparison of basophil gene expression derived from different tissues.
(M) Gene expression of basophil hallmark genes (*Mcpt8*, *Cpa3*, *Cd200r3*), as well as tissue specific genes (*Il6*, *Ccl3*), across basophils collected from lung, tumor microenvironment, blood, spleen and liver of 8 weeks old mice. Non-basophils indicate cells collected and filtered as outliers.
(N) Distribution of gene expression signature of the lung basophils (Figure S4G) across basophils derived from different tissues. *$p < 0.05$, ***$p < 0.001$.

Discussion

The lung is a complex organ, so a lot of precise and tightly controlled steps are required to ensure its correct development. In mature adult lungs, remarkable repair mechanisms exist to regenerate lost or damaged cells, while on the other hand prenatal complications can result in life-long respiratory problems (Hogan et al., 2014). In the first phase of lung development, most cells are of non-immune origin, followed by the gradual infiltration of immune cells that are ultimately shaped by the local microenvironment. Before the two studies of this thesis were published, the crosstalk between non-immune and immune cells during lung development was never investigated to this extent.

In the first publication, summarized in Fig. 9, we could show that AEC II, important structural cells of the lung, produce and release the cytokine IL-33 upon the expansion of the alveoli during the first breathing movements. IL-33, in turn, triggers the activation of IL-33 receptor (ST-2) expressing ILC2s, a cell type that elicits a type-2 response. As such, IL-5 and IL-13 are released by ILC2s, which results in eosinophil influx, induced by IL-5, and polarization of AMs to an anti-inflammatory phenotype, which is IL-13 dependent. The anti-inflammatory phenotype of AMs is marked by lowered expression of pro-inflammatory cytokines such as TNF (tumor necrosis factor) and KC (CXCL1, chemokine ligand 1). Even if an anti-inflammatory macrophage phenotype is crucial during lung homeostasis to prevent excessive inflammation this comes at the expense of a delayed response to infectious agents like the Gram-positive bacteria *Streptococcus pneumoniae*.

Alarmins like IL-33 are released from necrotic cells after cell damage or mechanical injury to alert the immune system (Cayrol and Girard, 2014), which corresponds to the inflammatory milieu that develops shortly after birth following alveolar expansion and structural changes induced by exposure to the outer environment. An increase of IL-33 can also be measured during inflammation, for example in asthma patients (Préfontaine et al., 2010). It was shown that IL-33 is constitutively expressed in humans and mice as a nuclear cytokine, especially in epithelial cells of mucosal tissues and in fibroblastic reticular cells of lymphoid tissues (Pichery et al., 2012). But it is also detectable in lung AEC II before birth (Treutlein et al., 2014), which is quite surprising as drivers of IL-33 up-regulation are still missing. How IL-33 expression is regulated during embryogenesis, is still not understood. One possible regulatory mechanism is the binding of IL-33 to chromatin via short binding motifs (Travers et al., 2018). It would be interesting to study the role of nuclear IL-33 in epithelial cells shortly before birth to see if chromatin binding of IL-33 influences gene expression.

To gain more insight into the role of IL-33, one experiment was the mechanical expansion of late embryonic lungs in a negative pressure chamber, which resulted in an up-regulation of IL-33 while the cells were still viable and undamaged. This would suggest that IL-33 is not

only a passively released alarmin but also has an additional function in lung development, for example as a “mechanosensor”. As mentioned in the introduction, fetal breathing movements can lead to enhanced differentiation of epithelial cells at the end of the pseudoglandular phase. It would be exciting to study if this is accompanied by an up-regulation of IL-33 and if it has any influence on the surfactant production in preterm infants. The expression of IL-33 before birth could also explain why low numbers of ILC2s in the lung can already be detected at a late embryonic stage (Lai et al., 2016). Parabiosis experiments showed that ILC2s are tissue-resident cells and only after a nematode challenge were donor-derived ILC2s detectable in the host system (Gasteiger et al., 2015; Moro et al., 2016). This opens up a lot of questions about the homing of ILCs during embryogenesis and tissue-specific factors that shape their expression pattern similar to the imprinting described for tissue-resident macrophages.

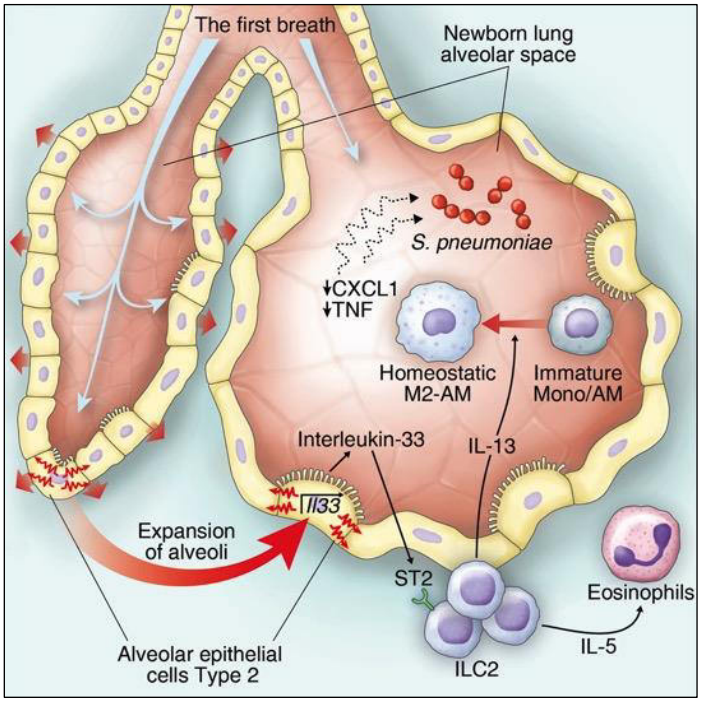

Fig. 9 – Working model “First-breath-induced type 2 pathways shape the lung immune environment”. Taken from (Saluzzo et al., 2017).

ILC2s were just recently found, but received much attention since then, as they orchestrate innate and adaptive immune responses in various tissues. The IL33/ILC2 axis in the lung plays a role in viral infections where it is important to restore airway integrity after an influenza infection (Monticelli et al., 2011) on the other hand it was also shown to trigger airway hyper-reactivity (Chang et al., 2011). With our study we add one important aspect to their role in development (summarized in Fig.9), but which role ILCs play in other tissues that are exposed to cell damage and mechanical stress during birth, still needs to be addressed (Mindt et al., 2018).

In the second paper we aimed for a system-wide approach to better understand the crosstalk of cell types during lung development. Within the lung, signal-transmitting cells secrete growth factors and cytokines thereby regulating cellular composition. By mapping these interactions using single cell RNA-sequencing we could not only confirm the role of ILC2s as a development driving cell population but also identify a basophil population that expresses a tissue-specific profile. Basophils are thought to be short-lived granulocytic cells that are important for the induction of Th2 responses in allergy but we could show that they also play a role in lung development and homeostasis. As the exact timing is essential for proper tissue development and function, we analyzed time points ranging from early fetal development up to adulthood, as seen in the upper panel of Fig.10. In the upper left box a summary of all cell types of the immune and non-immune niche that were found by single cell sequencing are shown. Using a curated ligand-receptor list, potential interactions between cell types were mapped and projected onto the cell type atlas as depicted in the left panels in Fig. 10. As an example AEC II that express IL-33 and basophils that express the IL-33 receptor, ST2, are shown. To ensure proximity of the involved cell type pairs found via the ligand-receptor expression, immunohistochemistry staining was performed, showing prosurfactant protein C (proSP-C) expressing AEC II and Mcpt8 positive basophils. Using *in vivo* mouse models such as ST2 deficient mice and basophil depletion using an antibody based strategy, or genetically modified mice, as well as *in vitro* cell assays, we could show that AEC II produce IL-33 and GM-CSF (Csf2) that activate ILC2s and lung basophils. In response, lung basophils and ILC2s produce GM-CSF and IL-13, which we showed to play a role in generating an anti-inflammatory phenotype in lung macrophages, which is graphically depicted on the right panel of Fig. 10.

Profiling of the basophil population revealed a lung specific phenotype that was distinct to the expression pattern found in peripheral circulating basophils. Using mice that lack the IL-33 receptor (ST2 KO mice) or *ex vivo* cultures we found that IL-33 in combination with GM-CSF was required to induce this tissue-specific phenotype. This led to questions that were not within the scope of the published study and that are still open as for example how long do these basophils reside in the tissue and what is driving them to enter the organ during late embryogenesis. It would also be interesting to use inducible depletion strategies to establish the role of these tissue basophils in adulthood and determine if this population has self-renewing capacities. Understanding cellular circuits during development can shed light on the crosstalk between cell types during infection or chronic inflammation.

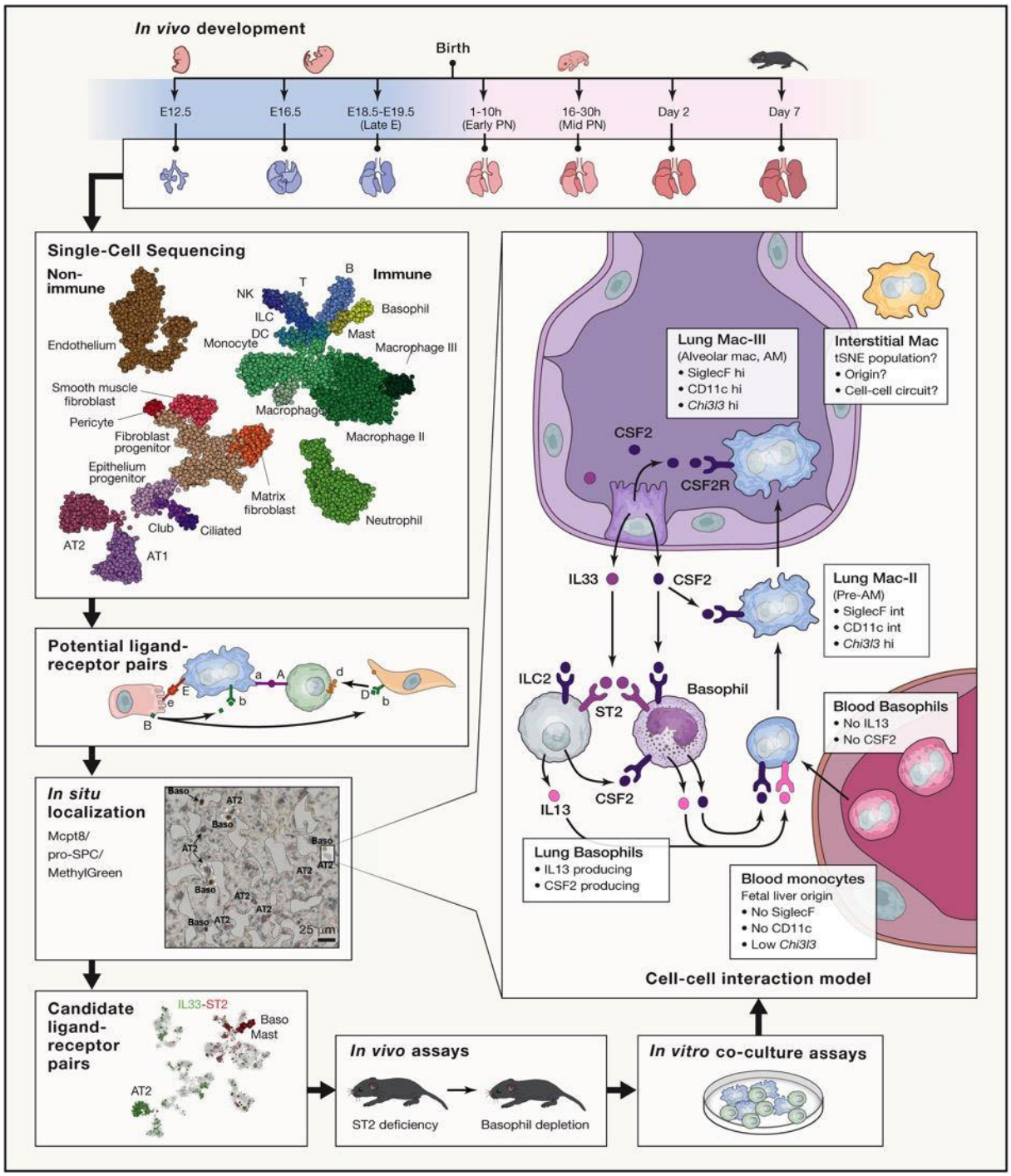

Fig. 10 – Working model "Lung single-cell signaling interaction map reveals basophil role in macrophage imprinting". Taken from (Scott and Guilliams, 2018).

In both publications we could demonstrate the impact of a small immune cell population on the maturation of alveolar macrophages (AM). In the developmental cell atlas we identified dynamic trajectories, including three waves of AM development starting from primitive yolk sac macrophages, followed by the income of fetal liver monocytes that differentiated into mature AMs shortly after birth. This nicely confirms the published results of other groups (Guilliams et al., 2013; van de Laar et al., 2016). To our surprise we couldn't find interstitial macrophages (IMs, Fig. 10 upper right), a second group of tissue-resident lung macrophages that develop from yolk sac macrophages and lack the surface marker SiglecF and are not

auto-fluorescent in contrast to AMs (Schyns et al., 2018). The lack of IMs could be explained by different preparation protocols or even the potential of AMs to acquire different surface markers when microenvironmental factors change.

Tissue-resident macrophages in general display substantial functional and morphological heterogeneities, depending on the tissue they reside in. Knowledge on the identity-defining changes can be deducted from both, transcriptional and epigenetic profiling. Epigenetic marks regulate gene expression levels and cellular identity, and are as such differentially regulated within specific macrophage populations. Indeed, a number of hallmark publications demonstrated that local, microenvironmental factors are indispensable for determining subset-specific gene expression patterns and enhancer landscapes in resident tissue macrophage populations at steady state (Amit et al., 2016; Gautier et al., 2012; Gosselin et al., 2014; Lavin et al., 2014). By creating a single cell RNA-seq lung cell atlas we took the first step to profile lung development but soon system-wide studies on an epigenetic and metabolite level should follow to further characterize lung subsets and their interactions.

The biggest difference between the role of ILC2s and basophils on AM development seems to be that ILC2s effect the polarization of AMs to a more M2-like phenotype but are not important for AM maintenance or proliferation as the AM number was comparable between IL-13 deficient and WT mice. Basophil depletion on the other hand, seems to influence the AM maturation and functionality as fewer AMs were detectable in the bronchoalveolar lavage of adult mice that moreover showed reduced phagocytic capacities. In the first paper we found that IL-33 abrogation is not sufficient to completely abolish the M2-like phenotype of AMs. This already suggested that an additional cell population is important for AM differentiation. Besides the basophil population, which we found to also depend on IL-33, there might be even more unidentified cell populations that shape AM identity.

Despite the fact that the lung is quite an elastic and flexible organ with reparative capacities, chronic pathologies like fibrosis develop. Using our knowledge we gained from extensively studying lung development we can now go one step further and apply these information to a model of lung injury to better understand the regenerative ability within the lung at different ages. In addition, we need to apply similar strategies to the human lung. Human AMs express the mannose receptor CD206 on their surface, which is a M2-like marker (Bharat et al., 2015; Kaku et al., 2013). In newborns, high levels of soluble ST2 and IL-13 can be measured (Belderbos et al., 2013), which would correspond to the data we found in mice. As respiratory diseases are still the third leading cause of mortality and morbidity in industrialized countries, lung development and interactions between lung cell types should continue to be the focus of extensive investigations.

3. References

Albrengues, J., Shields, M.A., Ng, D., Park, C.G., Ambrico, A., Poindexter, M.E., Upadhyay, P., Uyeminami, D.L., Pommier, A., Küttner, V., et al. (2018). Neutrophil extracellular traps produced during inflammation awaken dormant cancer cells in mice. Science *361*.

Amit, I., Winter, D.R., and Jung, S. (2016). The role of the local environment and epigenetics in shaping macrophage identity and their effect on tissue homeostasis. Nat Immunol *17*, 18–25.

Arinobu, Y., Iwasaki, H., and Akashi, K. (2009). Origin of basophils and mast cells. Allergol Int *58*, 21–28.

Artis, D., and Spits, H. (2015). The biology of innate lymphoid cells. Nature *517*, 293–301.

Bain, C.C., Bravo-Blas, A., Scott, C.L., Gomez Perdiguero, E., Geissmann, F., Henri, S., Malissen, B., Osborne, L.C., Artis, D., and Mowat, A.M. (2014). Constant replenishment from circulating monocytes maintains the macrophage pool in the intestine of adult mice. Nature Immunology *15*, 929–937.

Barkauskas, C.E., Chung, M.-I., Fioret, B., Gao, X., Katsura, H., and Hogan, B.L.M. (2017). Lung organoids: current uses and future promise. Development *144*, 986–997.

Belderbos, M.E., Levy, O., Meyaard, L., and Bont, L. (2013). Plasma-mediated immune suppression: a neonatal perspective. Pediatr Allergy Immunol *24*, 102–113.

Berger, A. (2000). Th1 and Th2 responses: what are they? BMJ *321*, 424.

Bharat, A., Bhorade, S.M., Morales-Nebreda, L., McQuattie-Pimentel, A.C., Soberanes, S., Ridge, K., DeCamp, M.M., Mestan, K.K., Perlman, H., Budinger, G.R.S., et al. (2015). Flow Cytometry Reveals Similarities Between Lung Macrophages in Humans and Mice. Am J Respir Cell Mol Biol *54*, 147–149.

Bilsland, C.A., Diamond, M.S., and Springer, T.A. (1994). The leukocyte integrin p150,95 (CD11c/CD18) as a receptor for iC3b. Activation by a heterologous beta subunit and localization of a ligand recognition site to the I domain. J. Immunol. *152*, 4582–4589.

Boucher, E., Provost, P.R., and Tremblay, Y. (2015). C21-steroids inactivation and glucocorticoid synthesis in the developing lung. J. Steroid Biochem. Mol. Biol. *147*, 70–80.

Bourbon, J., Boucherat, O., Chailley-Heu, B., and Delacourt, C. (2005). Control mechanisms of lung alveolar development and their disorders in bronchopulmonary dysplasia. Pediatr. Res. *57*, 38R-46R.

Bradley, L.M., Dalton, D.K., and Croft, M. (1996). A direct role for IFN-gamma in regulation of Th1 cell development. J. Immunol. *157*, 1350–1358.

Brinkmann, V., Reichard, U., Goosmann, C., Fauler, B., Uhlemann, Y., Weiss, D.S., Weinrauch, Y., and Zychlinsky, A. (2004). Neutrophil extracellular traps kill bacteria. Science *303*, 1532–1535.

Cayrol, C., and Girard, J.-P. (2014). IL-33: an alarmin cytokine with crucial roles in innate immunity, inflammation and allergy. Curr. Opin. Immunol. *31*, 31–37.

Chang, Y.-J., Kim, H.Y., Albacker, L.A., Baumgarth, N., McKenzie, A.N.J., Smith, D.E., Dekruyff, R.H., and Umetsu, D.T. (2011). Innate lymphoid cells mediate influenza-induced airway hyper-reactivity independently of adaptive immunity. Nat. Immunol. *12*, 631–638.

Chirumbolo, S. (2012). State-of-the-art review about basophil research in immunology and allergy: is the time right to treat these cells with the respect they deserve? Blood Transfus *10*, 148–164.

Cho, J.Y., Song, D.J., Pham, A., Rosenthal, P., Miller, M., Dayan, S., Doherty, T.A., Varki, A., and Broide, D.H. (2010). Chronic OVA allergen challenged Siglec-F deficient mice have increased mucus, remodeling, and epithelial Siglec-F ligands which are up-regulated by IL-4 and IL-13. Respir. Res. *11*, 154.

Coalson, J.J. (2003). Pathology of new bronchopulmonary dysplasia. Semin Neonatol *8*, 73–81.

D'Angio, C.T., and Maniscalco, W.M. (2004). Bronchopulmonary dysplasia in preterm infants: pathophysiology and management strategies. Paediatr Drugs *6*, 303–330.

Denzel, A., Maus, U.A., Gomez, M.R., Moll, C., Niedermeier, M., Winter, C., Maus, R., Hollingshead, S., Briles, D.E., Kunz-Schughart, L.A., et al. (2008). Basophils enhance immunological memory responses. Nature Immunology *9*, 733–742.

Desai, T.J., Brownfield, D.G., and Krasnow, M.A. (2014). Alveolar progenitor and stem cells in lung development, renewal and cancer. Nature *507*, 190–194.

Domyan, E.T., Ferretti, E., Throckmorton, K., Mishina, Y., Nicolis, S.K., and Sun, X. (2011). Signaling through BMP receptors promotes respiratory identity in the foregut via repression of Sox2. Development *138*, 971–981.

Eberl, G., Colonna, M., Di Santo, J.P., and McKenzie, A.N.J. (2015). Innate lymphoid cells. Innate lymphoid cells: a new paradigm in immunology. Science *348*, aaa6566.

El Kasmi, K.C., Qualls, J.E., Pesce, J.T., Smith, A.M., Thompson, R.W., Henao-Tamayo, M., Basaraba, R.J., König, T., Schleicher, U., Koo, M.-S., et al. (2008). Toll-like receptor-induced arginase 1 in macrophages thwarts effective immunity against intracellular pathogens. Nat. Immunol. *9*, 1399–1406.

Epelman, S., Lavine, K.J., Beaudin, A.E., Sojka, D.K., Carrero, J.A., Calderon, B., Brija, T., Gautier, E.L., Ivanov, S., Satpathy, A.T., et al. (2014). Embryonic and Adult-Derived Resident Cardiac Macrophages Are Maintained through Distinct Mechanisms at Steady State and during Inflammation. Immunity *40*, 91–104.

Evans, M.J., Cabral, L.J., Stephens, R.J., and Freeman, G. (1975). Transformation of alveolar type 2 cells to type 1 cells following exposure to NO2. Exp. Mol. Pathol. *22*, 142–150.

van Furth, R., and Cohn, Z.A. (1968). The origin and kinetics of mononuclear phagocytes. J. Exp. Med. *128*, 415–435.

van Furth, R., Cohn, Z.A., Hirsch, J.G., Humphrey, J.H., Spector, W.G., and Langevoort, H.L. (1972). The mononuclear phagocyte system: a new classification of macrophages, monocytes, and their precursor cells. Bull. World Health Organ. *46*, 845–852.

Gasteiger, G., Fan, X., Dikiy, S., Lee, S.Y., and Rudensky, A.Y. (2015). Tissue residency of innate lymphoid cells in lymphoid and nonlymphoid organs. Science *350*, 981–985.

Gautier, E.L., Shay, T., Miller, J., Greter, M., Jakubzick, C., Ivanov, S., Helft, J., Chow, A., Elpek, K.G., Gordonov, S., et al. (2012). Gene-expression profiles and transcriptional regulatory pathways that underlie the identity and diversity of mouse tissue macrophages. Nat Immunol *13*, 1118–1128.

Gauvreau, G.M., Lee, J.M., Watson, R.M., Irani, A.M., Schwartz, L.B., and O'Byrne, P.M. (2000). Increased numbers of both airway basophils and mast cells in sputum after allergen inhalation challenge of atopic asthmatics. Am. J. Respir. Crit. Care Med. *161*, 1473–1478.

Giangreco, A., Reynolds, S.D., and Stripp, B.R. (2002). Terminal bronchioles harbor a unique airway stem cell population that localizes to the bronchoalveolar duct junction. Am. J. Pathol. *161*, 173–182.

Gieseck, R.L., Wilson, M.S., and Wynn, T.A. (2018). Type 2 immunity in tissue repair and fibrosis. Nat. Rev. Immunol. *18*, 62–76.

Ginhoux, F. (2014). Fate PPAR-titioning: PPAR-γ "instructs" alveolar macrophage development. Nat. Immunol. *15*, 1005–1007.

Ginhoux, F., Greter, M., Leboeuf, M., Nandi, S., See, P., Gokhan, S., Mehler, M.F., Conway, S.J., Ng, L.G., Stanley, E.R., et al. (2010). Fate Mapping Analysis Reveals That Adult Microglia Derive from Primitive Macrophages. Science *330*, 841–845.

Ginhoux, F., Schultze, J.L., Murray, P.J., Ochando, J., and Biswas, S.K. (2016). New insights into the multidimensional concept of macrophage ontogeny, activation and function. Nat. Immunol. *17*, 34–40.

Gordon, S., and Martinez, F.O. (2010). Alternative Activation of Macrophages: Mechanism and Functions. Immunity *32*, 593–604.

Goss, A.M., Tian, Y., Tsukiyama, T., Cohen, E.D., Zhou, D., Lu, M.M., Yamaguchi, T.P., and Morrisey, E.E. (2009). Wnt2/2b and beta-catenin signaling are necessary and sufficient to specify lung progenitors in the foregut. Dev. Cell *17*, 290–298.

Gosselin, D., Link, V.M., Romanoski, C.E., Fonseca, G.J., Eichenfield, D.Z., Spann, N.J., Stender, J.D., Chun, H.B., Garner, H., Geissmann, F., et al. (2014). Environment drives selection and function of enhancers controlling tissue-specific macrophage identities. Cell *159*, 1327–1340.

Guilliams, M., Kleer, I.D., Henri, S., Post, S., Vanhoutte, L., Prijck, S.D., Deswarte, K., Malissen, B., Hammad, H., and Lambrecht, B.N. (2013). Alveolar macrophages develop from fetal monocytes that differentiate into long-lived cells in the first week of life via GM-CSF. Journal of Experimental Medicine *210*, 1977–1992.

Gury-BenAri, M., Thaiss, C.A., Serafini, N., Winter, D.R., Giladi, A., Lara-Astiaso, D., Levy, M., Salame, T.M., Weiner, A., David, E., et al. (2016). The Spectrum and Regulatory Landscape of Intestinal Innate Lymphoid Cells Are Shaped by the Microbiome. Cell *166*, 1231-1246.e13.

Hammad, H., Plantinga, M., Deswarte, K., Pouliot, P., Willart, M.A.M., Kool, M., Muskens, F., and Lambrecht, B.N. (2010). Inflammatory dendritic cells—not basophils—are necessary and sufficient for induction of Th2 immunity to inhaled house dust mite allergen. J Exp Med *207*, 2097–2111.

Hashimoto, D., Chow, A., Noizat, C., Teo, P., Beasley, M.B., Leboeuf, M., Becker, C.D., See, P., Price, J., Lucas, D., et al. (2013). Tissue-resident macrophages self-maintain locally

throughout adult life with minimal contribution from circulating monocytes. Immunity *38*, 792–804.

Heinz, S., Benner, C., Spann, N., Bertolino, E., Lin, Y.C., Laslo, P., Cheng, J.X., Murre, C., Singh, H., and Glass, C.K. (2010). Simple combinations of lineage-determining transcription factors prime cis-regulatory elements required for macrophage and B cell identities. Mol. Cell *38*, 576–589.

Herriges, M., and Morrisey, E.E. (2014). Lung development: orchestrating the generation and regeneration of a complex organ. Development *141*, 502–513.

Herriges, M.J., Swarr, D.T., Morley, M.P., Rathi, K.S., Peng, T., Stewart, K.M., and Morrisey, E.E. (2014). Long noncoding RNAs are spatially correlated with transcription factors and regulate lung development. Genes Dev. *28*, 1363–1379.

Herriges, M.J., Tischfield, D.J., Cui, Z., Morley, M.P., Han, Y., Babu, A., Li, S., Lu, M., Cendan, I., Garcia, B.A., et al. (2017). The NANCI-Nkx2.1 gene duplex buffers Nkx2.1 expression to maintain lung development and homeostasis. Genes Dev. *31*, 889–903.

Hiemstra, P.S., McCray, P.B., and Bals, R. (2015). The innate immune function of airway epithelial cells in inflammatory lung disease. Eur. Respir. J. *45*, 1150–1162.

Hoeffel, G., Chen, J., Lavin, Y., Low, D., Almeida, F.F., See, P., Beaudin, A.E., Lum, J., Low, I., Forsberg, E.C., et al. (2015). C-Myb+ Erythro-Myeloid Progenitor-Derived Fetal Monocytes Give Rise to Adult Tissue-Resident Macrophages. Immunity *42*, 665–678.

Hogan, B.L.M., Barkauskas, C.E., Chapman, H.A., Epstein, J.A., Jain, R., Hsia, C.C.W., Niklason, L., Calle, E., Le, A., Randell, S.H., et al. (2014). Repair and regeneration of the respiratory system: complexity, plasticity, and mechanisms of lung stem cell function. Cell Stem Cell *15*, 123–138.

Hong, K.U., Reynolds, S.D., Watkins, S., Fuchs, E., and Stripp, B.R. (2004). In vivo differentiation potential of tracheal basal cells: evidence for multipotent and unipotent subpopulations. Am. J. Physiol. Lung Cell Mol. Physiol. *286*, L643-649.

Hussell, T., and Bell, T.J. (2014). Alveolar macrophages: plasticity in a tissue-specific context. Nat Rev Immunol *14*, 81–93.

Jaitin, D.A., Kenigsberg, E., Keren-Shaul, H., Elefant, N., Paul, F., Zaretsky, I., Mildner, A., Cohen, N., Jung, S., Tanay, A., et al. (2014). Massively parallel single-cell RNA-seq for marker-free decomposition of tissues into cell types. Science *343*, 776–779.

Jobe, A.H., and Ikegami, M. (1998). Mechanisms initiating lung injury in the preterm. Early Hum. Dev. *53*, 81–94.

Joza, S., and Post, M. (2015). Development of the Respiratory System (Including the Preterm Infant). In Pediatric and Neonatal Mechanical Ventilation: From Basics to Clinical Practice, P.C. Rimensberger, ed. (Berlin, Heidelberg: Springer Berlin Heidelberg), pp. 3–25.

Kaku, Y., Imaoka, H., Takenaka, S., Oda, H., Matsuoka, M., Morimatu, Y., Kawayama, T., and Hoshino, T. (2013). M2 Macrophage Marker CD163 And CD204 Expression On Alveolar Macrophages In The Lungs Of Patients With COPD. In C43. CHRONIC OBSTRUCTIVE PULMONARY DISEASE: PATHOGENETIC MECHANISMS, (American Thoracic Society), pp. A4233–A4233.

Kang, J., and Coles, M. (2012). IL-7: the global builder of the innate lymphoid network and beyond, one niche at a time. Semin Immunol *24*, 190–197.

Kim, C.F.B., Jackson, E.L., Woolfenden, A.E., Lawrence, S., Babar, I., Vogel, S., Crowley, D., Bronson, R.T., and Jacks, T. (2005). Identification of bronchioalveolar stem cells in normal lung and lung cancer. Cell *121*, 823–835.

Kimura, S., Hara, Y., Pineau, T., Fernandez-Salguero, P., Fox, C.H., Ward, J.M., and Gonzalez, F.J. (1996). The T/ebp null mouse: thyroid-specific enhancer-binding protein is essential for the organogenesis of the thyroid, lung, ventral forebrain, and pituitary. Genes Dev. *10*, 60–69.

Knapp, S., Leemans, J.C., Florquin, S., Branger, J., Maris, N.A., Pater, J., van Rooijen, N., and van der Poll, T. (2003). Alveolar macrophages have a protective antiinflammatory role during murine pneumococcal pneumonia. Am. J. Respir. Crit. Care Med. *167*, 171–179.

Kobayashi, Y., and Tata, P.R. (2018). Pulmonary Neuroendocrine Cells: Sensors and Sentinels of the Lung. Dev. Cell *45*, 425–426.

Kumar, M.E., Bogard, P.E., Espinoza, F.H., Menke, D.B., Kingsley, D.M., and Krasnow, M.A. (2014). Mesenchymal cells. Defining a mesenchymal progenitor niche at single-cell resolution. Science *346*, 1258810.

La Manno, G., Soldatov, R., Zeisel, A., Braun, E., Hochgerner, H., Petukhov, V., Lidschreiber, K., Kastriti, M.E., Lönnerberg, P., Furlan, A., et al. (2018). RNA velocity of single cells. Nature *560*, 494–498.

van de Laar, L., Saelens, W., De Prijck, S., Martens, L., Scott, C.L., Van Isterdael, G., Hoffmann, E., Beyaert, R., Saeys, Y., Lambrecht, B.N., et al. (2016). Yolk Sac Macrophages, Fetal Liver, and Adult Monocytes Can Colonize an Empty Niche and Develop into Functional Tissue-Resident Macrophages. Immunity *44*, 755–768.

Lai, D.-M., Shu, Q., and Fan, J. (2016). The origin and role of innate lymphoid cells in the lung. Mil Med Res *3*, 25.

Lavin, Y., Winter, D., Blecher-Gonen, R., David, E., Keren-Shaul, H., Merad, M., Jung, S., and Amit, I. (2014). Tissue-resident macrophage enhancer landscapes are shaped by the local microenvironment. Cell *159*, 1312–1326.

Lawrence, T., and Natoli, G. (2011). Transcriptional regulation of macrophage polarization: enabling diversity with identity. Nat. Rev. Immunol. *11*, 750–761.

LeVine, A.M., Whitsett, J.A., Gwozdz, J.A., Richardson, T.R., Fisher, J.H., Burhans, M.S., and Korfhagen, T.R. (2000). Distinct effects of surfactant protein A or D deficiency during bacterial infection on the lung. J. Immunol. *165*, 3934–3940.

Lignell, A., Kerosuo, L., Streichan, S.J., Cai, L., and Bronner, M.E. (2017). Identification of a neural crest stem cell niche by Spatial Genomic Analysis. Nat Commun *8*, 1830.

Linnarsson, S., and Teichmann, S.A. (2016). Single-cell genomics: coming of age. Genome Biol *17*.

Liu, M., and Post, M. (2000). Invited review: mechanochemical signal transduction in the fetal lung. J. Appl. Physiol. *89*, 2078–2084.

López-Rodríguez, C., Chen, H.M., Tenen, D.G., and Corbí, A.L. (1995). Identification of Sp1-binding sites in the CD11c (p150,95 alpha) and CD11a (LFA-1 alpha) integrin subunit promoters and their involvement in the tissue-specific expression of CD11c. Eur. J. Immunol. *25*, 3496–3503.

Macosko, E.Z., Basu, A., Satija, R., Nemesh, J., Shekhar, K., Goldman, M., Tirosh, I., Bialas, A.R., Kamitaki, N., Martersteck, E.M., et al. (2015). Highly Parallel Genome-wide Expression Profiling of Individual Cells Using Nanoliter Droplets. Cell *161*, 1202–1214.

Madurga, A., Mizíková, I., Ruiz-Camp, J., and Morty, R.E. (2013). Recent advances in late lung development and the pathogenesis of bronchopulmonary dysplasia. Am. J. Physiol. Lung Cell Mol. Physiol. *305*, L893-905.

Mantovani, A., Sica, A., Sozzani, S., Allavena, P., Vecchi, A., and Locati, M. (2004). The chemokine system in diverse forms of macrophage activation and polarization. Trends Immunol. *25*, 677–686.

Marone, G., Rossi, F.W., Detoraki, A., Granata, F., Marone, G., Genovese, A., and Spadaro, G. (2007). Role of superallergens in allergic disorders. Chem Immunol Allergy *93*, 195–213.

Mason, R.J., and Voelker, D.R. (1998). Regulatory mechanisms of surfactant secretion. Biochim. Biophys. Acta *1408*, 226–240.

Mattner, J., and Wirtz, S. (2017). Friend or Foe? The Ambiguous Role of Innate Lymphoid Cells in Cancer Development. Trends Immunol. *38*, 29–38.

Mebius, R.E., Rennert, P., and Weissman, I.L. (1997). Developing lymph nodes collect CD4+CD3- LTbeta+ cells that can differentiate to APC, NK cells, and follicular cells but not T or B cells. Immunity *7*, 493–504.

Mills, C.D., Kincaid, K., Alt, J.M., Heilman, M.J., and Hill, A.M. (2000). M-1/M-2 macrophages and the Th1/Th2 paradigm. J. Immunol. *164*, 6166–6173.

Mindt, B.C., Fritz, J.H., and Duerr, C.U. (2018). Group 2 Innate Lymphoid Cells in Pulmonary Immunity and Tissue Homeostasis. Front Immunol *9*, 840.

Minoo, P. (2000). Transcriptional regulation of lung development: emergence of specificity. Respir. Res. *1*, 109–115.

Monticelli, L.A., Sonnenberg, G.F., Abt, M.C., Alenghat, T., Ziegler, C.G.K., Doering, T.A., Angelosanto, J.M., Laidlaw, B.J., Yang, C.Y., Sathaliyawala, T., et al. (2011). Innate lymphoid cells promote lung-tissue homeostasis after infection with influenza virus. Nat. Immunol. *12*, 1045–1054.

Moro, K., Kabata, H., Tanabe, M., Koga, S., Takeno, N., Mochizuki, M., Fukunaga, K., Asano, K., Betsuyaku, T., and Koyasu, S. (2016). Interferon and IL-27 antagonize the function of group 2 innate lymphoid cells and type 2 innate immune responses. Nat. Immunol. *17*, 76–86.

Morrisey, E.E., and Hogan, B.L.M. (2010). Preparing for the first breath: genetic and cellular mechanisms in lung development. Dev. Cell *18*, 8–23.

Mosmann, T.R., Cherwinski, H., Bond, M.W., Giedlin, M.A., and Coffman, R.L. (1986). Two types of murine helper T cell clone. I. Definition according to profiles of lymphokine activities and secreted proteins. J. Immunol. *136*, 2348–2357.

Mosser, D.M., and Edwards, J.P. (2008). Exploring the full spectrum of macrophage activation. Nat Rev Immunol *8*, 958–969.

Motomura, Y., Morita, H., Moro, K., Nakae, S., Artis, D., Endo, T.A., Kuroki, Y., Ohara, O., Koyasu, S., and Kubo, M. (2014). Basophil-derived interleukin-4 controls the function of natural helper cells, a member of ILC2s, in lung inflammation. Immunity *40*, 758–771.

Mucenski, M.L., Wert, S.E., Nation, J.M., Loudy, D.E., Huelsken, J., Birchmeier, W., Morrisey, E.E., and Whitsett, J.A. (2003). beta-Catenin is required for specification of proximal/distal cell fate during lung morphogenesis. J. Biol. Chem. *278*, 40231–40238.

Murray, P.J., and Wynn, T.A. (2011). Protective and pathogenic functions of macrophage subsets. Nat. Rev. Immunol. *11*, 723–737.

Murray, P.J., Allen, J.E., Biswas, S.K., Fisher, E.A., Gilroy, D.W., Goerdt, S., Gordon, S., Hamilton, J.A., Ivashkiv, L.B., Lawrence, T., et al. (2014). Macrophage activation and polarization: nomenclature and experimental guidelines. Immunity *41*, 14–20.

Nicolás-Ávila, J.Á., Adrover, J.M., and Hidalgo, A. (2017). Neutrophils in Homeostasis, Immunity, and Cancer. Immunity *46*, 15–28.

Nkadi, P.O., Merritt, T.A., and Pillers, D.-A.M. (2009). An overview of pulmonary surfactant in the neonate: genetics, metabolism, and the role of surfactant in health and disease. Mol. Genet. Metab. *97*, 95–101.

Nutku, E., Aizawa, H., Hudson, S.A., and Bochner, B.S. (2003). Ligation of Siglec-8: a selective mechanism for induction of human eosinophil apoptosis. Blood *101*, 5014–5020.

Ohnmacht, C., and Voehringer, D. (2009). Basophil effector function and homeostasis during helminth infection. Blood *113*, 2816–2825.

Okabe, Y., and Medzhitov, R. (2014). Tissue-specific signals control reversible program of localization and functional polarization of macrophages. Cell *157*, 832–844.

O'Koren, E.G., Hogan, B.L.M., and Gunn, M.D. (2013). Loss of basal cells precedes bronchiolitis obliterans-like pathological changes in a murine model of chlorine gas inhalation. Am. J. Respir. Cell Mol. Biol. *49*, 788–797.

Oliphant, C.J., Hwang, Y.Y., Walker, J.A., Salimi, M., Wong, S.H., Brewer, J.M., Englezakis, A., Barlow, J.L., Hams, E., Scanlon, S.T., et al. (2014). MHCII-mediated dialog between group 2 innate lymphoid cells and CD4(+) T cells potentiates type 2 immunity and promotes parasitic helminth expulsion. Immunity *41*, 283–295.

Pan, J., Copland, I., Post, M., Yeger, H., and Cutz, E. (2006). Mechanical stretch-induced serotonin release from pulmonary neuroendocrine cells: implications for lung development. Am. J. Physiol. Lung Cell Mol. Physiol. *290*, L185-193.

Pardo-Saganta, A., Law, B.M., Tata, P.R., Villoria, J., Saez, B., Mou, H., Zhao, R., and Rajagopal, J. (2015). Injury induces direct lineage segregation of functionally distinct airway basal stem/progenitor cell subpopulations. Cell Stem Cell *16*, 184–197.

Pepicelli, C.V., Lewis, P.M., and McMahon, A.P. (1998). Sonic hedgehog regulates branching morphogenesis in the mammalian lung. Curr. Biol. *8*, 1083–1086.

Pichery, M., Mirey, E., Mercier, P., Lefrancais, E., Dujardin, A., Ortega, N., and Girard, J.-P. (2012). Endogenous IL-33 is highly expressed in mouse epithelial barrier tissues, lymphoid organs, brain, embryos, and inflamed tissues: in situ analysis using a novel Il-33-LacZ gene trap reporter strain. J. Immunol. *188*, 3488–3495.

Préfontaine, D., Nadigel, J., Chouiali, F., Audusseau, S., Semlali, A., Chakir, J., Martin, J.G., and Hamid, Q. (2010). Increased IL-33 expression by epithelial cells in bronchial asthma. J. Allergy Clin. Immunol. *125*, 752–754.

Que, J., Okubo, T., Goldenring, J.R., Nam, K.-T., Kurotani, R., Morrisey, E.E., Taranova, O., Pevny, L.H., and Hogan, B.L.M. (2007). Multiple dose-dependent roles for Sox2 in the patterning and differentiation of anterior foregut endoderm. Development *134*, 2521–2531.

Reynolds, S.D., Reynolds, P.R., Snyder, J.C., Whyte, F., Paavola, K.J., and Stripp, B.R. (2007). CCSP regulates cross talk between secretory cells and both ciliated cells and macrophages of the conducting airway. Am. J. Physiol. Lung Cell Mol. Physiol. *293*, L114-123.

Robb, L., Drinkwater, C.C., Metcalf, D., Li, R., Köntgen, F., Nicola, N.A., and Begley, C.G. (1995). Hematopoietic and lung abnormalities in mice with a null mutation of the common beta subunit of the receptors for granulocyte-macrophage colony-stimulating factor and interleukins 3 and 5. Proc. Natl. Acad. Sci. U.S.A. *92*, 9565–9569.

Rock, J.R., Gao, X., Xue, Y., Randell, S.H., Kong, Y.-Y., and Hogan, B.L. (2011). Notch-dependent differentiation of adult airway basal stem cells. Cell Stem Cell *8*, 639–648.

Rogelj, S., Klagsbrun, M., Atzmon, R., Kurokawa, M., Haimovitz, A., Fuks, Z., and Vlodavsky, I. (1989). Basic fibroblast growth factor is an extracellular matrix component required for supporting the proliferation of vascular endothelial cells and the differentiation of PC12 cells. J. Cell Biol. *109*, 823–831.

Ryan, R.M., Ahmed, Q., and Lakshminrusimha, S. (2008). Inflammatory mediators in the immunobiology of bronchopulmonary dysplasia. Clin Rev Allergy Immunol *34*, 174–190.

Saluzzo, S., Gorki, A.-D., Rana, B.M.J., Martins, R., Scanlon, S., Starkl, P., Lakovits, K., Hladik, A., Korosec, A., Sharif, O., et al. (2017). First-Breath-Induced Type 2 Pathways Shape the Lung Immune Environment. Cell Reports *18*, 1893–1905.

Sans-Fons, M.G., Yeramian, A., Pereira-Lopes, S., Santamaría-Babi, L.F., Modolell, M., Lloberas, J., and Celada, A. (2013). Arginine transport is impaired in C57Bl/6 mouse macrophages as a result of a deletion in the promoter of Slc7a2 (CAT2), and susceptibility to Leishmania infection is reduced. J. Infect. Dis. *207*, 1684–1693.

Sawa, S., Lochner, M., Satoh-Takayama, N., Dulauroy, S., Bérard, M., Kleinschek, M., Cua, D., Di Santo, J.P., and Eberl, G. (2011). RORγt+ innate lymphoid cells regulate intestinal homeostasis by integrating negative signals from the symbiotic microbiota. Nat. Immunol. *12*, 320–326.

Scandella, E., Bolinger, B., Lattmann, E., Miller, S., Favre, S., Littman, D.R., Finke, D., Luther, S.A., Junt, T., and Ludewig, B. (2008). Restoration of lymphoid organ integrity through the interaction of lymphoid tissue-inducer cells with stroma of the T cell zone. Nat. Immunol. *9*, 667–675.

Schittny, J.C. (2017). Development of the lung. Cell Tissue Res. *367*, 427–444.

Schneider, C., Nobs, S.P., Kurrer, M., Rehrauer, H., Thiele, C., and Kopf, M. (2014). Induction of the nuclear receptor PPAR-γ by the cytokine GM-CSF is critical for the differentiation of fetal monocytes into alveolar macrophages. Nat. Immunol. *15*, 1026–1037.

Schulz, C., Gomez Perdiguero, E., Chorro, L., Szabo-Rogers, H., Cagnard, N., Kierdorf, K., Prinz, M., Wu, B., Jacobsen, S.E.W., Pollard, J.W., et al. (2012). A lineage of myeloid cells independent of Myb and hematopoietic stem cells. Science *336*, 86–90.

Schyns, J., Bureau, F., and Marichal, T. (2018). Lung Interstitial Macrophages: Past, Present, and Future. J Immunol Res *2018*, 5160794.

Scott, C.L., and Guilliams, M. (2018). Tissue Unit-ed: Lung Cells Team up to Drive Alveolar Macrophage Development. Cell *175*, 898–900.

Scott, C.L., T'Jonck, W., Martens, L., Todorov, H., Sichien, D., Soen, B., Bonnardel, J., De Prijck, S., Vandamme, N., Cannoodt, R., et al. (2018). The Transcription Factor ZEB2 Is Required to Maintain the Tissue-Specific Identities of Macrophages. Immunity *49*, 312-325.e5.

Shu, W., Guttentag, S., Wang, Z., Andl, T., Ballard, P., Lu, M.M., Piccolo, S., Birchmeier, W., Whitsett, J.A., Millar, S.E., et al. (2005). Wnt/beta-catenin signaling acts upstream of N-myc, BMP4, and FGF signaling to regulate proximal-distal patterning in the lung. Dev. Biol. *283*, 226–239.

Siracusa, M.C., Saenz, S.A., Hill, D.A., Kim, B.S., Headley, M.B., Doering, T.A., Wherry, E.J., Jessup, H.K., Siegel, L.A., Kambayashi, T., et al. (2011). TSLP promotes interleukin-3-independent basophil haematopoiesis and type 2 inflammation. Nature *477*, 229–233.

Snapper, C.M., and Paul, W.E. (1987). Interferon-gamma and B cell stimulatory factor-1 reciprocally regulate Ig isotype production. Science *236*, 944–947.

Snyder, E.L., Watanabe, H., Magendantz, M., Hoersch, S., Chen, T.A., Wang, D.G., Crowley, D., Whittaker, C.A., Meyerson, M., Kimura, S., et al. (2013). Nkx2-1 represses a latent gastric differentiation program in lung adenocarcinoma. Mol. Cell *50*, 185–199.

Snyder, J.C., Reynolds, S.D., Hollingsworth, J.W., Li, Z., Kaminski, N., and Stripp, B.R. (2010). Clara cells attenuate the inflammatory response through regulation of macrophage behavior. Am. J. Respir. Cell Mol. Biol. *42*, 161–171.

Sørensen, O.E., and Borregaard, N. Neutrophil extracellular traps — the dark side of neutrophils. J Clin Invest *126*, 1612–1620.

Stein, M., Keshav, S., Harris, N., and Gordon, S. (1992). Interleukin 4 potently enhances murine macrophage mannose receptor activity: a marker of alternative immunologic macrophage activation. J. Exp. Med. *176*, 287–292.

Suzuki, T., Maranda, B., Sakagami, T., Catellier, P., Couture, C.-Y., Carey, B.C., Chalk, C., and Trapnell, B.C. (2011). Hereditary pulmonary alveolar proteinosis caused by recessive CSF2RB mutations. Eur. Respir. J. *37*, 201–204.

Tamoutounour, S., Guilliams, M., Montanana Sanchis, F., Liu, H., Terhorst, D., Malosse, C., Pollet, E., Ardouin, L., Luche, H., Sanchez, C., et al. (2013). Origins and Functional Specialization of Macrophages and of Conventional and Monocyte-Derived Dendritic Cells in Mouse Skin. Immunity *39*, 925–938.

Travers, J., Rochman, M., Miracle, C.E., Habel, J.E., Brusilovsky, M., Caldwell, J.M., Rymer, J.K., and Rothenberg, M.E. (2018). Chromatin regulates IL-33 release and extracellular cytokine activity. Nat Commun *9*, 3244.

Treutlein, B., Brownfield, D.G., Wu, A.R., Neff, N.F., Mantalas, G.L., Espinoza, F.H., Desai, T.J., Krasnow, M.A., and Quake, S.R. (2014). Reconstructing lineage hierarchies of the distal lung epithelium using single cell RNA-seq. Nature *509*, 371–375.

Vivier, E., Artis, D., Colonna, M., Diefenbach, A., Santo, J.P.D., Eberl, G., Koyasu, S., Locksley, R.M., McKenzie, A.N.J., Mebius, R.E., et al. (2018). Innate Lymphoid Cells: 10 Years On. Cell *174*, 1054–1066.

Voehringer, D. (2017). Recent advances in understanding basophil functions in vivo. F1000Res *6*, 1464.

Volckaert, T., and De Langhe, S. (2014). Lung epithelial stem cells and their niches: Fgf10 takes center stage. Fibrogenesis Tissue Repair *7*, 8.

Wada, T., Ishiwata, K., Koseki, H., Ishikura, T., Ugajin, T., Ohnuma, N., Obata, K., Ishikawa, R., Yoshikawa, S., Mukai, K., et al. (2010). Selective ablation of basophils in mice reveals their nonredundant role in acquired immunity against ticks. J Clin Invest *120*, 2867–2875.

Weaver, C.T., Harrington, L.E., Mangan, P.R., Gavrieli, M., and Murphy, K.M. (2006). Th17: an effector CD4 T cell lineage with regulatory T cell ties. Immunity *24*, 677–688.

Xue, J., Schmidt, S.V., Sander, J., Draffehn, A., Krebs, W., Quester, I., De Nardo, D., Gohel, T.D., Emde, M., Schmidleithner, L., et al. (2014). Transcriptome-based network analysis reveals a spectrum model of human macrophage activation. Immunity *40*, 274–288.

Yu, Y., and Su, K. (2013). Neutrophil Extracellular Traps and Systemic Lupus Erythematosus. J Clin Cell Immunol *4*.

Yu, X., Buttgereit, A., Lelios, I., Utz, S.G., Cansever, D., Becher, B., and Greter, M. (2017). The Cytokine TGF-β Promotes the Development and Homeostasis of Alveolar Macrophages. Immunity *47*, 903-912.e4.

Zhang, M., Angata, T., Cho, J.Y., Miller, M., Broide, D.H., and Varki, A. (2007). Defining the in vivo function of Siglec-F, a CD33-related Siglec expressed on mouse eosinophils. Blood *109*, 4280–4287.

Zheng, D., Yin, L., and Chen, J. (2014). Evidence for Scgb1a1(+) cells in the generation of p63(+) cells in the damaged lung parenchyma. Am. J. Respir. Cell Mol. Biol. *50*, 595–604.

Ziegenhain, C., Vieth, B., Parekh, S., Reinius, B., Guillaumet-Adkins, A., Smets, M., Leonhardt, H., Heyn, H., Hellmann, I., and Enard, W. (2017). Comparative Analysis of Single-Cell RNA Sequencing Methods. Mol. Cell *65*, 631-643.e4.

Curriculum vitae

Personal details

Full name	Anna-Dorothea Gorki
Date of Birth	19.07.1990
Place of Birth	Grevesmühlen, Germany
Nationality	German
Address	CeMM - Research Center for Molecular Medicine of the Austrian Academy of Sciences Medical University of Vienna, Department of Medicine1, Laboratory of Infection Biology Währinger Gürtel 18 – 20, 1090 Vienna, Austria
E-Mail	Tgorki@cemm.oeaw.ac.at

Research interests

Basic and translational immunology, Host-pathogen interaction, Systems biology, Macrophage biology

Academic career

08/2018-present	Master's degree studies in Bioinformatics at the University of Applied Sciences, Vienna
10/2013-present	**PhD Thesis** within the interdisciplinary FWF-funded PhD-program "Cell Communication in Health and Disease" (CCHD) under the supervision of Prof. Sylvia Knapp, MD, PhD at the Medical University of Vienna, Austria Title: "The underdogs: How small immune cell populations shape lung macrophage development""
08/2016 – 03/2017	Research internship in the lab of Prof. Ido Amit at the Weizmann Institute of Science, Rehovot, Israel Title: "Single-cell sequencing during lung development"
03/2014 – 03/2016	Deputy Speaker of the Students Council of the Doctoral Program "Cell Communication in Health and Disease" (CCHD) at the Medical University of Vienna, Austria
02/2013-10/2013	**Master Thesis** in the lab of Predrag Slijepcevic, PhD, at Brunel University, West London, UK Title: "The role of telomere maintenance in DNA damage response- The effect of the telomerase activator TA-65 on the γH2AX foci formation in a lymphoblastoid cell line"
02/2013-10/2013	Master's degree studies of Molecular Medicine at Brunel University, West London, UK
01/2012-06/2012	**Bachelor Thesis** in the lab of Prof. Philipp Henneke, MD, PhD at the Centre of Chronic Immunodeficiency; Freiburg, Germany

	Title: "The role of the inflammasome in the reactive oxygen species response to streptococci"
06/2011-06/2012	Research Assistant at the Centre of Chronic Immunodeficiency in the lab of Prof. Philipp Henneke, MD, PhD
10/2009-06/2012	Bachelor's degree studies of Molecular Medicine at the Albert-Ludwigs-University, Freiburg, Germany

Awards and Fellowships

06/2017	EFIS Conference Support Grant to participate and present at the "Development of tissue- and pathogen-specific cellular innate immunity" conference, Freiburg, Germany
11/2016	EMBO Short-term fellowship for an internship in the lab of Prof. Ido Amit, Weizmann Institute of Science, Rehovot, Israel
11/2015	Travel Grant to participate and present at the "Inflammation-Bonfire from Within" conference, Weizmann Institute of Science, Rehovot, Israel
06/2015	Travel Grant to participate and present at the 2nd "Systems biology of infection symposium", Ascona, Switzerland
10/2012 – 10/2013	German Academic Exchange Service (DAAD) Scholarship for master studies, Brunel University, UK

Teaching

10/2018-ongoing	Co-supervision (together with Prof. Sylvia Knapp, MD, PhD) of PhD student Asma Farhat at the Medical University of Vienna
08/2018-ongoing	Supervision of medical student Dörte Symmank at the Medical University of Vienna
12/2016-ongoing	Co-supervision (together with Prof. Sylvia Knapp, MD, PhD) of PhD student Sophie Zahalka at the Medical University of Vienna

Publications

1. Cohen, M.*, Giladi, A.*, **Gorki, A.-D.***, Solodkin, D.G., Zada, M., Hladik, A., Miklosi, A., Salame, T.-M., Halpern, K.B., David, E., Itzkovitz, S., Harkany, T., Knapp, S., Amit, I., 2018. Lung Single-Cell Signaling Interaction Map Reveals Basophil Role in Macrophage Imprinting. Cell 175, 1031-1044.e18. https://doi.org/10.1016/j.cell.2018.09.009

   * Authors contributed equally

2. Saluzzo, S., **Gorki, A.-D**., Rana, B.M.J., Martins, R., Scanlon, S., Starkl, P., Lakovits, K., Hladik, A., Korosec, A., Sharif, O., Warszawska, J.M., Jolin, H., Mesteri, I., McKenzie, A.N.J., Knapp, S., 2017. First-Breath-Induced Type 2 Pathways Shape the

Lung Immune Environment. Cell Reports 18, 1893–1905. https://doi.org/10.1016/j.celrep.2017.01.071

3. Martins, R., Maier, J., **Gorki, A.-D.**, Huber, K.V.M., Sharif, O., Starkl, P., Saluzzo, S., Quattrone, F., Gawish, R., Lakovits, K., Aichinger, M.C., Radic-Sarikas, B., Lardeau, C.-H., Hladik, A., Korosec, A., Brown, M., Vaahtomeri, K., Duggan, M., Kerjaschki, D., Esterbauer, H., Colinge, J., Eisenbarth, S.C., Decker, T., Bennett, K.L., Kubicek, S., Sixt, M., Superti-Furga, G., Knapp, S., 2016. Heme drives hemolysis-induced susceptibility to infection via disruption of phagocyte functions. Nat. Immunol. 17, 1361–1372. https://doi.org/10.1038/ni.3590

Conference Participation

02/2018	Next Gen Immunology Conference, WIS, Rehovot, Israel
10/2017	Human Cell Atlas General Meeting, WIS, Rehovot, Israel
10/2017	Single cell genomics 2017, WIS, Rehovot, Israel
09/2017	Development of tissue- and pathogen-specific cellular innate immunity conference, Freiburg, Germany (Poster presentation)
02/2016	Next Gen Immunology Conference, WIS, Rehovot, Israel
11/2015	Inflammation-Bonfire from Within Symposium, WIS, Rehovot, Israel (Poster presentation)
09/2015	18th International Summer School on Immunology (FEBS Advanced Lecture Course) (Poster presentation)
09/2015	2nd Systems Biology of Infection Symposium, Ascona, Switzerland (Talk and poster presentation)
06/2015	11th PhD-Symposium of the Medical University of Vienna, 2015 (Poster presentation)
02/2015	8th Bridging the Gap Symposium – part of organizing committee
10/2014	28th Annual conference of the European Macrophage and Dendritic Cell Society, Vienna, Austria
02/2014	7th Bridging the Gap Symposium – part of organizing committee

Memberships

03/2016-present	Member of the Austrian Association for Allergy and Immunology (ÖGAI)
07/2015-present	Member of the Austrian Association of Molecular Life Sciences and Biotechnology (ÖGMBT)